PHASE-SEPARATING MICROBUBBLES FUNCTIONING AS VACCINE DEPOTS

A Thesis

by

JIHUI LEE

Submitted to the Office of Graduate and Professional Studies of
Texas A&M University
in partial fulfillment of the requirements for the degree of

MASTER OF SCIENCE

Chair of Committee,	Corey J. Bishop
Committee Members,	Daniel L. Alge
	M.N.V. Ravi Kumar
Head of Department,	Michael J. McShane

December 2017

Major Subject: Biomedical Engineering

ABSTRACT

        Failure in receiving a booster for specific vaccines contributes to incomplete

seroconversion, particularly in the developing world. Single injection vaccine

technology could potentially be a solution such that health care personnel would not

need to meet patients multiple times at designated points in time thereafter. The main

challenge for single injection vaccine systems to date is controlling the stability of the

antigen. to maintain the antigenic protein structure while in the physiological

environment. We engineered a novel phase-separating microbubble technology which

could function as an injectable depot which we hypothesize will enable us to control the

microenvironment of the antigen for the durations required, in addition to controlling the

antigen release time.

        We have successfully accomplished the following Main Specific Aims and sub-

aims:

Main Specific Aim 1: Synthesize polymers for microbubbles formation and Engineer

    methods for stabilizing Microbubbles:

  1A: Synthesize PCL and PLGA library at different molecular weights and

        characterizing the polymers

  1B: Synthesize acrylate polymers for microbubbles

  1C: Engineer stable microbubble through UV cure and lyophilization

  1D: Engineering the microbubbles to be stationary for maintaining sphere shape during

        the curing process and the inject of the cargo

1E: Engineering the cargo to be stationary within the polymeric microbubble to maximize the release time

1F: Quantify the diameter of the microbubble by varying syringe pump rate and comparing diameter pre- and post-lyophilization

1G: Quantify the angle of the micromotor for injecting cargo into the center of the microbubbles

1H: Engineer a self-contained lyophilization-capable system for the microbubbles

Main Specific Aim 2: Engineering cargo release time of the microbubbles:

2A: Quantify how different molecular weights of PCL affect release time of the microbubbles

2C: Quantify how varying the microbubbles' thickness of the shell controls the release time

Main Specific Aim 3: Quantify stability of HIV and Hepatitis B antigens:

3A: Quantify how the HIV gp120/41 and HBsAg ayw antigens are stable in time in an aqueous environment versus in a cryo-protectant context at varying temperatures

Our novel phase-separating technology which can form microbubble vaccine depots is a promising method to alleviate stability issues which hinders the single injection vaccine field. Enhancement of antigen stability in the microbubbles will be determined in future work.

DEDICATION

This work is dedicated to the living God and my Lord, Jesus Christ.

But he knows the way that I take;

when he has tested me, I will come forth as gold. (Job 23:10)

ACKNOWLEDGEMENTS

I would like to express my deepest gratitude to my committee chair, Dr. Bishop, for giving me the great opportunity to do my thesis in Pharmacoengineering lab. This thesis would never have done without his incredible patience and support throughout my time as his student. I have learned not only how to carry out research but also how to motivate people and how not to lose humor in any situations. It was a great honor to study under his guidance.

I would like to thank my committee members, Dr. Alge and Dr. Majeti, for their thoughtful guidance and support throughout the course of this research.

Thanks also go to all graduate and undergraduate members of Pharmacoengineering lab. In particular, I would like to thank Shree and Yongyu for their help and understanding for all the times. I have been lucky to have you guys as colleagues and friends.

I would also like to thank the department faculty and staff for making my experience at Texas A&M University a great experience.

Last, but not least, I send big thanks to my dear family for their prayers and caring and to my Andrei for his endless support and love.

CONTRIBUTORS AND FUNDING SOURCES

NOMENCLATURE

^{1}H NMR	Proton NMR
3D	Three-dimensional
AIDS	Acquired Immunodeficiency Syndrome
APC	Antigen Presenting Cell
B/CS	Bryan/College Station
bNAB	broadly Neutralizing Antibody
BSA	Bovine Serum Albumin
CCR5	C-C Receptor Type 5
CF	Correction Factor
CMC	Carboxymethyl Cellulose
CpG	Cytosine-phophodiester bond-guanine
CPP	Cell-penetrating Peptides
CS	Chitosan
CTL	Cytotoxic T Lymphocyte
DCM	Dichloromethane
DI	Deionized
DMPA	2,2-Dimethoxy-2-Phenylacetophonone
DMSO	Dimethyl Sulfoxide
DNA	Deoxyribonucleic Acid
DSC	Differential Scanning Calorimetry

DTP3	Three-dose Diphtheria-Tetanus-Pertussis
DTPA	Diethylenetriaminepentaacetic Acid
DTS	DNA Targeting Sequence
EDTA	Ethylene Diamine Tetra-acetic Acid
ELISA	Enzyme-Linked Immunosorbent Assay
EPO	Eudragit® E PO
FDA	Food and Drug Administration
G	Glycolide monomer
gp120	Glycoprotein 120 kDa
gp41	Glycoprotein 41 kDa
HBsAg	Hepatitis B Surface Agent
HBV	Hepatitis B Virus
HEMA	Hydroxyethyl Methacrylate
HIV	Human Immunodeficiency Virus
HIV-1	HIV subtype 1
HIV-2	HIV subtype 2
HRP	Horseradish Peroxidase
HSUS	Humane Society of the United States
ICMV	Interbilayer-crosslinked multilamellar lipid vesicles
IFN	Interferon
Ig	Immunoglobulin
IL	Interleukin

IPV	Inactivated Poliovirus Vaccine
IV	Inactivated Vaccine
L	Lactide monomer
LAV	Live Attenuated Vaccine
Lbl	Layer-by-layer
M	Million
MHC I/II	Major Histocompatibility Complex (class I/class II)
MP	Microparticle
mPEG	Methoxypolyethylene Glycol
mRNA	Messenger RNA
MW	Molecular Weight
NMR	Nuclear Magnetic Resonance Spectroscopy
NP	Nanoparticle
OPV	Oral poliovirus vaccine;
OVA	Ovalbumin;
P	Pressure
P(A)	polyadenylation
PAA	polyacrylic acid
PAMP	Pathogen-associated Molecular Pattern
PBAE	Poly(β-amino ester)
PCL	Poly(ε-caprolactone)
PCLDA	PCL Diacrylate

PCLTA	PCL Triacrylate
PCPH	Poly[(1,6-bis-carboxyphenoxy) hexane]
PEG	Polyethylene Glycol
PEI	Polyethylamine Imine
PLGA	Poly(lactic-co-glycolic acid)
PLLA	Poly(L-lactic acid)
PMMA	Poly(methyl methacrylate);
ppm	Part per million
PNA	Peptide Nucleic Acid
PVA	Polyvinyl Alcohol
RNA	Ribonucleic Acid
SEM	Scanning Electron Microscopy
SO	Tin(II) 2-ethylhexanoate
SV40	Simian Virus 40
T	Time
TCEP	Tris-(2-carboxyethyl)phosphine
TCR	T Cell Receptor
TEA	Trimethylamine
TEGDMA	Triethylene Glycol Dimethacrylate
TGF	Transforming Growth Factor
Th	Helper T Cell
TLR	Toll-like Receptor

TMB	Tetramethylbezidine
TMC	N-trimethyl Chitosan Chloride
TNF	Tumor Necrosis Factor
T_g	Glass transition temperature
T_m	Melting temperature
TVA	Tennessee Valley Authority
TxDOT	Texas Department of Transportation
UV	Ultraviolet
VLP	Virus-like particle
WHO	World Health Organization

TABLE OF CONTENTS

LIST OF FIGURES

LIST OF TABLES

1   INTRODUCTION*

Infectious diseases are one of the main causes of death globally. For instance, lower respiratory infections are the third biggest killer (3.19 M deaths) following by ischemic heart disease (8.46 M deaths) and stroke (6.24 M deaths) in 2015 (**Figure 1**) [1]. Initially, vaccines were developed as a preventive treatment against infectious diseases but now vaccines are being used for therapeutic approaches (e.g. cancer therapy). Since the first vaccine against smallpox was developed by Edward Jenner, scientist eradicated numerous infectious diseases and the overall death rate has decreased continuously from 0.8% to 0.046% for the last 114 years.

Even though many vaccines were developed and they reduced the mortality rate due to infectious disease, death from several infectious diseases increased such as AIDS and vector-borne diseases [1]. This problem is more serious in developing countries. From 2015 to 2017, the 68 poorest countries presented an average coverage rate of 80% for the 3 doses of diphtheria-tetanus-pertussis (DTP3) (**Figure 2**). This means that 19.4 M children cannot receive DTP3 nowadays [2]. Another example is Hepatitis B. In the western pacific countries, the at-birth coverage rate for HBV was 79% while in the African region it was 11% [3]. The reason is that there are many barriers to increasing
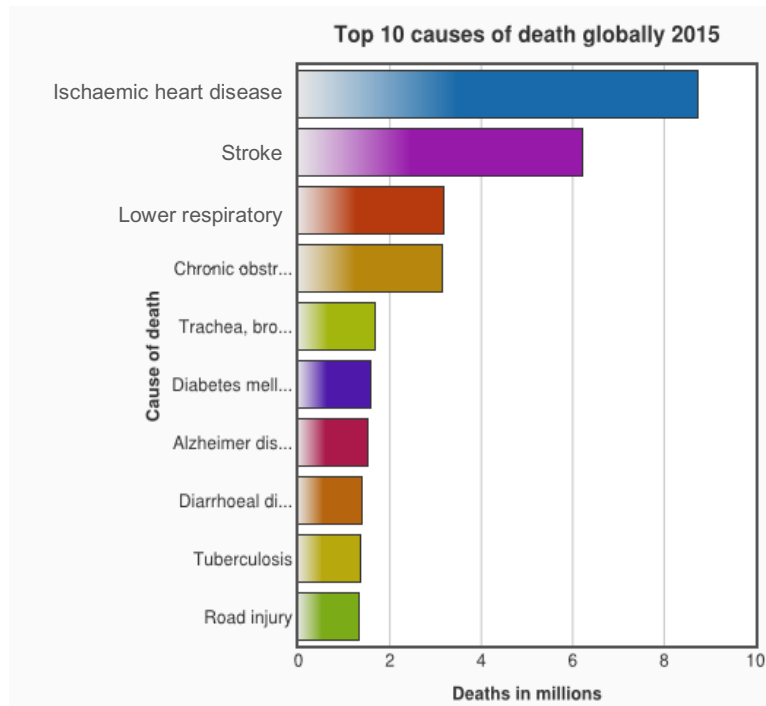
Figure 1 Top 10 causes of death globally published in 2015 by the WHO. Reprinted from [1]
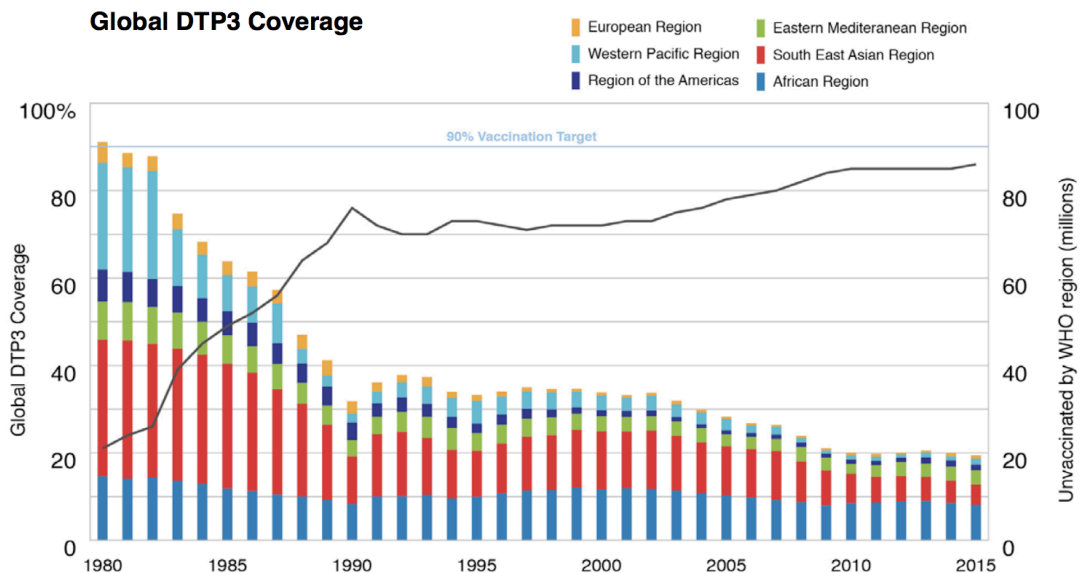
Figure 2 Timeline for the global DTP3 vaccine coverage published in 2015 by WHO. Adapted from [2]

the vaccine coverage rate in developing countries.

One of the main barriers is their poor health care system. According to the WHO, 2-3 million people can be saved from death by completing every dose of vaccination. However, most African countries and India have 1 doctor per 2000 people, in 2010 [4]. Therefore, visiting medical facilities every time to complete a vaccination is not easy for patients and the cost for every dosage is also a burden for them.

Another reason for poor vaccine coverage is issues with functionality because of the instability of antigens. For amino acid-based and protein-based vaccines, thermo-instability and hydrolysis greatly diminishes the vaccines efficacy. Proteins are exposed to harsh temperatures during poor transportation and storage conditions. Transportation systems in the developing world generally have an incomplete cold chain, causing antigen instability during transportation. A reasonable approach to tackle a number of these issues is the single injection vaccine based on non-viral polymeric delivery systems [5-7]. Through this single injection vaccine, multiple doses can be administered at once. Therefore, single injection vaccines reduce or eliminate the need for multiple visits to a medical facility. Furthermore, the burden of cost could be potentially mitigated with fewer visits to medical facilities for both the people to be vaccinated, as well as the medical personnel involved in the vaccination itself. The main challenges for single injection vaccines are engineering the release kinetics and the antigen stability. However, stabilizing the antigen is far more challenging than controlling the release kinetics over the durations needed for completing vaccination.

It is highly likely that novel release profiles may be more efficient than what is commonly done for a type of vaccine. For example, although 0, 1, and 6 months may be used for a vaccine, a limited number of permutations of the vaccine schedule has been tested.

For a single injection vaccine, every dosage that will be exposed to the patient's immune system is injected at the same time. Each dosage should be released at each expected date. For instance, a hepatitis B vaccine should release the second dosage and the third dosage at 1 month and 6 months from the injection, respectively. Also, the second and third antigen exposures should be in a conformation that will generate neutralizing antibodies against the antigen wild types. A great deal of research has shown successful results in controlling release kinetics, but they have difficulty in maintaining antigen stability over the durations required for complete seroconversion.

Although a number of research laboratories use traditional microparticles, there are a number of drawbacks such as loss of antigen stability due to contact with organic solvent during the precipitation processes. Furthermore, an antigen can lose its functionality due to ultrasound during the emulsification. The microparticles have an extremely high surface area of aqueous phase in contact with organic solvent for double-emulsion processes.
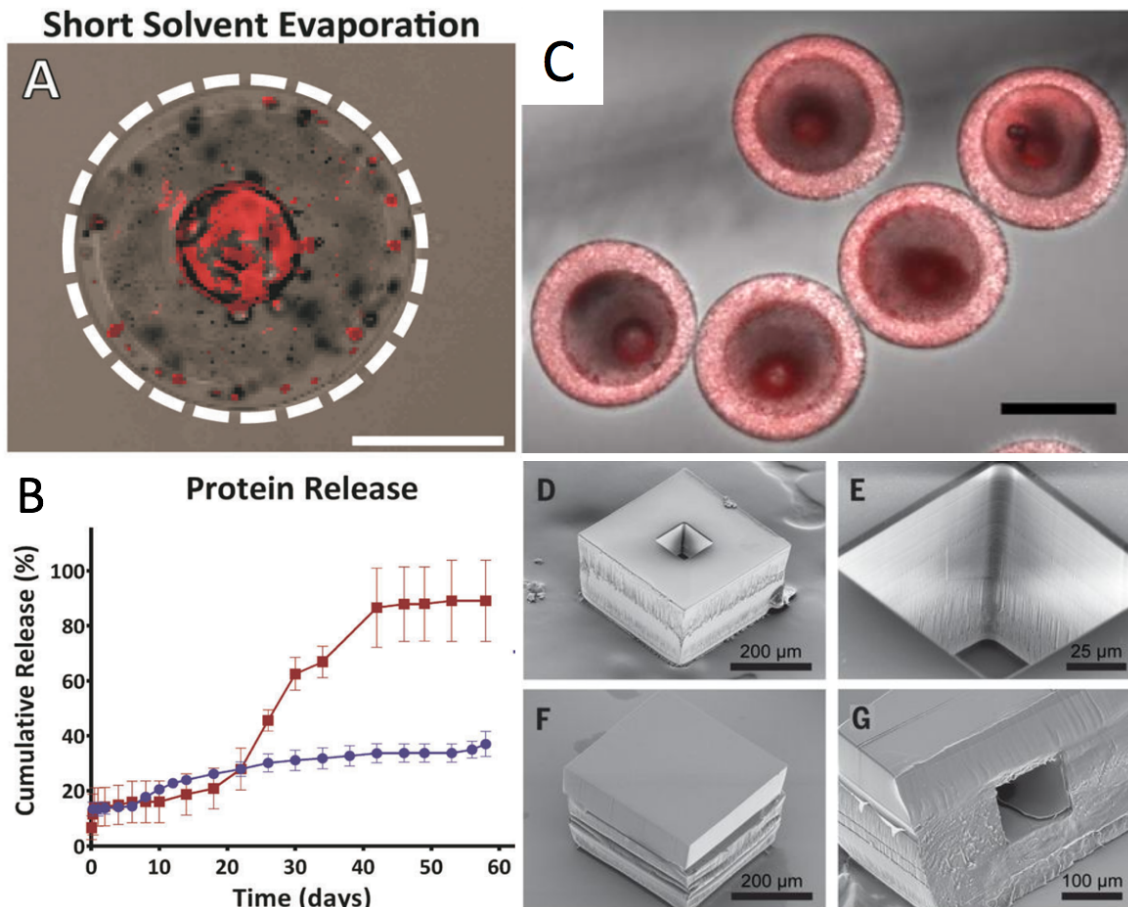
Figure 3 State-of-the-art for polymeric delivery systems (A) PLGA/PLLA microbubble confocal image of the short solvent evaporation group (B) PLGA/PLLA microbubble release profile. SEM images of (C) laser scanning confocal micrographs of PLGA/PCPH double-walled polymer microspheres (D) a single particle, (E) the core of a particle, and (F) a sealed particle. (G) A cross section of a single particle. Reprinted from [5, 8, 9].

In the study presented by Dutta, et al. using PLGA/poly(L-lactic acid) (PLLA) microparticles, protein is able to be distributed to varying degrees more towards the center (**Figure 3A**) [5] of the microparticle using combinations of long and short solvent evaporation times, as well as in the presence or absence of ethanol. Such formulations can result in a burst release profile (**Figure 3B**). Berkland, et al. produced double-walled

microparticles using PLGA and poly[(1,6-bis-carboxyphenoxy) hexane] (PCPH) (**Figure 3C**) [9]. Release profiles was controlled by controlling mass ratio of PCPH:PLG and the shell thickness. However, in both of these studies, there was an extremely high surface area where the protein was in direct contact with the organic solvent, denaturing the protein.

McHugh, et al. synthesized a PLGA-based vaccine depot on the order of a few hundred microns using a microfabrication technique involving photolithography to form a poly(dimethyl siloxane) (PDMS) mold which is then used as yet another mold for forming the micron-scale PLGA depots. A picoliter dispensing technology was used to fill the depots. A mask aligner was then used to align the caps for the micron-sized depots which had been filled with a cargo of interest (**Figure 3D-G**). Such microparticles allowed a highly controlled bolus release by varying the PLGA MOLECULAR WEIGHT and L:D monomer ratio [8], but the failure rates of capping the depots were high, which made predicting when they would burst difficult. The sealing of the depots was successful along a continuum, causing the burst release to occur anywhere from time 0 (improperly capped and easily apparent) up until when the depot was designed to be released. Screening for the depots which would release after time zero and prematurely is currently a challenge this technology faces. This technology could be incredibly impactful if the issue of predicting which particle will prematurely release is rectified.

Our proposed microbubbles will have no sealing of caps, homogenization or sonication, and a greatly minimized surface contact area of antigen directly in contact with organic solvent.
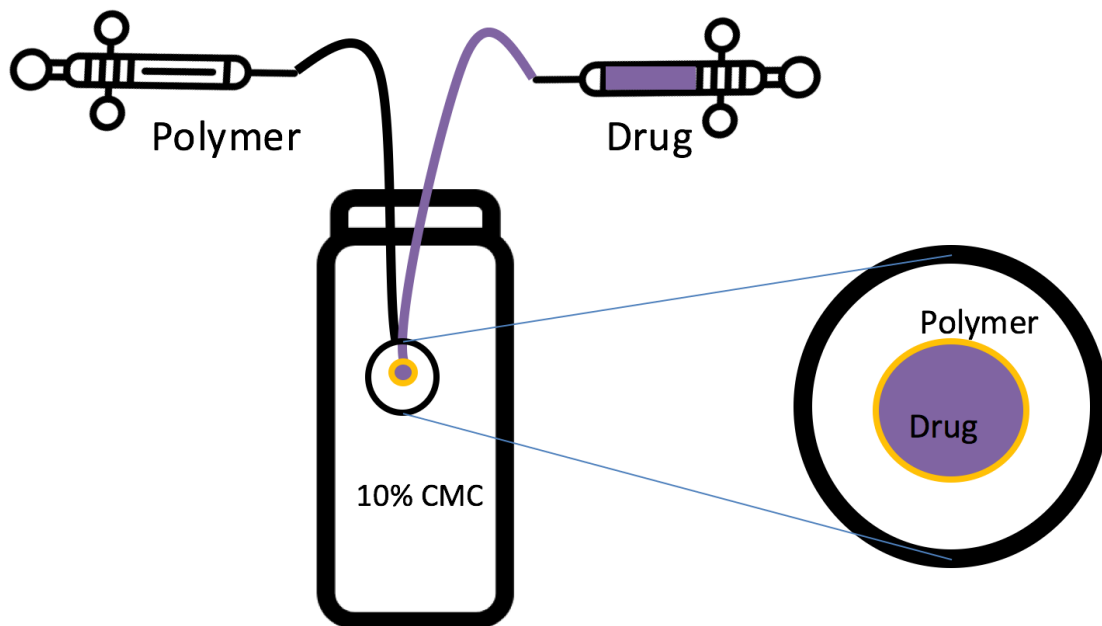
Figure 4 Concept of the microbubble fabrication system. Polymer and drug are injected using micromotors. Microbubble is supported into 10% CMC matrix, which also prevents drug leakage after injection within the microbubble.

In this work, we suggest a microbubble as a novel platform as a vaccine delivery carrier (**Figure 4**). This microbubble can reduce many downsides of emulsification and thermal treatment for sealing. First, our microbubbles can stabilize antigens because they do not need ultrasound and they do not have such large surface areas in contact with organic solvent. Our microbubbles will also lead to release kinetics that is a bolus

instead of sustained antigen release which is a common release profile when using traditional microparticles. Sustained release is known to cause T cell anergy. Causing T cell anergy may be useful for certain applications of anti-autoimmune disease formulations, however.

In addition, in this thesis, I describe the development of a phase-separating microbubble as a novel vaccine depot. Engineering the release time of the microbubble is crucial for the development of a single injection vaccine technology (Aim 1). Section 3.1 entails the synthesis of PLGA and PCL, and section 3.2 describes the development of microbubbles using a blend of poly(ε-caprolactone) (PCL) and PCL triacrylate (PCLTA). Section 3.3 shows how lyophilization improves stability of the microbubble post UV curing. Also, section 3.4 describes how the microbubble maintains its shape and can be suspended during the formation and injection processes. Section 3.5 entails how to engineer the cargo to stay centered within the microbubble. Section 3.6 quantifies how the diameter of the microbubble varies as a function of the syringe pump rate and also how pre- and post-lyophilization affects the diameter. Section 3.7 quantifies the angle of the micromotor necessary for injecting cargo within the microbubbles. Section 3.8 describes engineering a self-contained system which will enable lyophilization of the microbubbles.

Main Specific Aim 2 entails engineering the release time of the microbubbles. Section 4.1 quantifies how different molecular weights of PCL affect release times of the microbubbles. Section 4.2 quantifies how varying the microbubbles' thickness of the shell controls the release time.

Section 5 quantifies stability of HIV and Hepatitis B antigens in a non-microbubble context as a positive control for the antigen protection within the microbubble (ongoing work). Section 5 describes how the HIV gp120/41 and HBsAg ayw antigens are stable in time in an aqueous environment versus in a cryo-protectant context at varying temperatures.

Section 6 entails conclusions and future direction of this work. Finally, section 7 provides a thorough review of literature regarding amino acid- and protein-based vaccines for anti-infectious disease applications.

2   BACKGROUND*

2.1   CHALLENGES IN VACCINE COVERAGE

The World Health Organization (WHO) estimated that 19.5 M infants annually cannot receive adequate vaccination throughout the world [2]. Two of the biggest impediments which inhibit improving vaccination coverage rates is the poor medical facilities and general medical welfare found in the developing countries. Statistics show that the people-to-doctor ratio of African countries is less than 3333 to 1; whereas, more than 110 countries have at least one doctor per 1000 people. Such statistics become increasingly worse when multiple doses, long administration regimens, and cold chain distribution are required.

2.2   HEPATITIS B AND STATE OF THE ART FOR VACCINES

The hepatitis B virus (HBV) and induces a liver infection, which contributes to diseases such as cirrhosis or hepatocellular carcinoma [10]. More than 248 million people have chronic hepatitis B disease globally, and 25% of those who are infected with HBV in infancy have a higher risk of developing the primary liver cancer or cirrhosis as

adults [11]. According to the statistics of the WHO, several African countries such as Equatorial Guinea, Central African Republic, and Guinea have a low coverage rate of Hepatitis B vaccine, therefore the mortality rate of babies who is 0 year old is 2-5 times higher than that in other African countries [3].

HBsAg constitutes four serotypes: ayw, ayr, adw, and adr, which is geographically dependent. For example, most countries on the American continent have the adw serotype, and most African countries have the ayw serotype. High mortality countries in the north of the southern Africa countries, such as Angola, Vanuatu, and Chad usually involve the ayw serotype [12]. However, current commercialized HBsAg-based vaccines (e.g. Recombivax HB® and Engerix-B®) are for the immunization against the adw serotype, which is common in the Americas. We will be developing a vaccine depot system for the ayw serotype, which will dually function as a proof-of-concept for such a delivery system that would be far more convenient in the developed world as well.

Vaccine schedules for the hepatitis B vaccine (HBsAg) for babies are currently at 0, 1, and 6-month bolus injections, starting at birth [3]. However, the completion of all requisite inoculations is difficult for poor medical facilities. A study about the coverage of vaccination against hepatitis B in the rural population of China showed that people with lower incomes tend to present with higher rates of ineffective vaccination [13]. If all the vaccines in the schedule could be delivered in a single injection vaccine containing three microbubbles with different releasing time points, the vaccine coverage rate would increase significantly.

Projections for 2015-2030 indicate a reduction of 90% of new chronic hepatitis B cases and a 65% decrease in the mortality rate, once the vaccine coverage achieves 90% of infants, 80% of neonates [14].

2.3   HIV AND STATE OF THE ART FOR VACCINES

HIV can cause AIDS, and currently there is no commercially available prophylactic therapy. Globally, 36.7 M people (2015), and 1.2 M people in the United States are living with HIV, and this number is increasing annually. Fourteen percent of the infected population are unaware of their condition, which unintentionally exposes uninfected people.

In regard to subtypes, HIV-1 is more pathogenic than the HIV-2; both are capable of infecting T cells. However, only HIV-1 can escape the innate immune system recognition which is primarily accomplished by avoiding dendritic cells. HIV-1 presents a high evolution rate and wide genetic variability, which are challenges to the development of antiretroviral drugs and vaccines [15, 16].

It is crucial to choose adequately conserved antigens for subunit vaccines. Thus, viral capsid glycoprotein (gp) molecules, which are highly conserved sequences, may provide such reliability required for developing vaccines [17, 18]. There are many clinical trials employing the gp120 and gp41 as an HIV-1 vaccine but to date there has not been satisfactory seroconversion for adequate protection [15]. Furthermore, developing broadly neutralizing antibodies against HIV vaccine is a highly sought after

objective [19], in addition to developing stable antigens to enable transportation of the vaccine itself to enhance coverage [20].

2.4   SINGLE INJECTION VACCINES

Generally, live attenuated vaccines are lyophilized in order to enhance stability. The storage and transportation temperature should remain between 2 ℃ to 8 ℃, which is the same temperature range recommended to store and distribute inactivated and subunit vaccines [21, 22]. Temperature oscillation and long-term exposure to out-of-range temperatures can reduce the antigen functionality of a recombinant protein vaccine (i.e. HBsAg ayw for hepatitis B and gp120/gp41 for HIV-1). Enhanced antigen stability in ambient temperatures and single injection technology could potentially enable improved immunization coverage for more people. For developing countries, a thermostable vaccine would be able to bypass cold chain shipment issues. For developed countries, thermostable single injection vaccines will bring a convenient will bring a convenient alternative to avoid several visits to healthcare centers.

Current studies involving single injection vaccines struggle to control antigen stability over the duration required for boosting. Nano/microparticles based on biocompatible and biodegradable polymers have been widely investigated for bolus, pulsatile, and sustained release applications using a number of different polymers (e.g. PLGA, PCL) [20].

13

There are several studies focused on enhancing the thermal and long-term antigen encapsulated stability (i.e. up to 12 months within carriers for specific antigens which are considered relatively easier to stabilize) [23]. This has been mainly accomplished by various freeze-drying procedures in conjunction with the use of cryo- or lyoprotectants that improve vaccine shelf-life and stability during transportation in the presence or in the absence of complete cold chain distribution capabilities.

However, these studies did not focus on preserving the antigenicity after administration for long-term self-boosting delivery [24, 25]. It is necessary to (1) ensure the pH is not damagingly low for the antigen; (2) optimize the antigen/cryo-protectant ratio to preserve precious antigen cargo space within the depot; (3) optimize the lyophilization to properly remove water to the extent necessary; and, lastly, (4) ensure the particles auto-boost at the expected times.

2.5   UTILITY OF PLGA FOR DRUG DELIVERY SYSTEMS

Poly(lactic-co-glycolic acid) (PLGA) is a biodegradable and relatively biocompatible copolymer which has been approved for clinical use for specific applications by the US Food and Drug Administration (FDA) and the European Medicines Agency. Successful encapsulation in PLGA nanoparticle/microparticle (NP/MP) depot as injectable delivery systems was reported for anticancer drugs [26], peptides/proteins [27], DNA [28], and RNA [29]. The hydrolytic degradation of the PLGA backbone produces lactic and glycolic acids (**Figure 5**), and which can be

biologically incorporated within the body, causing minimal damage [30]. Loss of

conformation or denaturation of peptides/proteins encapsulated in PLGA due to the

acidic degradation of PLGA may be controlled by using internal buffers and neutralizing

reagents [25], or blending PLGA with pH-sensitive polymers [31].

PLGA: Poly(D,L-lactide-co-glycolide)

Breakdown by hydrolysis

Lactic acid   Glycolic acid
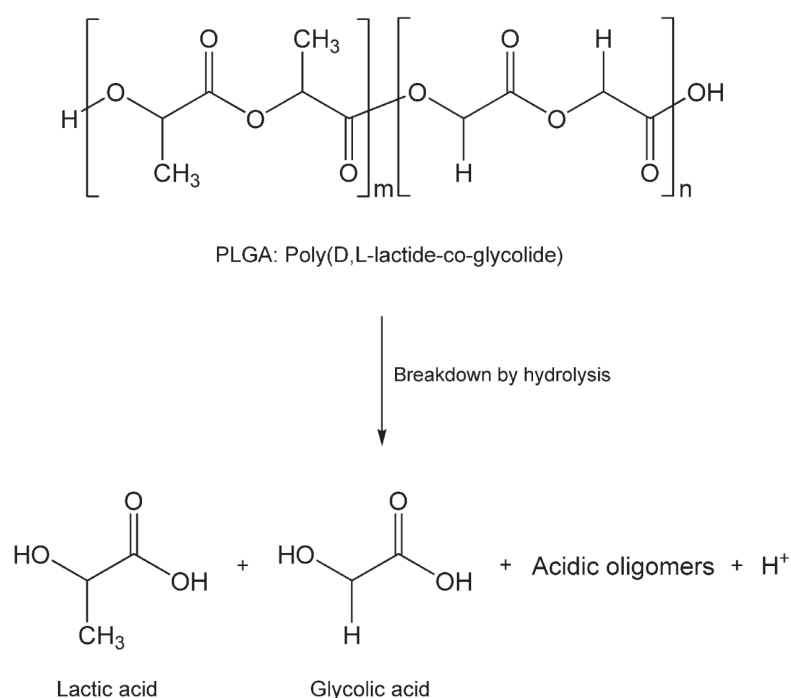
Figure 5 De-esterification of PLGA backbone in an aqueous environment producing lactic acid, glycolic acid, acidic oligomers, and free protons which self-catalyze the degradation further and can cause issues with pH regulation for antigen stability. Adapted from [32]

Currently, there is an extensive variety of PLGA-based biomedical technologies,

such as orthopedic implants [33], bone regenerative scaffolds [34], surgical devices [35],

and drug delivery systems [36]. This versatility is due to PLGA's highly tunable

chemical properties. The hydrophilicity and hydrophobicity of PLGA can be controlled by increasing the glycolide and lactide monomer ratios, respectively, or by combining with other monomers in a conjugated fashion. For instance, mPEG (methoxypolyethylene glycol) can be added to PLGA in a diblock copolymer manner to control the hydrophilic/hydrophobic balance [37]. However, inflammatory responses have been reported as a side effect of PLGA implants due to the long-term acidic degradation [45] and should be carefully assessed during the development of such polymer-based applications to ensure all safety requirements are appropriately satisfied.

In 2016, there were 15 FDA-approved drugs for the US market using PLGA as a delivery platform [38]. In the past ten years, several intrinsic drawbacks of PLGA have been studied [39]. The PLGA cell-recognition capacity and susceptibility to opsonization can be potentially mitigated by surface modification of PLGA NPs/MPs [40-42]. Also, surface modifications may be used to modify the kinetics of cellular uptake by endocytic pathways [6].

Thermostabilization of PLGA-encapsulated drugs for storage and transportation purposes can be achieved by a freeze-drying technique and the use of lyo-/cryo-protectants such as trehalose [43].

2.6 UTILITY OF PCL FOR DRUG DELIVERY SYSTEMS

Poly(ε-caprolactone) (PCL) is a biodegradable and biocompatible polymer used in several FDA-approved biomedical devices. The PCL structure is hydrophobic in nature and contains semi-crystalline domains, and has relatively low glass transition temperature (-60 ºC for a MW 65K) [44]. The PCL`s long degradation rate (up to a year) [45] has been used for bone regeneration applications [46], three-dimensional (3D) tissue scaffolds [44], 3D-printed resorbable membranes for bone regeneration and bone integration [47], and drug delivery systems intended for long durations[48].

PCL is commonly conjugated with another polymer to produce multi-block copolymers in order to obtain specific properties. For instance, PCL/PLGA conjugates are studied in different compositions. Block copolymers of PCL and PLGA (i.e. tri-block PLGA-PCL-PLGA) phase separate and results in a flexible material at room temperature because the temperature is above PCL's T_g. Because room temperature is generally below PLGA's T_g, PLGA is more glass-like state and the resulting tri-block PLGA-PCL-PLGA is similar to a rubbery material where there are domains which are able to move translationally while other domains do not. Chou, et al. employed PCL/PLGA (20:80) to produce fibers for drug delivery. Such composition allowed differential drug partitioning between the PCL and PLGA phases and the PLGA promoted faster drug release [49].

3 SYNTHESIZE POLYMERS FOR MICROBUBBLE FORMATION AND ENGINEER METHODS FOR STABILIZING MICROBUBBLES*

3.1 SYNTHESIZE PCL AND PLGA LIBRARY AT DIFFERENT MOLECULAR WEIGHTS AND CHARACTERIZING THE POLYMERS

3.1.1 Introduction

Certain vaccines require multi-dose regimens to enable complete seroconversion. According to the Advisory Committee on Immunization Practices, hepatitis B requires an immunization schedule of 0, 1, 6-month [50]. A multiple-dose vaccine regimen can be administered in a single vaccine administration, and there is no need for a second or third visit to a medical facility to receive those doses. From a kinetic engineering point of view, it is necessary to control the (i) long-term release (i.e. months) and ensure a (ii) bolus release to prevent T cell anergy.

We hypothesized that different molecular weights of polymers would have different release kinetics because longer chains of higher molecular weight polymer can entrap cargo longer due to a greater extent of hydrolysis required. In order to assess how

_____

*Adapted with permission from: Kweon, et al. *Biomaterials*. **2003**, 24, 801-8, Copyright © 2017 Elsevier;

18

molecular weight controlled the releases kinetics of PLGA and PCL, a low, medium, and high molecular weight of each were synthesized initially. Because of PCL's is more hydrophobic in comparison to PLGA due to the 5 carbons between each of the ester groups, we hypothesized that PCL would take more time to release than PLGA because erosion by aqueous environments is faster in PLGA. The dynamic viscosity, glass transition temperature (T_g), and NMR of synthesized polymers were characterized.

3.1.2   Materials and Methods

3.1.2.1 Materials

1-dodecanol (Acros organics) was used for the terminating end group for PLGA. Tin(II) 2-ethylhexanoate (96% SO) (Alfa Aesar) was used as a catalyst. Chloroform (Fisher Chemical) was used for the solvent, and anhydrous ethyl ether (Fisher Chemical) was used for purification purposes. ε-caprolactone (Alfa Aesar) was the main monomer used for PCL synthesis. 1,4-Dioxane-2,5-dione (Alfa Aesar) and DL-Lactide were the main monomers for PLGA synthesis.

3.1.2.2 PCL synthesis

An Oil bath was heated at 110 ºC. 1-Dodecanol was then aliquoted into a glass vial at varying masses to control the targeted molecular weight. For higher molecular

weight PCL, 0.037 g (0.045 mL) of 1-dodecanol was added to the round bottom flask.

9.276 mL of ε-caprolactone was added to the flask. The ε-caprolactone mass was the

same in every synthesis with varying molecular weights, but the 1-dodecanol mass was

increased to reduce the molecular weights of PCL The molecular weight of the PCL was

controlled by the ratio between 1-dodecanol and the repeating unit.
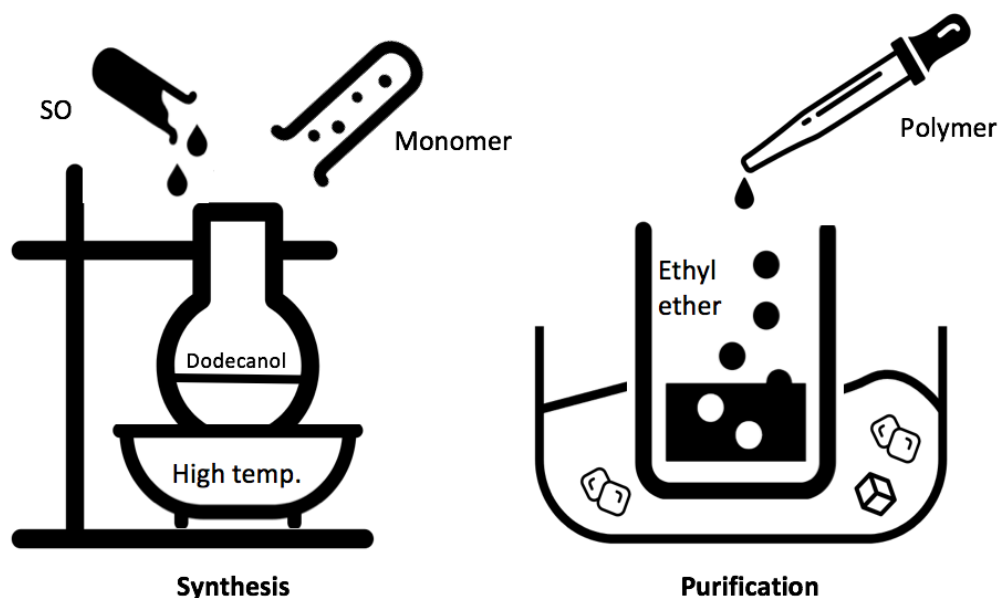
Polymer	PCL	PLGA
Temperature	110 ℃	140 ℃
Monomer	ε-caprolactone	1,4-Dioxane-2,5-dione and DL-Lactide
Endcap	1-dodecanol	
Catalyst	Tin(II) 2-ethylhexanoate (96% SO)	

Figure 6 PLGA and PCL synthesis.

The synthesis was carried out in a neat fashion and the reaction proceeded under an argon atmosphere. 40 µL of stock SO was added to the flask. Due to the increasing viscosity as the synthesis continued, the stir bar would become gradually slower and would stop. The round bottom flask was subsequently covered with foil and placed in the vacuum chamber overnight.

For the first purification, a water bath was heated at 50 ºC in order to help solve the polymer into chloroform. Subsequently, a 250 mL beaker was filled with ethyl ether (three-fold the polymer solution that would eventually be added to the ether for crashing out the polymer. The ethyl ether-filled beaker was placed in a bucket, which was filled with ice and water to aid the precipitation of the polymer into the ether for purification purposes. Polymer solution was added to the ethyl ether dropwise. After the precipitated polymer fell to the bottom, the ethyl ether was decanted. The remaining ethyl ether was evaporated in the vacuum chamber, the and polymer underwent a second purification in a similar manner (**Figure 6**).

3.1.2.3 PLGA synthesis

L and G were allowed to warm to room temperature before opening the vial to avoid forming condensation on the monomer in the main container which helped not introducing water from the ambient atmosphere into the container. The mineral oil bath was heated to 140 ºC and contained a stir bar to help maintain an even distribution of

temperature throughout. 44.8 μL of 1-dodecanol was added to flask used for polymer synthesis. 5.5412 g of the L monomer and 4.4609 g of the G monomer was measured; this was a 50:50 monomeric L:G ratio. The weighed L and G monomers were then added to the flask which was placed in the secondary container with the mineral oil. The monomers melted together and were thoroughly mixed with another magnetic stir bar within the synthesis flask. The stirring was accomplished under an argon atmosphere.

Like PCL, PLGA molecular weights were also controlled by the mass ratio of 1-dodecanol and the mass of L and G present. As soon as the monomer was completely melted, 40 μL of stock SO was added to the flask. The stir bar was increasingly slowed down as the reaction proceeded due to the increasing viscosity of the polymer. The purification step was same as what was previously described above for purifying PCL. After the purification step, to remove the residual ether, the polymer was left in the vacuum chamber overnight.

3.1.2.4 Polymer Characterization

Each polymer was characterized via differential scanning calorimetry (DSC), rheometery, and nuclear magnetic resonance (NMR) spectroscopy. The dynamic viscosity was analyzed by DSC Q20 (TA Instruments), and the melting point of PCL and the glass transition of PLGA were measured using Physica MCR 301(Anton Paar). Mercury 300 was used for recording ^{1}H NMR spectra.

3.1.3 Results and discussion

Each polymer was prepared in three different molecular weights, using monomeric ratios that would theoretically target 10 kDa to 100 kDa; which we term Low, Med, and High MW PLGA or PCL.
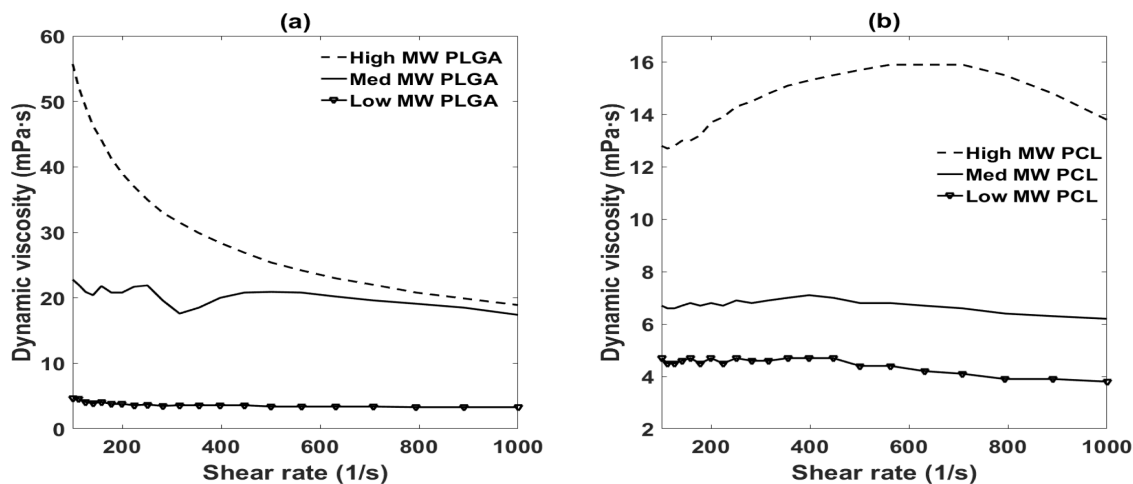
Figure 7 Average dynamic viscosity of (a) PLGA and (b) PCL using a shear rate which varied from 100 to 1000 (1/s).

The dynamic viscosity of each polymer using a polymer concentration of 100 mg/mL in chloroform was measured using a rheometer at a shear rate ranging from 100 to 1000 1/s. For both PCL and PLGA, their dynamic viscosity increased as their MOLECULAR WEIGHTS increased. More specifically, the average dynamic viscosity of High, Med, and Low MW PCL were 13.56 mPa·s, 6.52 mPa·s, and 4.69 mPa·s when

using a shear rate that range from 100 to 1000 1/s. (**Figure 7b**). Similar behavior was observed for PLGA. The average dynamic viscosity of the High, Med, and Low MW PLGAs were 33.51 mPa·s, 20.29 mPa·s, and 3.70 mPa·s (**Figure 7a**). Thus, PCL had a narrower dynamic viscosity range when compared to PLGA.
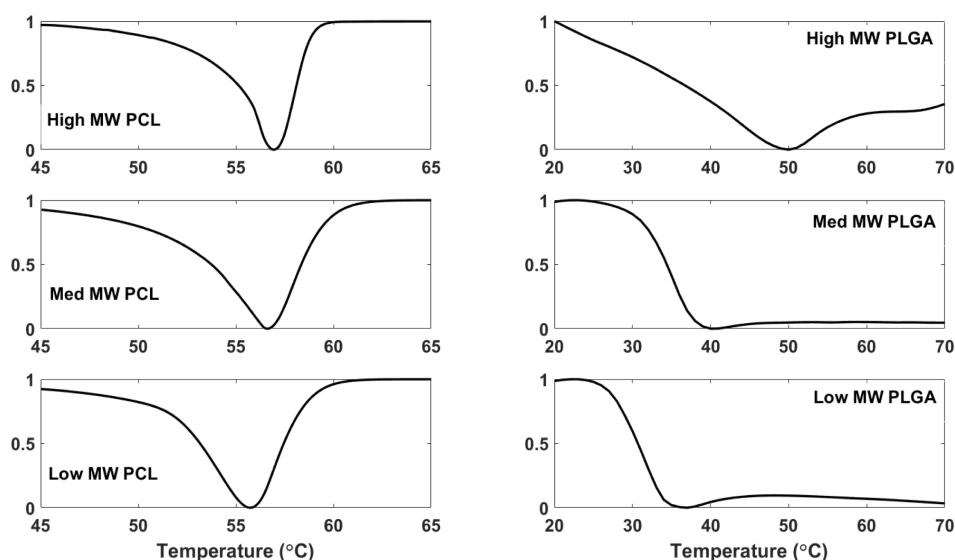
Figure 8 DSC curves of PCL from 45 to 65 ºC and PLGA from 20 to 70 ºC.

Another key parameter quantified was the glass transition temperature and melting temperature (T_g and T_m), which was measured by DSC. The T_g for PLGA and T_m of PCL are presented as DSC curves in **Figure 8**. The T_m of PCL was identified between 50-55 ºC and the T_g of PLGA was detected between 35-50 ºC. It is preferable that the body temperature is not higher in comparison to the T_g for PLGA or T_m for PCL, as it otherwise could potentially cause excessive polymer relaxation and likely not allow for long term antigen delivery.

24
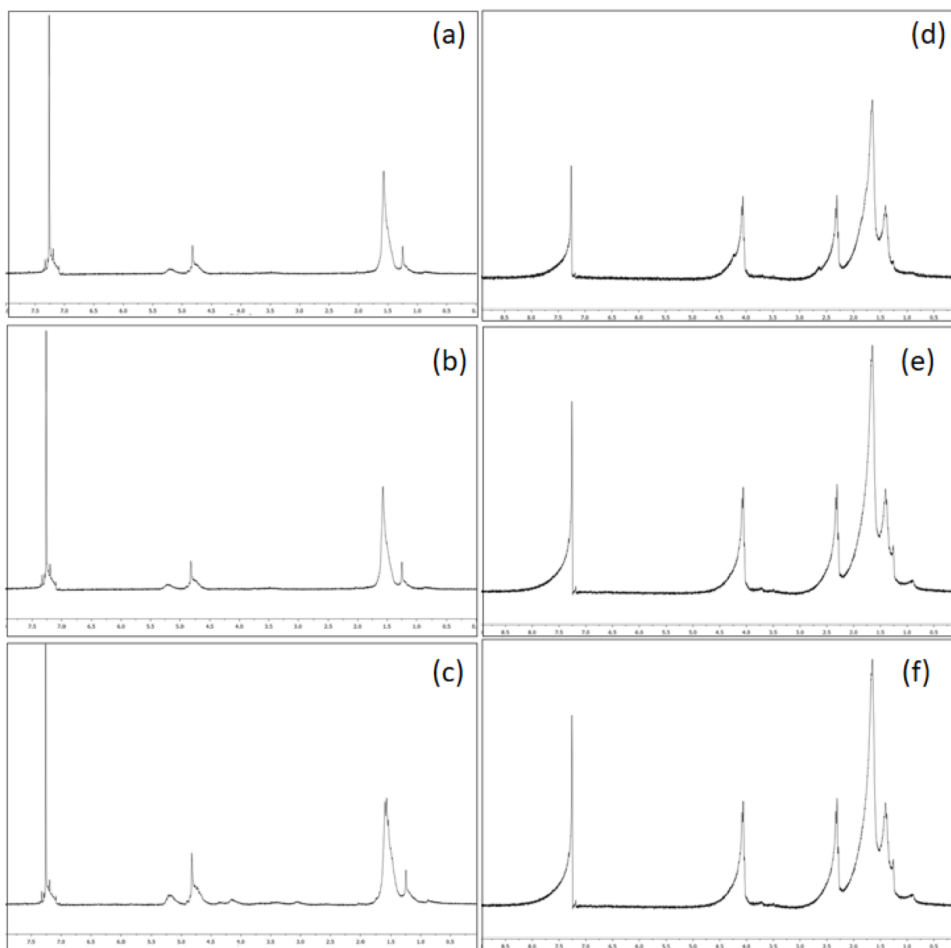
Figure 9 NMR spectra for (a) High MW PLGA, (b) Med MW PLGA, and (c) Low MW PLGA (d) High MW PCL (e) Med MW PCL (f) Low MW PCL.

PLGA (CDCL3: 7.26ppm)

0.88 ppm: **CH3**(CH2)10(CH2)O-O-[(CO)CH(CH3)]x-[O(CO)(CH2)O]y-H

1.25 ppm: CH3**(CH2)10**(CH2)O-O-[(CO)CH(CH3)]x-[O(CO)(CH2)O]y-H

1.55-1.0 ppm: CH3(CH2)10(CH2)O-O-[(CO)CH(**CH3**)]x-[O(CO)(CH2)O]y-H

2.03ppm: CH3(CH2)10(CH2)O-O-[(CO)CH(CH3)]x-[O(CO)(CH2)O]y-**H**

4.16ppm: CH3(CH2)10(**CH2**)O-O-[(CO)CH(CH3)]x-[O(CO)(CH2)O]y-H

4.73-4.83ppm: CH3(CH2)10(CH2)O-O-[(CO)CH(CH3)]x-[O(CO)(**CH2**)O]y-H

5.20ppm: CH3(CH2)10(CH2)O-O-[(CO)**CH**(CH3)]x-[O(CO)(CH2)O]y-H

PCL (CDCL3: 7.26ppm)

0.9ppm: **H[(CH2)**(CH2)(CH2)(CH2)(CH2)(CO)O]n-O(CH2)(CH2)10**CH3**

1.25-1.35ppm: H[(CH2)(CH2)(CH2)(CH2)(CH2)(CO)O]n-O(CH2)(CH2)**(CH2)9**CH3

1.38-1.42ppm: H[(CH2)**(CH2)(CH2)**(CH2)(CH2)(CO)O]n-O(CH2)(CH2)(CH2)9CH3

1.62-1.71ppm: H[(CH2)(CH2)(CH2)**(CH2)**(CH2)(CO)O]n-O(CH2)(CH2)(CH2)9CH3

2.28-2.60ppm: H[(CH2)(CH2)(CH2)(CH2)**(CH2)**(CO)O]n-O(CH2)(CH2) (CH2)9CH3

4.04-4.09ppm: H[(CH2)(CH2)(CH2)(CH2)(CH2)(CO)O]n-O**(CH2)**(CH2) (CH2)9CH3

The ^{1}H NMR spectra were used to confirm the identity of the synthesized polymers and were also used to estimate the molecular weights based on the chemical shifts and integration ratios for PCL and PLGA as described by Izunobi, et al. [51] (**Figure 9**). Estimation of MWs were 1700Da for high MW PCL, 900Da for med MW PCL and 600Da for low MW PCL.

3.1.4 Conclusion

To vary release time of cargo from the polymer, it is likely possible by having different molecular weights (or L:G ratios or varying thicknesses of the microbubble shell). Therefore, three different molecular weights of both PLGA and PCL was synthesized and characterized. Firstly, ^{1}H NMR spectra confirmed the successful synthesis of PCL and PLGA and MWs were estimated as 1.7 kDa for High MW PCL, 0.9 kDa for Med MW PCL and 0.6 kDa for Low MW PCL by NMR peak calculation.

DSC analysis revealed a T_m value ranging between 45-65 ℃ of for PCL and a T_g ranging from 20-70 ℃ for PLGA. PCL showed a lower and narrower dynamic viscosity range (4-16 mPa.s) than PLGA (4-60 mPa.s) when shear stress rates were varied from 100 to 1000 1/s.

3.2 SYNTHESIZE ACRYLATE POLYMER FOR MICROBUBBLE

3.2.1 Introduction

The initial attempts to synthesize the PCL microbubble indicated there were structural defects. Regardless of the concentration of PCL microbubbles, pores with 20-38 μm diameter were observed from the surface of the PCL microbubbles (**Figure 10**). Such defects were possibly caused by the diffusion of the dissolved chloroform from the

PCL microbubble before and possibly during the initial stages of lyophilization. The cargo could escape from the microbubble before the expected release date through these defects. Thus, using non-cured PCL microbubbles were considered an insufficient polymer for forming microbubbles Because of the structural issue of the PCL microbubbles, three-dimensional PCL acrylate networks were explored as an alternative. The PCL acrylate was also synthesized in-house. Synthesized PCLTA was mixed with purchased Mn 14 kDa PCL, since the microbubble, which was fabricated using synthesized high MW PCL (around 900 Da MW), was not rigid enough after lyophilization.
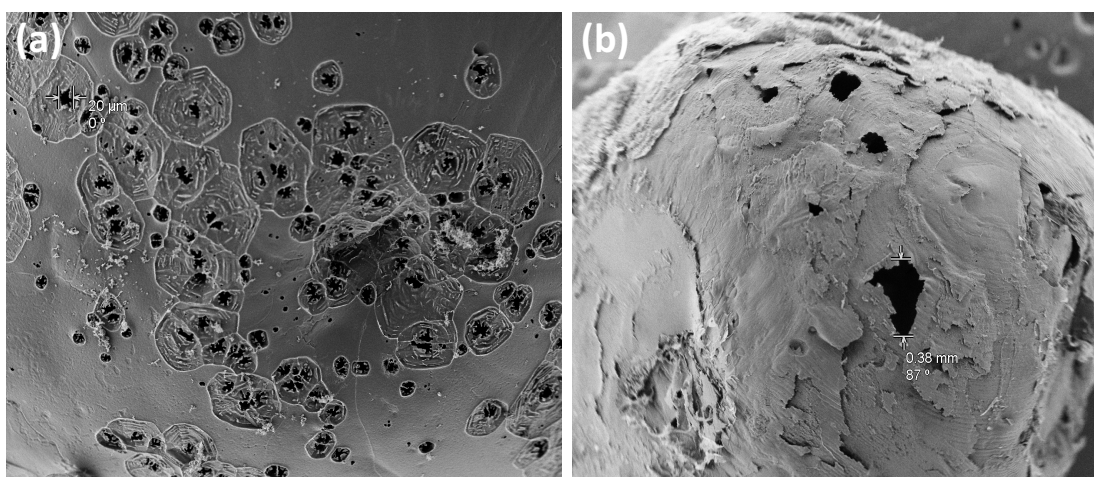
Figure 10 Scanning electron microscopy (SEM) imaging depicts pores and defects on the surface of PCL.

PCL acrylate was synthesized from PCL triol which was acrolyated into a PCL triacrylate (PCLTA). Cai, et al. described a synthetic pathway that employs potassium carbonate (K_2CO_3) as a proton scavenger instead of trimethylamine (TEA) [52]. TEA

complexes with acryloyl chloride and can produce a colorized compound that can affect the photo-crosslinking and cytotoxicity [52]. The relevant features of the PCL acrylate synthesis are (i) room temperature synthesis, (ii) adjustable and fast UV curing, and the (iii) TEA-related cytotoxicity could be eliminated.

This section describes the synthesis of PCLTA as an alternative of PCL microbubbles. To choose the adequate synthesis, two PCLTA syntheses were performed. One used TEA and another used K_2CO_3. In order to optimize the ratio between PCL and PCLTA, varying ratios were made and cured under UV. We also wanted to determine the minimum UV curing time to prevent unnecessary exposure of the cargo which could be potentially damaged by the UV.

3.2.2 Materials and Methods

3.2.2.1 Materials

Poly(ε-caprolactone) triacrylate (PCLTA) was synthesized using acryloyl chloride (Alfa Aesar), K_2CO_3 (ACROS Organics), poly(caprolactone)triol (PCL triol, average MW 300 Da) (ACROS Organics). Dichloromethane (DCM) (ACROS Organics) is used for the solvent.

Synthesized PCLTA and other reagents included poly(ε-caprolactone) (PCL, average Mn 14 kDa (we purchased this PCL because our previously synthesized PCL was insufficient, even after many batches for forming microbubbles and keeping the

29

cargo within)) (Sigma Aldrich), chloroform (Fisher Chemical), ethyl ether (Fisher Chemical) and 2-Hydroxy-2-methylpropiophenone relatively more hydrophobic photo initiator, in comparison to traditional irgacure) (TCI AMERICA) were used for curing the polymer.

3.2.2.2   PCLTA synthesis

PCLTA was synthesized with two different methods based on papers. The main difference between two methods is the proton scavenger. One of them used TEA and the other one used K_2CO_3. The method using TEA started by loading 2 mM (561 µL) of PCL triol to the round bottom flask (**Figure 11**). 40 µL of toluene was added to dissolve PCL triol. The solution was stirred in the 80 ºC oil bath. 4.5 mM (630 µL) of TEA and 4.5 mM (370 µL) of acryloyl chloride were added dropwise. After 3 hours of reaction, the mixture was filtered and purified using hexane in the ice bath. The product was dried in the reduced vacuum at 40 ºC for 24 hours, and analyzed by NMR.
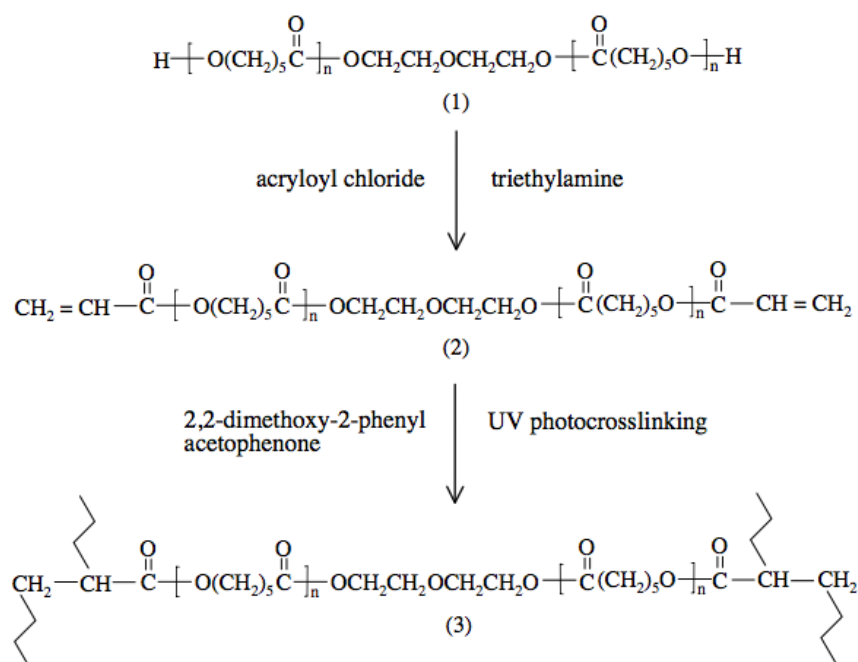
Figure 11 Synthesis of PCLTA using TEA [53]. © 2003 Elsevier

The second method used K_2CO_3. K_2CO_3, PCL triol, and acryloyl chloride were measured in a 3:1:3 molar ratio. 4.1463 g of $K_2CO_3$was dried in a 97.5 °C oven overnight. 3.2 mL of PCL triol stock was placed in a round bottom flask and also dried under reduced pressure at 50 °C using a secondary mineral oil container overnight. 2-fold volume excess of DCM was added to the PCL triol and continuously stirred at room temperature. K_2CO_3 was then added to the PCL triol. 2.72 mL of acryloyl chloride which was mixed with 10-fold volume excess of DCM was added to the mixture of K_2CO_3 and PCL triol, in a dropwise fashion. The reaction was allowed to continue for 24 hrs and the mixture was then vacuum-filtered. For purification, the filtered mixture was added drop-by-drop in 3-fold volume excess of diethyl ether which was in a secondary container functioning as an ice bath. After overnight in a vacuum chamber, the purified PCLTA

was collected. NMR was used for confirming the acrylate peaks in the final PCLTA product. The same method was used to synthesize PCLDA. The synthesis of PCLDA and PCLTAs is described in **Figure 12**.
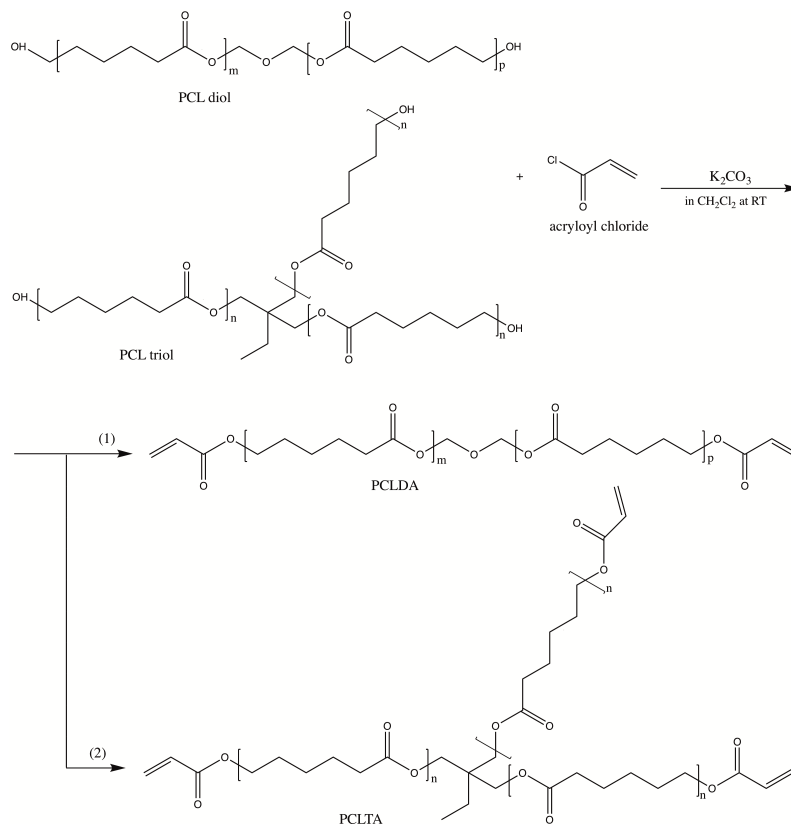
Figure 12 Synthesis of PCL acrylates (PCL diacrylate from PCL diol and PCL triacrylate from PCL triol) using K_2CO_3 in DCM at room temperature.

3.2.2.3   Curing PCL/PCLTA

PCL (Mn 14 kDa) was dissolved in chloroform at a concentration of 600 mg/mL. This PCL solution was mixed with the previously synthesized PCLTA in various volume

ratios (PCL:PCLTA=1:0, 1:1, 1:3, 3:1, and 0:1). The photoinitiator was dissolved in

chloroform at a 5 mg/mL concentration (or 0.5%, assuming the density of water). The

photoinitiator solution was then added in 1:1 volume ratios with various mixtures of

PCL/PCLTA. 150 µL of the 1:1 mixture was then added in the caps of 0.5 mL tubes.

Each of the caps filled with acrylate-terminated and non-acrylate-terminated polymers at

various ratios were cured under the UV lamp for 20 minutes using an inert atmosphere

of argon.

To determine the minimum curing time required for curing PCL (14 kDa 800

mg/mL):PCLTA:photoinitiator (5 mg/mL) was mixed at a 1:2:1 volume ratio. 150 µL of

the PCL/PCLTA and photoinitiator mixtures were added within the 0.5 mL tubes, and

each of the solutions were cured for under the UV lamp for 5, 10, 15 and 20 minutes.

3.2.3 Results and discussion

3.2.3.1 PCLTA synthesis

The NMR results from PCLTA using TEA and PCLDA using K_2CO_3 did not detect

acrylate peaks. However, PCLTA using K_2CO_3 did detect acrylate peaks between 6.40

and 5.75 ppm (**Figure 13**).
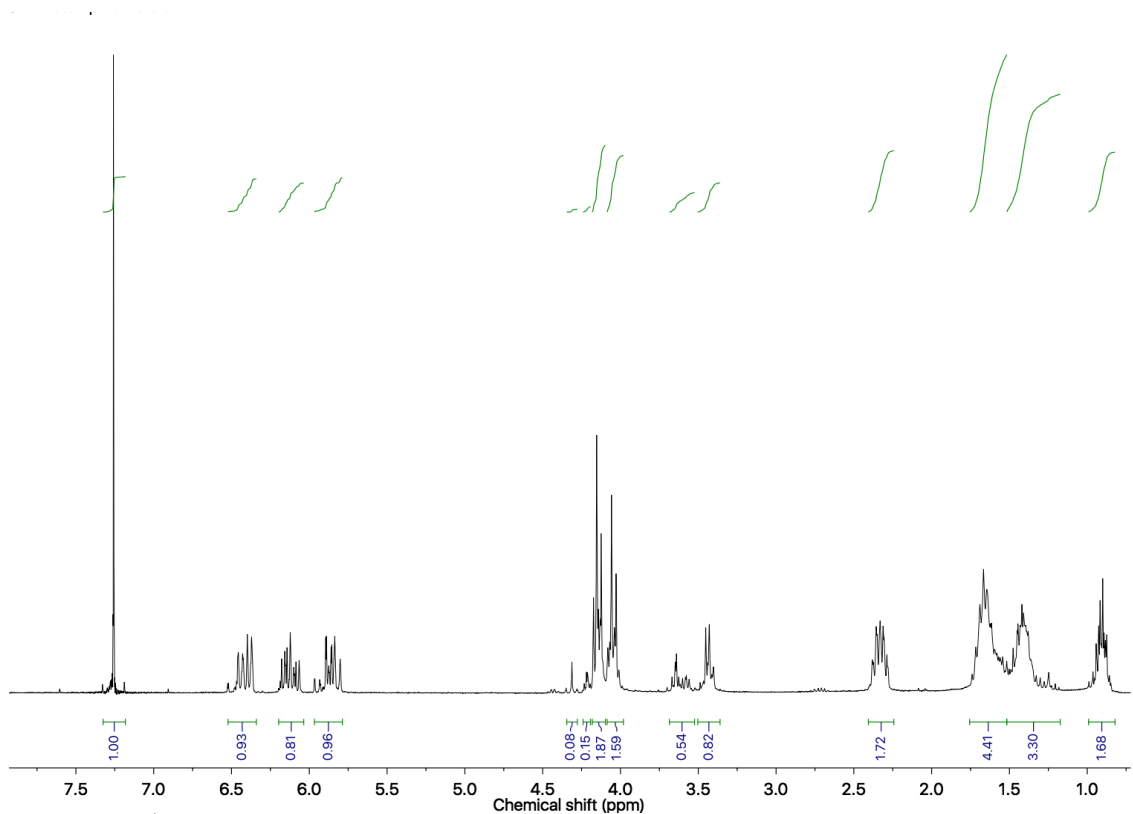
Figure 13 ¹H NMR spectra for PCLTA.

PCLTA(CDCL3: 7.26ppm)

5.73, 5.97ppm: [(**CH2**)(CH)(CO)O]3[(CH2)(CH2)(CH2)(CH2)(CH2)(CO)O]n(CH2)3-C(CH2)(CH3)

6.11ppm: [(CH2)(**CH**)(CO)O]3[(CH2)(CH2)(CH2)(CH2)(CH2)(CO)O]n(CH2)3-C(CH2)(CH3)

4.16ppm: [(CH2)(CH)(CO)O]3[(**CH2**)(CH2)(CH2)(CH2)(CH2)(CO)O]n(CH2)3-C(CH2)(CH3)

1.66ppm: [(CH2)(CH)(CO)O]3[(CH2)(**CH2**)(CH2)(CH2)(CH2)(CO)O]n(CH2)3-C(CH2)(CH3)

1.41ppm: [(CH2)(CH)(CO)O]3[(CH2)(CH2)(**CH2**)(CH2)(CH2)(CO)O]n(CH2)3-C(CH2)(CH3)

1.61ppm: [(CH2)(CH)(CO)O]3[(CH2)(CH2)(CH2)(**CH2**)(CH2)(CO)O]n(CH2)3-C(CH2)(CH3)

2.31ppm: [(CH2)(CH)(CO)O]3[(CH2)(CH2)(CH2)(CH2)(**CH2**)(CO)O]n(CH2)3-C(CH2)(CH3)

4.08ppm: [(CH2)(CH)(CO)O]3[(CH2)(CH2)(CH2)(CH2)(CH2)(CO)O]n**(CH2)3**-C(CH2)(CH3)

1.69ppm: [(CH2)(CH)(CO)O]3[(CH2)(CH2)(CH2)(CH2)(CH2)(CO)O]n(CH2)3-C(**CH2**)(CH3)

0.82ppm: [(CH2)(CH)(CO)O]3[(CH2)(CH2)(CH2)(CH2)(CH2)(CO)O]n(CH2)3-C(CH2)(**CH3**)

3.2.3.2   Curing PCL/PCLTA

The following assessment within section 3.2.2.2 regarding the curing of PCL/PCLTA was qualitative in nature. The polymer mixture, which contained a higher PCLTA ratio, had greater rigidity after curing. Therefore, sample 5 (PCL:PCLTA= 0:1; control) was the most rigid polymer, which could not be punctured using pipette tips. Sample 1 (PCL:PCLTA=1:0) was not cured at all. The color of sample 2, 3, and 4 was cloudy but only PCL and only PCLTA polymer were clear after curing (**Figure 14**). We opted to go with the PCL:PCLTA 1:3 because we need to be able to add polymer of a

35

higher molecular weight than PCLTA which was only made from PCL-triol that was 300 Da.

To cure the all of the polymer, as indicated by the visual presence of uncured polymer, within the cap, it required at least 10 minutes. After curing for 5 minutes, only the surface of the polymer was cured and it was easily manually broken. At 10 minutes, all of the polymer was cured and it was difficult to break using pipette tips. At 15 minutes, the polymer was breakable using needles but not with pipette tips. Therefore, 10 minutes was applied for curing every microbubble.

Figure 14 PCLTA polymer with different ratios after UV curing (1) PCL:PCLTA=1:0 (2)PCL:PCLTA= 1:1 (3)PCL:PCLTA= 1:3 (4) PCL:PCLTA= 3:1(5) PCL:PCLTA= 0:1.

3.2.4 Conclusion

PCL microbubbles showed defects on the surface using the 14 kDa PCL polymer which was purchased during the lyophilization process of the formed microbubbles, regardless of the concentration used. Therefore, PCL alone in an uncured stated was considered to not form microbubbles well, leading us to endeavor curing the microbubble.

This limitation was mitigated by synthesizing the PCLTA polymer via K_2CO_3, acryloyl chloride, and PCL triol. The PCLTA was analyzed by NMR and the result indicated acrylate peaks which was also functionally demonstrated with the UV curing process itself. The crosslinking between PCLTA monomers occurred under UV light and this network was likely sufficiently rigid to form UV-curable microbubbles.
The PCLTA and PCL solution was mixed with different ratios. Higher PCLTA content resulted in more rigid polymers. Optimized ratios of PCL:PCLTA was 1:3, and the minimum curing time was 10 minutes.

3.3 ENGINEER STABLE MICROBUBBLES THROUGH UV CURE AND LYOPHILIZATION

3.3.1 Introduction

PCL is considered to be a relatively biocompatible polymer for specific applications. Generally, PCL degrades slower than most ester-based polymers used for drug delivery systems (i.e., vs PLGA). Due to its hydrophobic properties, PCL has been known to facilitate transportation across cellular membranes. PCL also has tunable properties which can be modified by altering the chemical structure in its backbone [54].

The microbubble topography was assessed by scanning electron microscopy (SEM). In this technique, a topographical image is obtained by the electron beam that scans the surface of the sample. When conducting SEM, the surface of the sample should be conductive or should present a conductive coating (e.g. gold). Also, conventional SEM operates in a vacuum and the sample must be previously dried. Thus, SEM has limitations when imaging biological samples (for example, plasma membrane interactions, cells, tissues), which can lose the native structure or surface properties) [55]. At the scale and resolution, we need to image the microbubble, however, SEM is of high utility.

In this work, PCL microbubbles were formed in DI water using various concentrations. Images of the surface of PCL microbubbles were taken by SEM after lyophilization, and the structural limitations were subsequently discussed.

PCL/PCLTA microbubbles were also formed in water. Through SEM images after UV curing and lyophilization, it was identified that UV curing of the PCL/PCLTA microbubble resolved the structural problems of the PCL microbubbles which were shown in **Figure 10**. The optimization of PCLTA cross-linking by UV curing enabled us to seal the cargo inside the PCLTA microbubble, which would then enable us to modulate the kinetics of the cargo release using the shell of the microbubble. The freeze-drying processes are expected to aid the removal of water which would otherwise affect the stability of the cargo within. Of note, initially we synthesized PCL which was excessively low in MW, which made it difficult to form microbubbles from so we began using commercially purchased 14 kDa PCL. Below we will be discussing the use of 14 kDa and 80 kDa PCL to enable us to compare MW differences. Unfortunately, in the end we were not able to mix PCLTA with 80 kDa PCL which is required to cure the polymer because they phase separated, thus we ended up not being able to continue using 80 kDa PCL for formation of the microbubbles. To compare differing molecular weights of polymer we ended up using 14 kDa PCL and 45 kDa PCL.

3.3.2   Materials and Methods

3.3.2.1 Materials

Chloroform (Fisher Chemical) and poly(ε-caprolactone) (PCL, average Mn 80 kDa) (Sigma Aldrich) was purchased to form PCL microbubbles. Synthesized PCLTA,

Poly(caprolactone) (PCL, average Mn 14 kDa) (Sigma Aldrich), and 2-Hydroxy-2-methylpropiophenone (photoinitiator) (TCI AMERICA) were used for PCL/PCLTA microbubbles. Legato 100 Syringe Pump (KD Scientific) was used for the microbubble injection. 1 dram of borosilicate glass vial (VWR) was used for microbubble container.

3.3.2.2 PCL microbubble (80 kDa)

14 kDa and 80 kDa PCL is used to 80 kDa PCL was dissolved in chloroform as various concentration; 100 mg/mL, 400 mg/mL, 600 mg/mL, 800 mg/mL, and 1000 mg/mL (not accounting for polymer volume itself; thus, these concentrations would be 90.9, 286, 375, 444, and 500 mg/mL, respectively, when accounting for polymer volume). Each polymer was aspirated from a primary container into a 250 mL glass syringe using a 21 G needle. A nickel titanium alloy (Nitinol) tube was used for injecting the organic solvent phase containing solvated polymer into the water phase. The Luer lock and the Nitinol tubing were glued together using epoxy glue and was allowed to dry overnight. DI water was filled in the borosilicate glass vial and polymer was injected into this vial through the Nitinol tube which was connected to a syringe pump. The polymer injection rate of the syringe was controlled by the syringe pump at a rate of 0.5 µL/sec. The formed bubble was frozen in liquid nitrogen for 20 minutes and lyophilized overnight. The microbubble surface was then analyzed by SEM. The inner portions of

the microbubble using the highest concentration (1000 mg/mL) was imaged by breaking

the microbubbles open with forceps.

3.3.2.3 PCL/PCLTA (14 kDa) microbubbles

14 kDa PCL was dissolved in chloroform and the concentration used was 800

mg/mL. This PCL was mixed with PCLTA and 0.005 g/mL photoinitiator as 1:3:2

volume ratio. The polymer was loaded and injected into the glass vial in the same way as

the aforementioned PCL microbubble (3.3.1.2). The formed microbubble was cured

under UV light for 10 minutes. After it was confirmed that the microbubble was cured, it

was frozen in liquid nitrogen for 20 minutes and lyophilized overnight. The surface of

PCL/PCLTA microbubbles were also analyzed by SEM.

3.3.3   Results and discussion

3.3.3.1 PCL microbubble (80 kDa)

PCL concentrations were varied from 100 mg/mL to 1000 mg/mL From 100

mg/mL to 400 mg/mL microbubbles were hollow, similar to (a) and (b) in **Figure 15**.

Therefore, they easily collapsed when they were picked up and removed from the

solution. From 600 mg/mL to 1000 mg/mL, microbubbles were rigid enough to take out
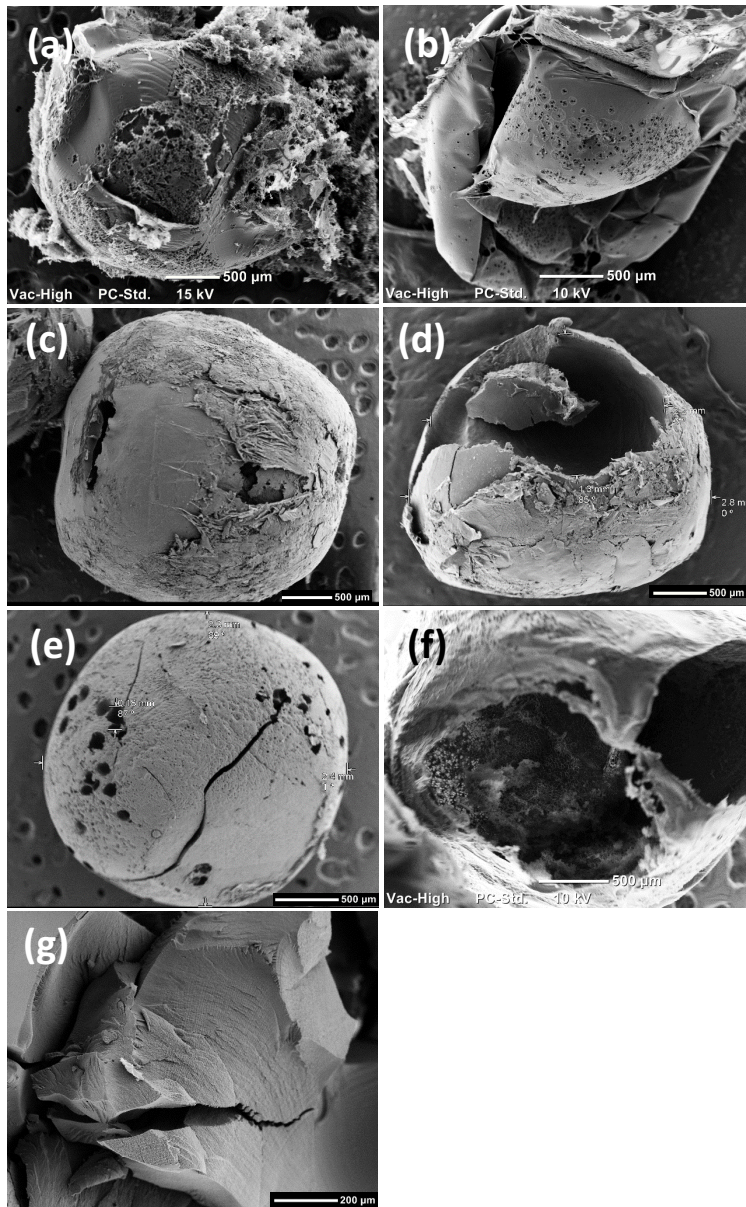
Figure 15 SEM images of 80 kDa PCL microbubbles surface at (a) 100 mg/mL, (b) 400 mg/mL, (c) 600 mg/mL, (d) 800 mg/mL, and (e) 1000 mg/mL and inside of PCL microbubbles at (f) 400 mg/mL and (g) 1000 mg/mL.

using forceps. However, these hard bubbles were cracked easily during the

lyophilization process. From the image of the inside of the microbubbles, denser inner

surfaces were observed using 1000 mg/mL (500 mg/mL accounting for polymer volume) microbubbles, while 100 mg/mL microbubble showed an inner surface with many pores.

3.3.3.2 PCL/PCLTA microbubbles

The main difference was shape when PCL and PCL/PCLTA microbubbles were formed in the glass vial. The PCL microbubble was spherical in shape from when it was formed to when it even sank to the bottom, but PCL/PCLTA microbubble became a hemisphere when it touched the bottom of the glass vial (**Figure 16**).
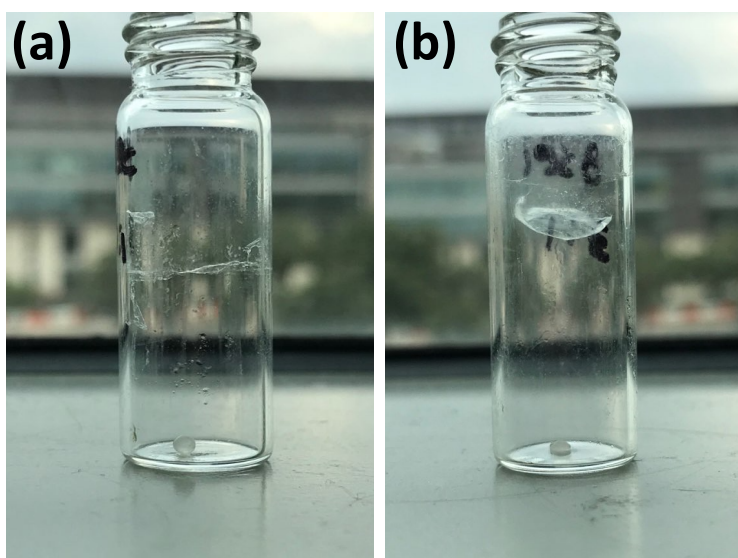
Figure 16 Shape of microbubbles formed in the water:
(a) 80 kDa PCL microbubble after lyophilization (UV curing was previously done on this and did not cure as expected so was not done so in this particular experiment) and (b) 14 kDa PCL/PCLTA microbubble after UV curing and lyophilization.

Also, when the microbubble became a hemisphere shape, as shown in **Figure 17**

the diameter of microbubble increased from 0.69 mm to 1.90 mm. Even though the

shape was a hemisphere, the SEM image showed that the defects of the microbubble

surface were rectified.
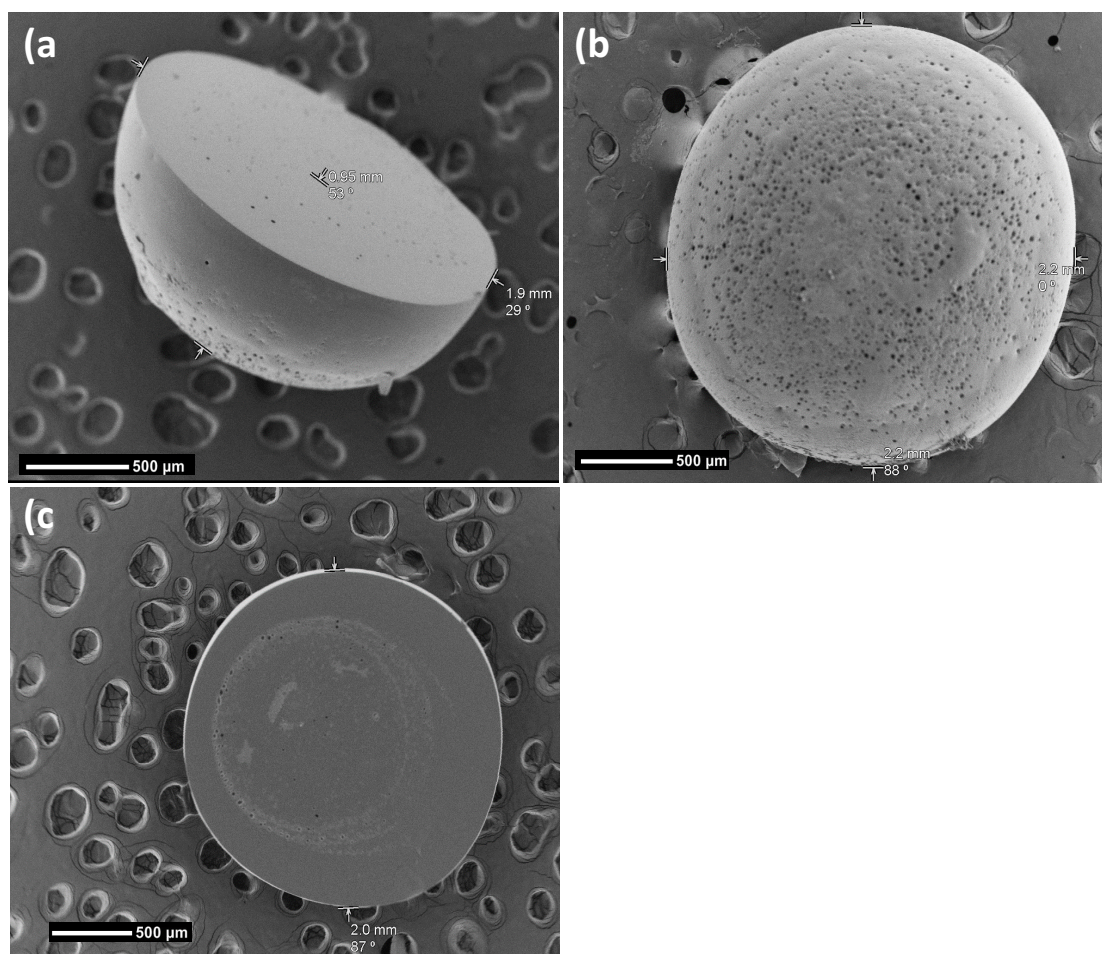
Figure 17 SEM images of PCL/PCLTA microbubbles from the (a) front, (b) bottom, (c) and side views.

3.3.4 Conclusion

The structure of PCL and PCL/PCLTA microbubbles were analyzed by SEM after formation, freezing, and lyophilization. PCL microbubbles showed different rigidity depending on the concentrations. For example, 100 and 400 mg/mL PCL microbubbles were unable to maintain their spherical shapes due to its hollow and porous structure. 600, 800, and 1000 mg/mL microbubbles maintained their spherical shapes, but they cracked during the lyophilization process. Regardless of the concentrations, 80 kDa PCL microbubbles at every concentration indicated surface defects.

PCL (14 kDa)/PCLTA microbubbles were formed as an alternative to PCL (80 kDa) microbubbles. Because PCL/PCLTA microbubbles are less rigid than PCL microbubbles, the surface that touched the glass vial became flat and it was cured in the hemisphere shape using UV light. However, we observed that there was no surface defect on the PCL/PCLTA microbubble surface.

Future work from this point will involve preserving the spherical shape of PCL/PCLTA microbubbles using various solutions.

3.4 ENGINEERING THE MICROBUBBLE TO BE STATIONARY FOR MAINTAINING SPHERICAL SHAPE DURING THE CURING PROCESS AND THE INJECTION OF THE CARGO

3.4.1 Introduction

In the previous section, we observed PCL/PCLTA sank in the glass vial, which was filled with water, and the microbubble formed a hemispherical shape. This hemispherical shape is not proper for controlling drug release because the distance from the cargo to the microbubble surface is not even as it is for a spherical shape. The hemisphere would make it unnecessarily difficult to control the release profile. Furthermore, it would likely be easier to have a spherical microbubble flow through the highest gauge needle possible, in comparison to the hemispherical shape. To maintain the spherical shape of microbubbles, the solution requires higher viscosity.

A direct injection of cargo into the microbubble requires a matrix that could provide enough mechanical support to hold the microbubble firmly during the injection in order to avoid the microbubble from touching the wall and lying flat. Moreover, the microbubble matrix should be transparent to UV light in order to allow for the PCLTA to cure. The microbubble matrix should avoid having the PCLTA diffuse through it to maintain the microbubble shape.

Several substances were tested as a microbubble matrix, such as polyethylene glycol (PEG) hydrogel, hydroxyethyl methacrylate (HEMA) hydrogels, a trehalose solution, agarose, and carboxymethyl cellulose (CMC; 5% and 10% solutions).

3.4.2   Materials and Methods

3.4.2.1 Materials

2,2-dimethoxy-2-phenylacetophenone (DMPA) (Acros Organics), ethylene glycol (Fisher Chemical), 2-hydroxyethyl methacrylate 97% (HEMA) (ACROS Organic), triethylene glycol dimethacrylate (TEGDMA) (TCI America) were used for HEMA gel.

carboxymethyl cellulose (CMC, sodium salt, low viscosity) (Millipore Sigma), agarose (Fisher BioReagents), trehalose (Acros Organics) were also purchased for preparing the solvent.

Synthesized PCLTA, Poly(ε-caprolactone) (PCL, average Mn 14 kDa) (Sigma Aldrich), and 2-hydroxy-2-methylpropiophenone (photoinitiator) (TCI AMERICA) were used for PCL/PCLTA microbubbles. A Legato 100 Syringe Pump (KD Scientific) was used for the microbubble injection. 1 dram of borosilicate glass vial (VWR) was filled with the various solutions as a primary microbubble container.

3.4.2.2 HEMA hydrogel

Three different HEMA hydrogels were synthesized. Before initiating the synthesis, HEMA and TEGDMA were passed through an inhibitor remover column and the solutions were then collected in glass vials. 5 mg of DMPA was measured, 10 µL of TEGDMA and 490 µL of HEMA were added together. 180 µL of ethylene glycol was added as a solvent and mixed. 100 µL, 200 µL, and 300 µL of water was added to render varying rigidities. The polymer was cured using UV for 10 minutes. The PCL/PCLTA microbubbles were injected through a 25 G needle.

3.4.2.3 HEMA hydrogel + 1.5% (final) CMC

CMC was dissolved in DI water as a 3% (w/v) solution. The same formulation of HEMA gel and 3% CMC solution was mixed in a 1:1 volume ratio. The mixture of HEMA and CMC was then cured using UV for 15 minutes. The PCL/PCLTA microbubbles were injected through a syringe pump at a rate of 0.5 µL/sec.

3.4.2.4 Trehalose

A 60% (w/v) trehalose solution was prepared by dissolving 6 mg of trehalose in 10 mL of DI water. 60% was used because 68% is the solubility limit and we wanted to make as viscous of a solution as possible without being concerned with the trehalose

being completely solvated. The PCL/PCLTA microbubbles were injected at a syringe pump rate of 0.5 µL/sec.

3.4.2.5 5% and 10% CMC

5% and 10% (w/v) CMC solutions were prepared by dissolving CMC in DI water. PCL/PCLTA microbubble was injected through syringe pump as 0.5 µL/sec rate.

3.4.3   Results and discussion

A microbubble could not be formed in a PEG hydrogel nor a HEMA hydrogel matrix (**Figure 18a**). These hydrogels were too dense, so the polymer was formed along the needle injection path, as the polymer solution followed the path of least resistance. The injected polymer was not able to be visualized in the HEMA hydrogel using 100 µL and 200 µL of water (**Figure 18b**). When HEMA hydrogel contained more than 400 µL of water, it turned even cloudier making the already not visible polymer even more difficult to see. We felt this would complicate the project so we opted to not use HEMA for our microbubble project.

There was another trial after injection to the hydrogels. The hydrogel was cured from the bottom of the glass vial. The glass vial was taken out from the UV station during the curing but before the gel was fully cured, and a microbubble was injected through the HEMA precursors onto the lower cured portion of HEMA. The curing likely

began from the bottom up, even though the UV light came from the top because there was less oxygen at the bottom, as this was not done under inert gas due to issues with the liquid spraying under the flow of the gas and difficulties with creating a gas chamber that would flow slowly enough into the vial. However, the microbubble surface, which came into contact with the HEMA hydrogel became flat, similar to previous observations when the microbubble touched the glass vial (**Figure 18c**). To increase the viscosity of the HEMA 5% CMC was mixed prior to UV curing. However, it was cloudy after UV curing (and became increasingly so with the addition of water), so the microbubble itself post-injection could not be visualized (**Figure 18d**).
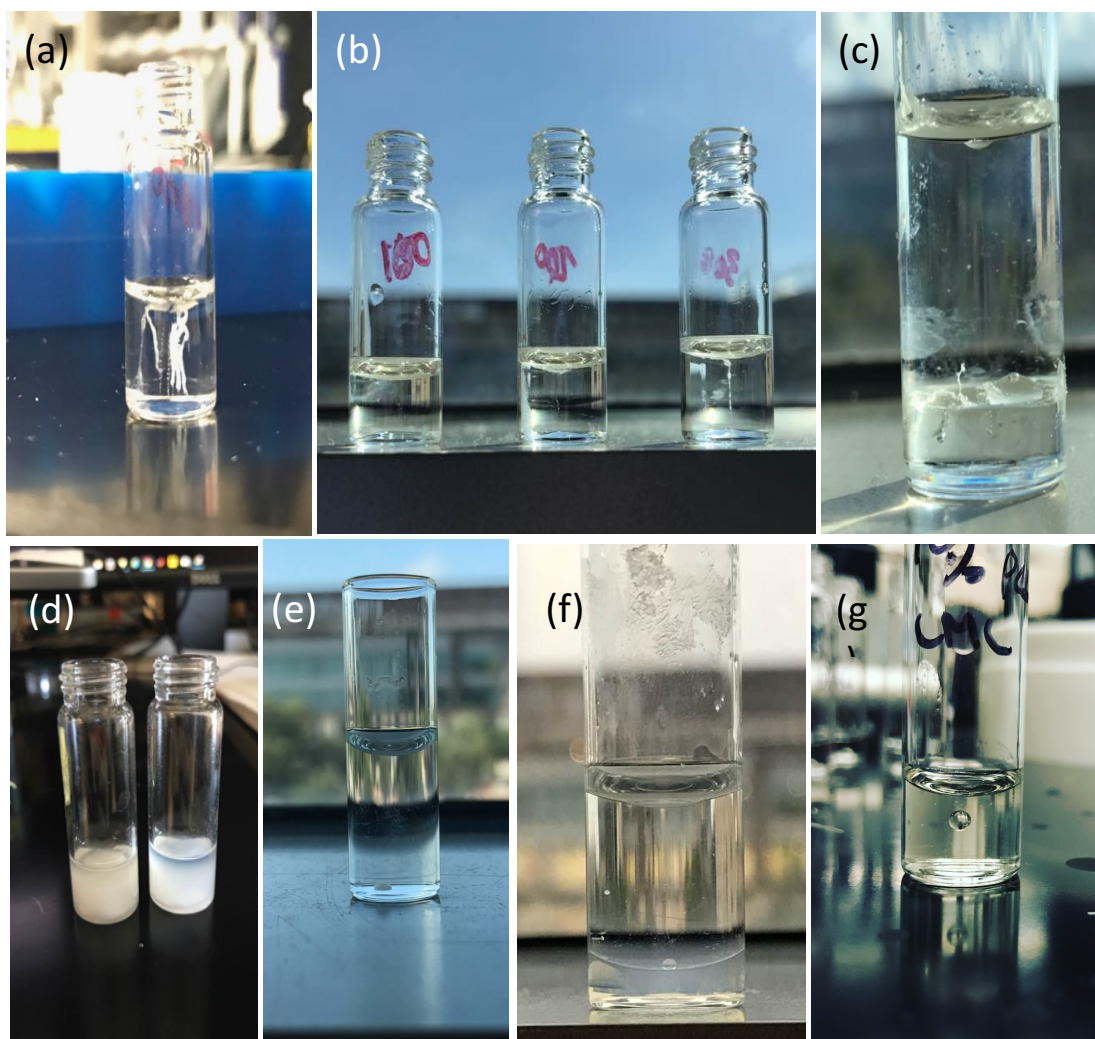
Figure 18 PCL/PCLTA polymer was injected in (a) PEG hydrogel and the polymer followed the path of the needle (b) a HEMA hydrogel with 13% (left), 23% (middle), and 31% (right) v/v water content; in (c)half-cured HEMA hydrogel (UV light directed from the top; the bottom portion likely cured first because it had less oxygen near the bottom of the vial; top contains uncured HEMA precursors) (d) HEMA+1.5% (final) CMC and subsequently cured (e) 60% (w/v) trehalose (f) agarose gel on the bottom with pure water atop (g) 10% CMC.

Even though the trehalose solution seemed to have had a higher viscosity than water, as literature indicates the microbubbles sank in the 60% (w/v) trehalose solution as fast as microbubbles in the DI water in the borosilicate glass vial. The microbubbles

in trehalose solution also became hemispherical when the microbubbles touched the

glass vial, similar to when the microbubbles were formed in the DI water. (**Figure 18e**).

Microbubbles on the agarose gel were closer to a sphere than other solution such

as the HEMA and PEG hydrogels or the trehalose solution, but the surface of

microbubbles which touched the agarose gel was more flat than other parts of the surface

(**Figure 18f**).
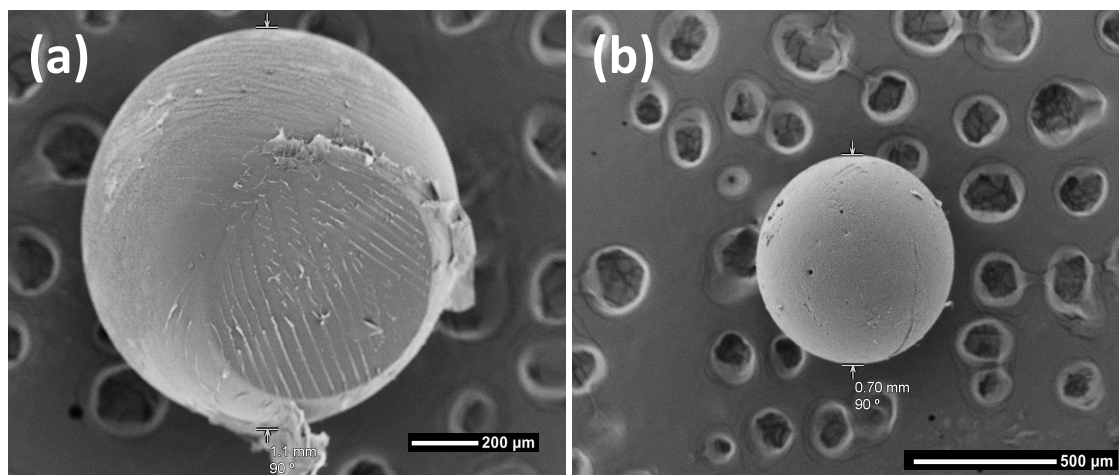
Figure 19. PCL/PCLTA microbubbles reached the bottom of the glass vial in a 5% CMC solution (a) which caused a flattened bottom on the microbubble and (b) the microbubble did not reach the bottom of the glass vial when using a 10% CMC solution.

Among the various solvents tested, the CMC solutions had the highest viscosity.

In a 5% CMC solution, the microbubbles sank slowly. After UV curing the microbubble

eventually did reach the bottom of the glass vial, so it resulted in a slightly flattened

bottom shape (**Figure 19a**). However, the microbubble was completely suspended in

10% CMC solution. Even after UV curing the microbubble was suspended in the same position which it was formed and also maintained the spherical shape (**Figure 18g** and **19b**).

3.4.4   Conclusion

As shown in section 3.3, PCL/PCLTA microbubbles are less rigid than PCL microbubbles. Therefore, PCL/PCLTA microbubbles changed the shape to be hemispherical when the microbubbles touched the glass vial. To avoid this shape change, various solutions were explored. PEG hydrogels and HEMA hydrogels were synthesized using different water contents. The half-cured HEMA hydrogel and the mixture of HEMA and 1.5% CMC were also used. Furthermore, a trehalose solution, an agarose gel, and 5% and 10% CMC solutions were prepared.

Microbubbles could not be formed into a spherical shape using PEG and HEMA hydrogels due to the hydrogel's density. In the context of the half-cured HEMA hydrogel, the microbubbles' surface, which touched the cured HEMA hydrogel, became flat. When the HEMA hydrogel was mixed with 5% CMC the gel changed to cloudy after curing, so microbubble could not be visualized. Microbubbles sank immediately in trehalose solution like that in water. 5% CMC was viscous but not enough to suspend microbubbles. Therefore, the microbubble sank slowly and touch the glass vial during the UV curing. However, the microbubble was suspended in 10% CMC. The only suitable solution for forming spherical microbubbles that allow for enough stability to

inject cargo was the 10% CMC. Even after curing and lyophilization, the shape was completely sphere.

Future work will entail ensuring the cargo within the microbubble remains stationary within the spherical microbubble to maximize the release kinetics for a given diameter of microbubble. The next section describes how to increase the viscosity of the cargo to cause the cargo bubble within the microbubble to not escape upwards into the outer 10% CMC solution.

3.5   ENGINEERING THE CARGO TO BE STATIONARY WITHIN THE POLYMERIC MICROBUBBLE TO MAXIMIZE THE RELEASE TIME

3.5.1   Introduction

Single- or double- emulsion techniques are the conventional methods for cargo encapsulation within PCL NPs and MPs [56, 57]. This size distribution affects to the kinetics of the drug release [58, 59], and it is common to observe sustained releases instead of bolus release from the NP/MP using emulsion methods because cargo is scattered throughout the microparticle whether it is homogeneously distributed (generally for hydrophobic cargo; single-emulsion) and distributed throughout in smaller aqueous pockets. Because of the cargo being distributed throughout, there is continual release generally for the duration that there is particle mass remaining. There has been reports, however, of catastrophic breakdown of ester-based polymers which degrade via

bulk degradation at later time points which could potentially serve as a secondary burst [25].

In this section, the encapsulation of cargo within the microbubble is accomplished by direct injection using needles. After direct injection, UV curing and freeze-drying processes were performed to stabilize the microbubble and avoid cargo leakage.

In order to study the kinetics of the drug release from the PCL/PCLTA microbubbles, a BSA conjugated to CF680 dye (BSA-CF680) was used as a model antigen which would be useful for *in vivo* imaging purposes due to the excitation/emission being in the near infrared region. We discovered later this excitation and emission could not be used with our confocal microscopy available to us at TAMU, thus we ended up using a BSA model antigen conjugated to a CF dye which is excited at 488 nm. Doxorubicin and acriflavine were used as fluorescence indicators for confocal microscopy purposes.

Until the end of UV curing, it is crucial to ensure that the cargo remains inside the microbubble. In this section, we ensured the cargo would remain stationary within the microbubbles using 3% and 5% CMC, which increased the viscosity of the cargo solution. Note that there is 10% CMC that the microbubble is injected into and then a 3% and 5% CMC solution of cargo is being injected within the microbubble for the internal cargo bubble to stay stationary.

3.5.2   Materials and Methods

3.5.2.1 Materials

Bovine serum albumin (BSA) (Fisher BioReagents) was conjugated with CF680, maleimide(Sigma Aldrich). Sephadex G-25 (Sigma Aldrich), anhydrous dimethylsulfoxide (DMSO) (Alfa Aesar), and Tris-(2-carboxyethyl)phosphine (TCEP) were other materials used for the BSA-CF680 conjugation reaction and purification steps.

This BSA-CF680, acriflavine (Chem-Impex International), and doxorubicin hydrochloride (Fisher BioReagents) were used for cargo. Carboxymethyl cellulose (CMC; sodium salt, low viscosity) (Millipore Sigma) was used for increasing viscosity of cargos.

Synthesized PCLTA, poly(ε-caprolactone) (PCL, average Mn 14 kDa) (Sigma Aldrich), and 2-hydroxy-2-methylpropiophenone (photoinitiator) (TCI AMERICA) were used for PCL/PCLTA microbubbles. A 0.5 dram borosilicate glass vial (VWR) was used for the primary microbubble container.

3.5.2.2 BSA-CF680 conjugation

12 mM of protein was prepared by dissolving 0.006 mmol of BSA in 0.5 mL PBS. A 10-fold molar excess of TCEP was added to reduce the disulfide bonds within the BSA to thiol groups. BSA with TCEP was stirred for 30 minutes under argon gas. 0.4 mL of anhydrous DMSO was added to 1μmole of CF680 maleimide, thus a 2.5 mM dye solution was prepared. The vial was vortexed to be fully dissolved and briefly centrifuged to collect as much of the solution as possible.

The 0.036 mL of dye stock was added to the stirring BSA solution in a dye/protein molar ratio of 15. The mixture was stirred at room temperature for 2 hours.

The Sephadex G-25 column was equilibrated in PBS buffer for separating the labeled BSA from the free dye. The Reaction Solution was loaded onto the column. The column was eluted with 1× PBS buffer. After excluding the first band, labeled BSA was collected.

3.5.2.3 Cargo injection with and without CMC

1% (w/v) acriflavine solution was prepared by dissolving 5 mg acriflavine in 0.5 mL PBS. 1% (w/v) doxorubicin was also prepared in the same way. BSA-CF680 conjugates, 1% (w/v) acriflavine and 1% (w/v) doxorubicin was loaded into the 1 mL syringe. The glass vial is filled with 10% CMC solution, and PCL/PCLTA microbubble

using 14 kDa 1000 mg/mL PCL was formed. The syringe pump rate was 0.5 µL/sec for 10 seconds, and three different cargo was injected into three different microbubbles using 34 G blunt tip needles.

To prepare cargo with CMC 9 mg, 15 mg of CMC is weighed in each microtube. By adding 0.3 mL of 1% (w/v) acriflavine solution to each CMC microtube, cargo with 3% and 5% (w/v) CMC were prepared. 1% (w/v) Doxorubicin and stock of BSA-CF680 in 3% and 5% CMC also prepared in same way. Microbubbles were formed in 10% CMC vial using same syringe pump rate. Six different cargo solutions were loaded into the 1 mL syringe and injected into the six different microbubbles using 34 G blunt tip needles.

3.5.3 Results and discussion

3.5.3.1 BSA-CF680 conjugation

After conjugation of CF680 and BSA, each concentration was calculated using the Beer-Lambert Law.

$A = \varepsilon c l$

A = the absorbance of dye or BSA

ε = the molar absorption coefficient or extinction coefficient (L mol^{-1} cm^{-1} or M^{-1}cm^{-1}).

c = the concentration of the dye or BSA (mol L^{-1})

l = the wavelength path length (cm).

For CF680 dye, the absorbance, the molar absorption or extinction coefficient, and the wavelength path length were 1.437, 210,000(L mol^{-1} cm$^-$1), and 0.294cm, respectively.

$1.437 = 210,000$ (L mol^{-1} cm^{-1}) x c x 0.294cm.

Therefore, the concentration of dye was 0.0232 mM.

For BSA, the absorbance, the molar absorption coefficient, and the wavelength path length were 0.149, 43,824(L mol^{-1} cm^{-1}), and 0.294cm, respectively.

$0.149 = 43,824$ (L mol^{-1} cm^{-1}) x c x 0.294cm.

Therefore, the concentration of BSA was 0.0115 mM. The concentration of BSA-CF680 conjugates was calculated using $A_{BSA(corrected)} = A_{280} - (Amax * CF)$.

A_{280} = absorbance readings of the conjugate at 280 nm

Amax = the absorption at 681 nm

CF = the absorbance correction factor

CF was 0.09 for CF680, therefore,

$A_{BSA(corrected)} = 1.437 - (0.149$ x $0.9) = 0.0193$.

$0.0193 = 43,824$ (L mol-1 cm-1) x c x 0.29422cm, so the corrected BSA concentration 0.0015 mM. The ratio of CF680 dye to BSA is 15.5 to 1.

Based on this calculation, the calibration curve using half dilution series of BSA-CF680 conjugates was prepared (**Figure 20**). There is a total of 17 disulfide bonds in BSA, thus after the reduction process there is a total of 34 thiol groups which could react with the maleimide. Because we had a ratio of 15.5:1 dye:BSA then we know that there the dye conjugation process was at 45.6% of the maximum saturation.
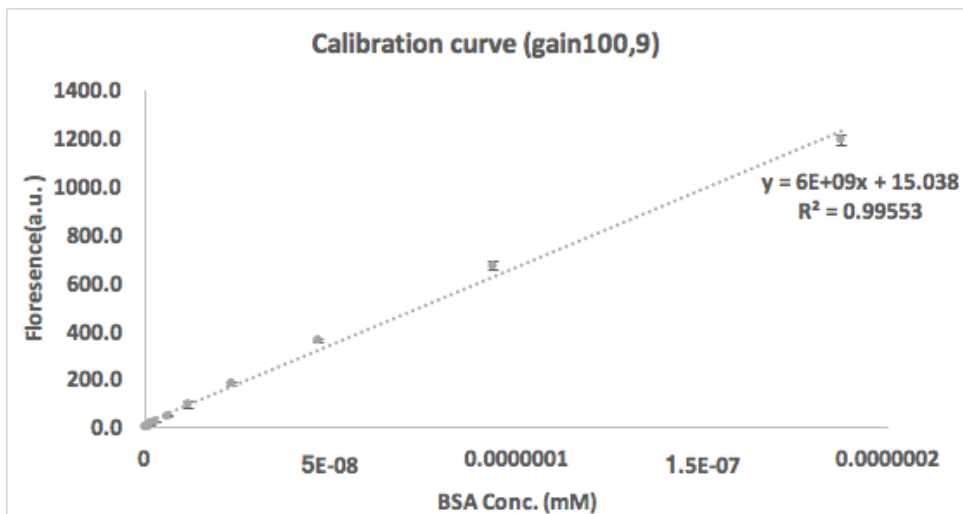
Figure 20. Calibration curve of BSA-CF680 conjugates (Cytation 5 was set to a gain of 100 and a bandwidth of 9 nm).

3.5.3.2 Cargo with CMC

Without CMC, the cargo inevitably escaped immediately upon injection within the microbubble, as shown in **Figure 21**. Through the confocal microscopy, the fluorescence dye was observed only from the surface of the microbubble but not inside the microbubble because the cargo escaped (**Figure 22a**). However, the cargo remained within the microbubble when injected with the CMC solution. However, an amount of the drug was also presumed to escape out of the conduit which the cargo tube had made while the cargo tube was pulled out of the shell of the microbubble. The dye preferentially would partition into the organic phase, as opposed to the aqueous phase which is why the outer perimeter fluoresces in the confocal microscopy images.

60
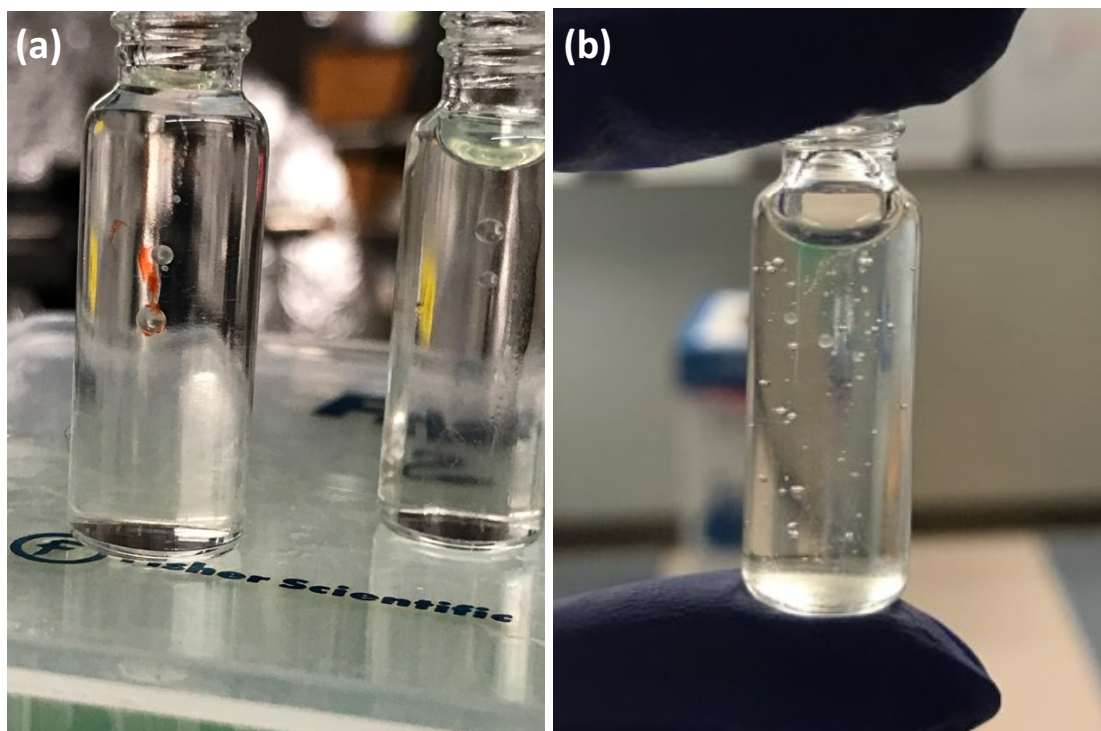
Figure 21. Cargos without CMC (a) 1% (w/v) doxorubicin (b)BSA-CF680.
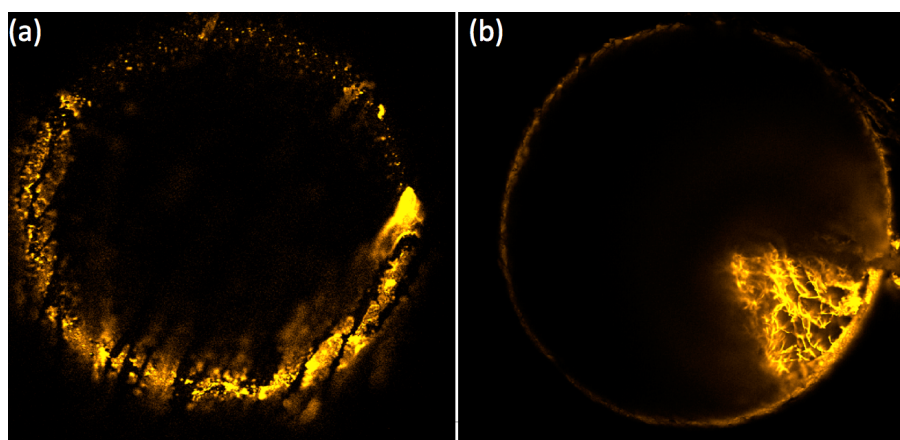
Figure 22. Confocal images after UV curing and lyophilization using (a) 1% (w/v) acriflavine without CMC and (b) 1% (w/v) acriflavine with 3% CMC.
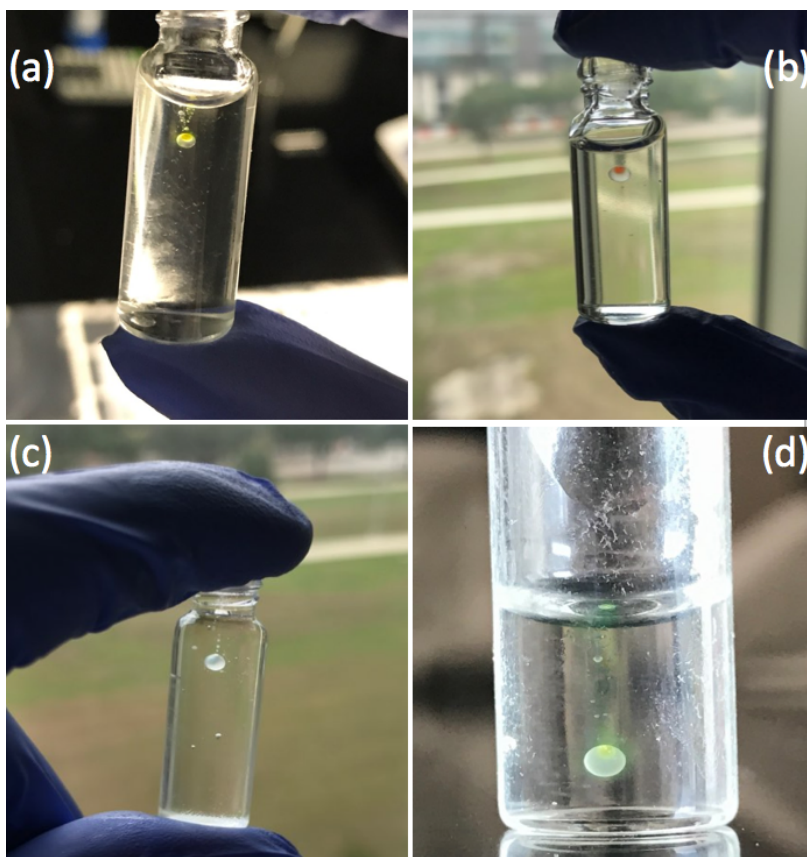
Figure 23. Inner cargo bubbles injected with 3% CMC within the microbubbles using (a) 1% (w/v) acriflavine (b) 1%(w/v) doxorubicin (c) BSA-CF680 (d) 1% (w/v) acriflavine after UV curing.

When cargo was injected with 3% CMC, they formed the expected inner bubble within the microbubble. However, the cargo bubble kept rising to the top of the microbubble through the microbubble's shell as shown in **Figure 22b** and **Figure 23**. Therefore, if there is a long-time interval between when the cargo is injected and when the UV curing takes place, the cargo may escape from the microbubble by migrating upwards. When the microbubble was cured immediately after the inner cargo bubble was injected using 3% CMC, the inner cargo bubble would migrate to the top of the microbubble within 1 minute and remain there (even throughout the remaining UV

curing duration and lyophilization. **Figure 23(d)** shows 1% (w/v) acriflavine with 3%

CMC after UV curing.

Figure 24. Cargo with 5% CMC using (a) 1% (w/v) acriflavine and (b) 1% (w/v) doxorubicin.

With 5% CMC, the inner cargo bubbles were stationary within the microbubbles.

Because of the viscosity of the inner cargo bubble, the cargo did not rise and stayed in

the middle of the microbubble even during the UV curing process (which the 3% CMC

was not able to do) and lyophilization. **Figure 24** and confocal image of **Figure 25**

demonstrate that the cargo using 5% CMC stayed stationary in the middle of the
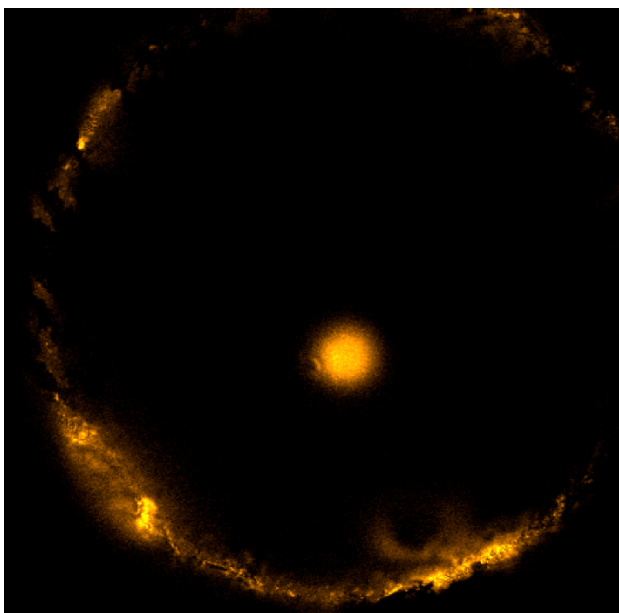
microbubbles.

Figure 25. Confocal image of 1% acriflavine with 5% CMC.

3.5.4 Conclusion

As the cargo, 1% (w/v) acriflavine, 1% (w/v) doxorubicin, and BSA-CF680 conjugate formulations were prepared and injected into the 14 kDa PCL/PCLTA microbubble. Again, at this stage we were not using the 80 kDa PCL because it could not be mixed with the PCLTA which is required for curing purposes. These drug formulations without CMC escaped as soon as they were injected. Cargo with 3% CMC was capable of creating an inner cargo bubble inside of the microbubble, but the inner cargo bubble would migrate upwards and remain at the top of the microbubble within 1 minute. Even though UV curing was started as soon as they were injected, the cargo stayed on the top of the microbubble.

To ensure the inner cargo bubble remained stationary, we found that a 5% CMC concentration was sufficient to keep the inner cargo bubble from migrating upwards even throughout the UV curing process (note that cargo can still escape during the initial phase of the curing process) as was demonstrated with the confocal microscopy images post-lyophilization.

3.6   QUANTIFY THE DIAMETERS OF THE MICROBUBBLE BY VARYING SYRINGE PUMP RATE AND COMPARING DIAMETERS PRE- AND POST-LYOPHILIZATION

3.6.1   Introduction

It is crucial to control the diameter of the microbubbles in order to control the drug release and the injectability through various desired gauges of needles. The repeatability of formation of the same diameter of microbubbles and injecting the same amount of drug are also important to maintain similar shell thicknesses. Varying diameters will affect the uniformity of drug release. The diameters of the microbubbles were varied by controlling the syringe pump rate and measured by taking photographs and using an electronic micrometer for the calibration of the image itself. The correlation between the syringe pump rates and the particle diameters gives us the ability to control the end microbubble diameter.

In addition, the actual volumes of microbubble using confocal microscopy were compared to the theoretical volumes based on the syringe pump rate and the duration of injection.

3.6.2   Materials and Methods

3.6.2.1 Materials

Synthesized PCLTA, poly(ε-caprolactone) (PCL, average Mn 14 kDa) (Sigma Aldrich), and 2-hydroxy-2-methylpropiophenone (photoinitiator) (TCI AMERICA) were used for PCL/PCLTA microbubbles. The glass syringe pump barrel and the tube was connected through luer locks. A P-662 female luer (Idex) is for the microbubble injection and one Hub Assembled with 12" of Tubing (30 gauge) (Hamilton) is for the drug injection. A Legato 100 Syringe Pump (KD Scientific) was used for controlling the microbubble injection rate. The micromotor (CONEX-AG-LS25-27P), Piezo Motor Linear Stage, was purchased from Newport. A 0.5 dram borosilicate glass vial (VWR) was used for the primary microbubble container.

3.6.2.2 Controlling the diameter of the microbubble by controlling the syringe
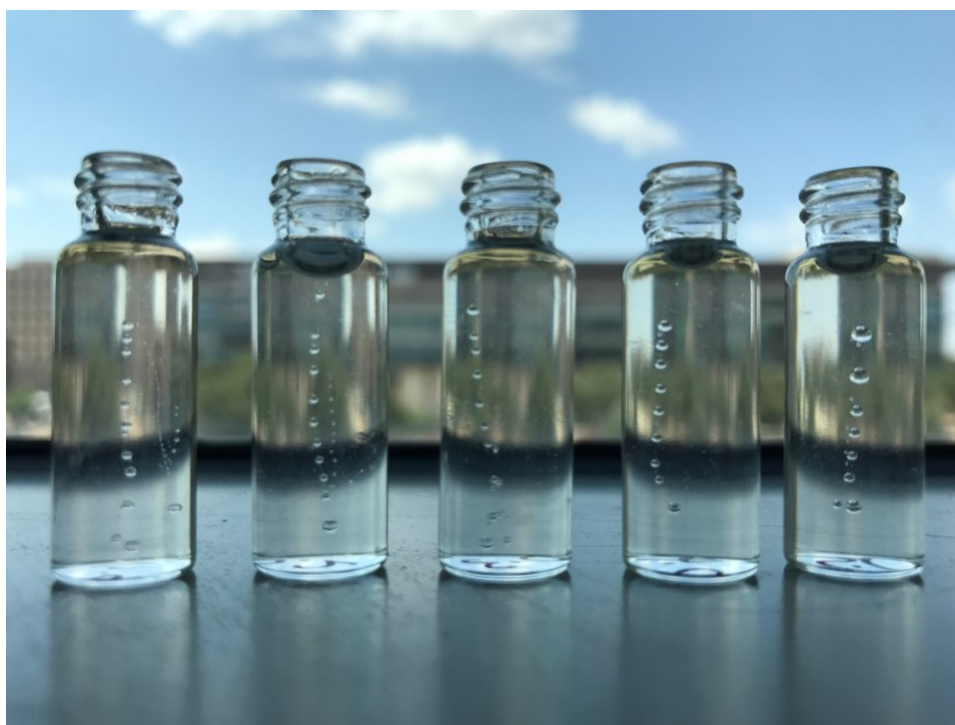
   pump rate

Figure 26. Microbubble diameter comparisons dictated by the syringe pump rate.

14 kDa PCL was dissolved in chloroform and the concentration was 800 mg/mL. This PCL was mixed with PCLTA as 1:3 volume ratio. 1 μL of the photoinitiator stock was added. The polymer was loaded within the glass barrel which was controlled by the syringe pump and the tube for the microbubble injection (polymer phase) was connected from the glass barrel to the micromotor. The glass vial was filled with 10% (w/v) CMC, and the tube was inserted near the bottom of the vial (but not so low that the injected polymer microbubble would contact the bottom of the glass vial). Using Labview® the

micromotor moved backwards (at the constant and manufacturer's set rate; the rate cannot be controlled by users) while the syringe pump was also extruding polymer. The syringe pump rate was controlled from 0.0005 to 1 µL/sec. A photo was taken of the vial (**Figure 26**), and the microbubble diameters were quantified via ImageJ® with the calibrated object in the image using the electronic micrometer.

Confocal microscopy is an optical microscopy technique with an enhanced resolution and contrast when compared to a regular micrograph. The main feature is imaging confocal planes through a spatial pinhole, which allows the selective observation of light from a specific plane and excluding the light from other planes. Therefore, the collection of z-stack confocal planes provide a three-dimensional image of the sample [69].

3.6.2.3 Diameter of the microbubble pre- and post-lyophilization

The precursor of the microbubbles was prepared in a similar manner as was described in section 3.6.2.2. The polymer was loaded within the glass barrel which was controlled by the syringe pump. The glass vial was filled with 10% (w/v) CMC, and the microbubble was injected using a syringe pump at a rate of 0.5 µL/sec. After the microbubbles were formed, they were cured by UV for 10 minutes.

Photos of the microbubbles within the glass vials were taken and the microbubble diameters were quantified via ImageJ® with a calibrated object in the photo using the electronic micrometer. After lyophilization the diameters of the microbubbles

were quantified using the electronic micrometer as well. The reason it is not possible to measure the diameters of the pre-cured microbubbles with the micrometer as they are in liquid form at that stage.

3.6.2.4 Diameter of the microbubbles pre- and post-cargo injection

The precursor of microbubbles was prepared similarly to the microbubbles in section 3.6.2.2. The polymer was loaded within the syringe pump's glass barrel. The borosilicate vial was filled with 10% (w/v) CMC, and the syringe pump was controlled. The syringe pump rate was controlled from 0.0005 to 1 µL/sec. After the microbubbles were formed, the 1% acriflavine using 5% CMC was injected into the microbubble using a 34 G needle. Before and after cargo injection, photos were taken of the microbubbles in the glass vial and the microbubble diameters were measured by ImageJ® using a calibrated object within the image as measured by the electronic micrometer.

3.6.3   Results and discussion

3.6.3.1 Controlling diameter of the microbubbles dictated by the syringe pump rate

As can be seen from **Figure 27**, the microbubble size increased from 325±20 µm to 799±71 µm when the syringe pump rate increased from 0.005 µL/sec to 1 µL/sec

69

while the micromotor was driven backwards at the constant manufacturer rate. There was an increase between 0.005 µL/sec and 0.01 µL/sec from 325 µm to 547 µm. Interestingly, the microbubble diameter is not reliable when the syringe pump rate is below than 0.005 µL/sec. The inaccuracy at this stage is likely due to the lower limit of the syringe pump rate which is 0.0003 µL/sec. It increased from 325±20 µm to 551±23 µm when the syringe pump rate decreased from 0.005 µL/sec to 0.001 µL/sec in two separate experiment.

The chart shows Microbubble Diameter (µm) on the y-axis versus Syringe pump rate (µL/sec) on the x-axis with the fitted equation:

$$y = -7.475x^4 + 94.031x^3 - 390.68x^2 + 532.5x + 571.27$$
$$R^2 = 0.99962$$
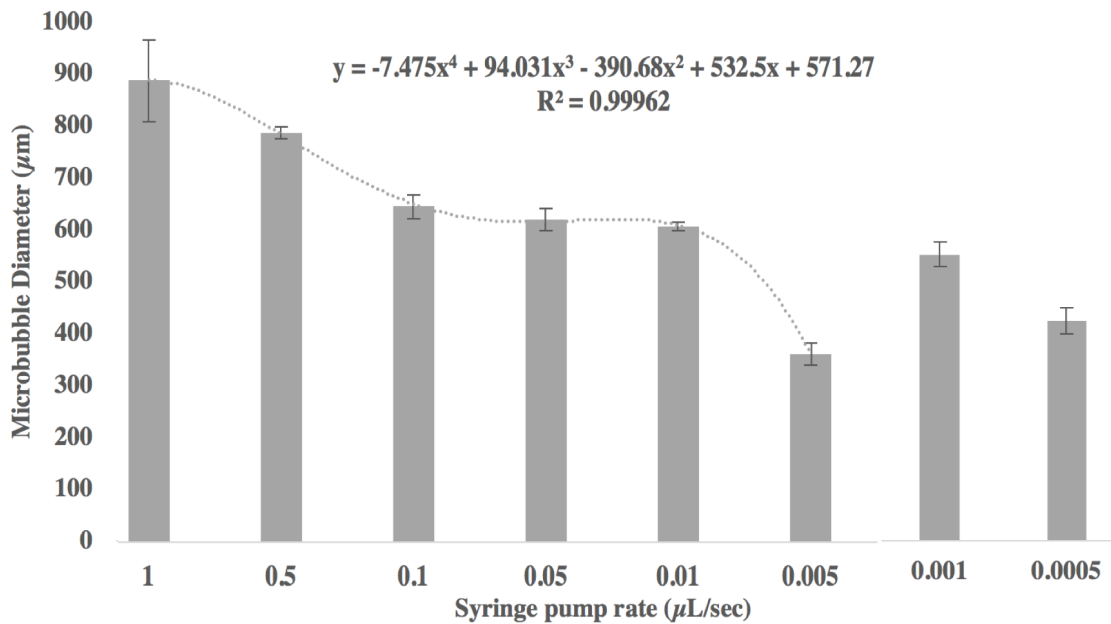
Figure 27. Microbubble diameters dictated by the syringe pump rate while the micromotors were driven backwards in space. The backwards motion causes microbubbles to separate.

When the microbubble was formed with 0.1 µL/sec rate for 5sec, the volume should be 0.5 µL. However, the actual volume was less than that, 0.473454 µL (r=

70

0.4835 mm). Because the syringe pump operation is performed manually, there was

5.4% of error between the theoretical and actual volumes.
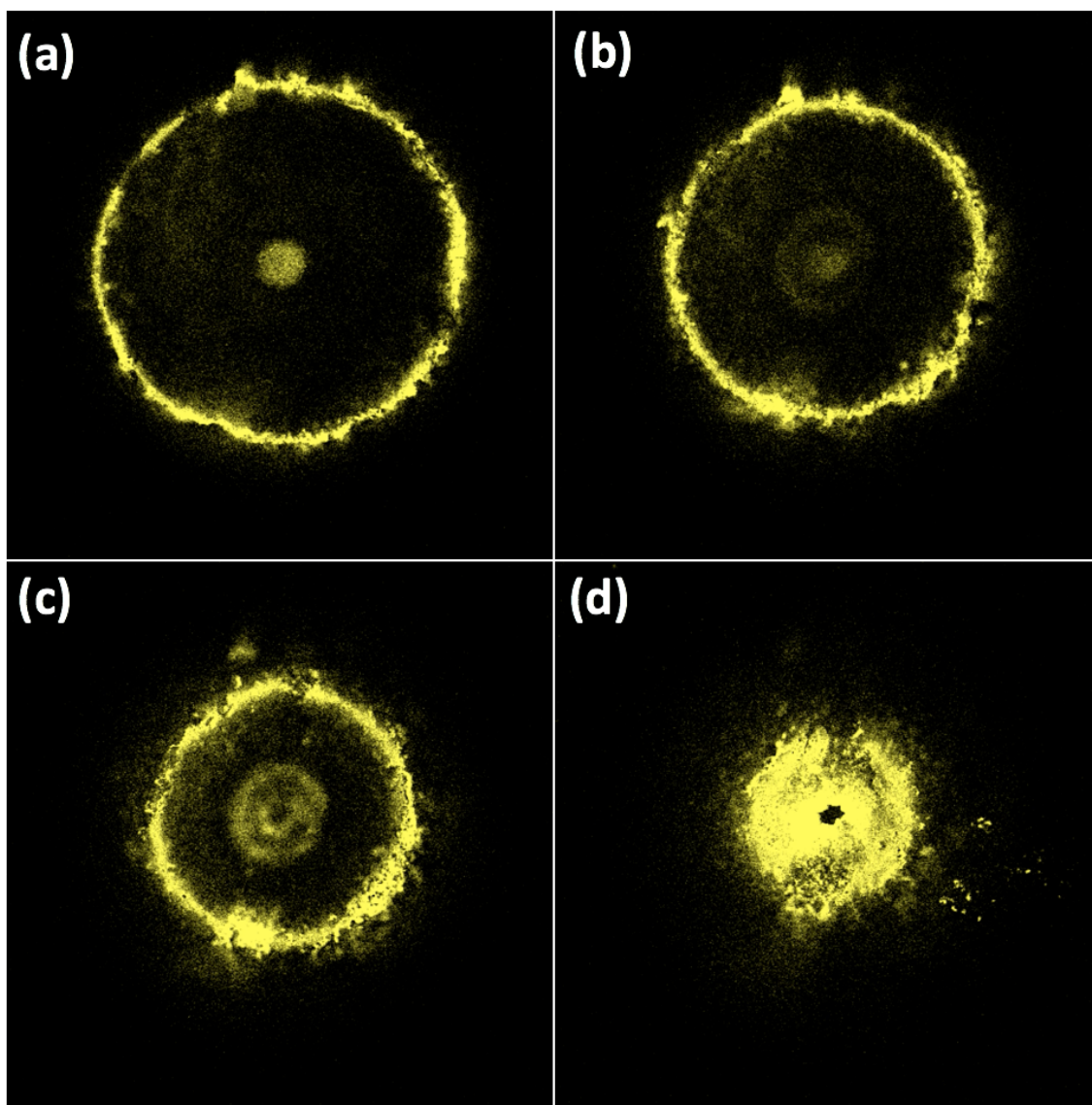
Figure 28 Confocal images of BSA-CF488 in the microbubble from the middle to the bottom of the microbubble (from (a) to (d)). The distance between each slice is 10 μm. Note that there is drug around the periphery which is due to the escape of the drug through the temporary conduit made as the tube used for the cargo injection is removed from the liquid shell of the microbubble. (The confocal video file was submitted as supplemental file)

A confocal microscopy is a characterization technique that helped assess the microbubble fabrication and cargo distribution throughout the microbubble (**Figure 28**).

3.6.3.2 Diameter of the microbubbles pre- and post-lyophilization
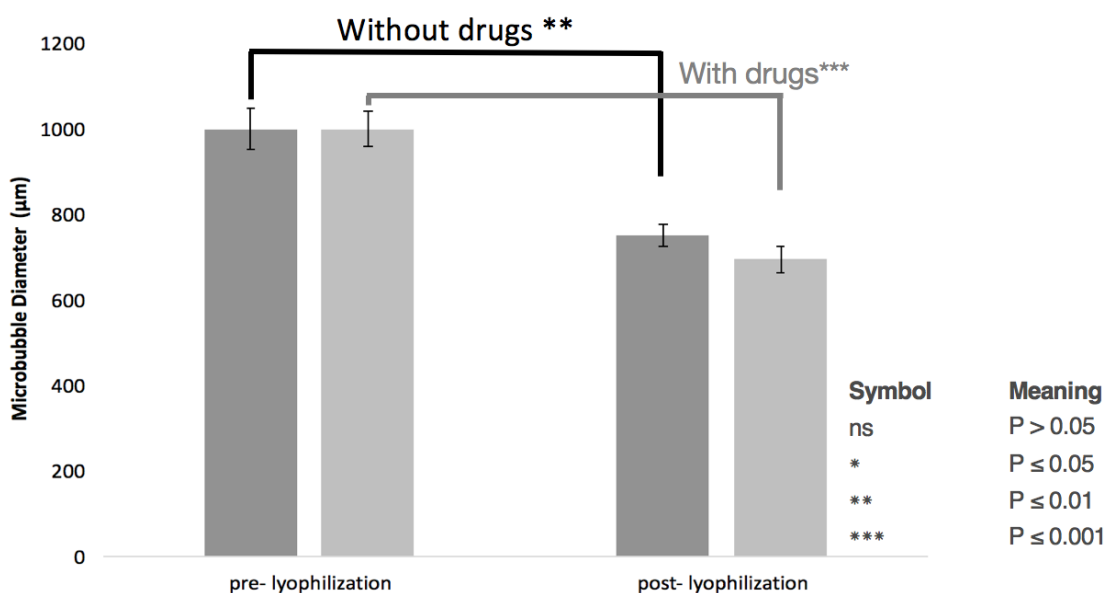
Figure 29 Microbubbles size comparison before and after lyophilization.

In both case, without drugs and with drugs, the microbubble was decreased post-lyophilization by $25\pm2.5\%$ and $31\pm3.2\%$, respectively (**Figure 29**). This is likely because the aqueous phase containing the cargo and chloroform of microbubbles were evaporated to the extent possible during the lyophilization. We suspect that the center is not as dry as it could be and studies investigating the inner water content will be

accomplished in the future as well as endeavoring to vent the inner cargo during the

lyophilization process, followed by a localized annealing process.

The diameter of the microbubbles was analyzed pre- and post-lyophilization

using a Student's t-test, and the quantified p-values were 0.0014 and 0.0009 for

microbubbles without drugs and with drugs, respectively. Both values were less than

0.05, so there were significant diameter differences pre- and post-lyophilization.

3.6.3.3 Size of the microbubble before and after cargo injection.
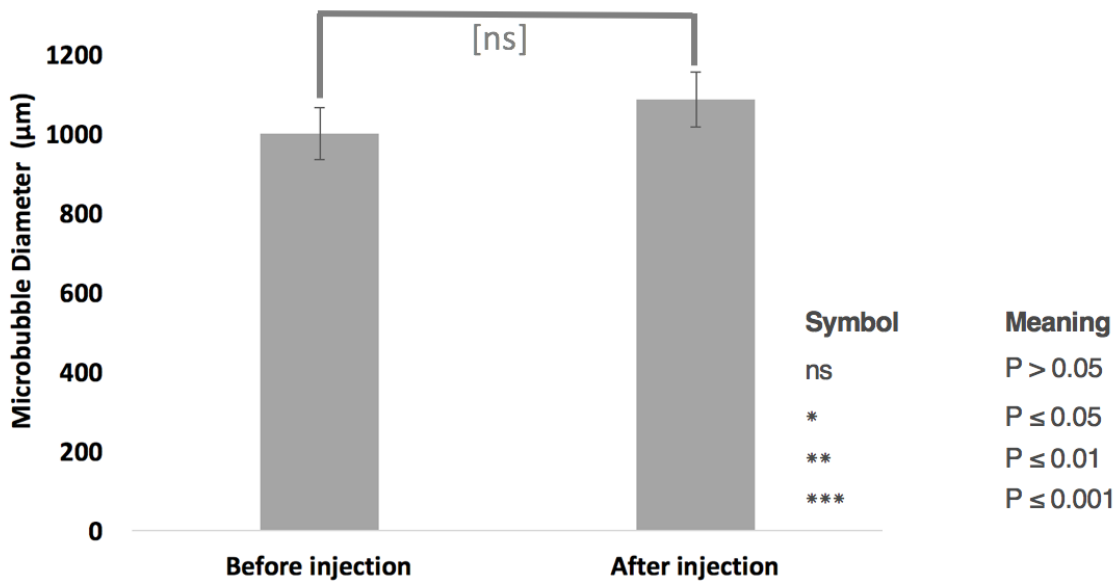
Figure 30. Microbubble diameter comparison before and after cargo injection.

When the diameter of the microbubbles before cargo injection was normalized to 1±0.064, the post-injection diameter was calculated to be 1.084±0.069 was gotten for the microbubble size after cargo injection (**Figure 30**). The volume increased 8.4%, but the size difference is not significant because the p-value was 0.199.

3.6.4   Conclusion

In this section, we were able to control the microbubble diameter using the syringe pump rate. The reliable range was from 0.005 to 1 µL/sec, and the microbubble diameters increased from 325±20 µm to 799±71 µm. The microbubble size before lyophilization was also compared to after lyophilization. For both microbubbles with and without drugs, the microbubble diameter decreased after lyophilization, and both p-values were less than 0.05. This demonstrates that the bubble diameters decrease significantly due to the solvent (water/organic solvent) evaporation. Even though the microbubble diameter increased because of the injected drug volume, it was not a significant increase (p-value: 0.199) but appeared to be trending towards significance.

These results enable us to know how to control the system for a given microbubble diameter. However, the automation system is required for the repeatability of microbubble formation which is an ongoing endeavor within the Pharmacoengineering Laboratory (Dr. Corey Bishop's Laboratory). The next chapter describes how to quantify the angle of the micromotors for enabling the polymer injection tube and the cargo tube

to meet at the same location within the borosilicate vial. These tubes can be controlled

by micromotors (translation of the tubes) and a goniometer (angling the tube).

3.7   QUANTIFYING THE ANGLE OF THE MICROMOTORS FOR

INJECTING CARGO INTO THE CENTER OF THE MICROBUBBLES

3.7.1   Introduction

After setting the initial conditions for the microbubble formation, it is important

to secure the repeatability. Since the microbubble fabrication was performed manually,

the bubble size and injected drug amount are slightly different every time. Also, the

position, which microbubbles are capable of forming, is variable in the outer 10% CMC

solution that the microbubbles are injected into when the system is not automated.

In order to form the microbubble, inject cargo, UV cure, freeze and lyophilize in an

automated fashion, this entire system needs to be self-contained in a container which can

withstand lyophilization-capable pressures. We intend to replace the glass vial used to

hold the 10% CMC every time and its position is related to the two micromotors.

The injection system should be able to place the microbubble in space

irrespective of how the personnel place the glass vial within a pre-designed holder.

Therefore, one platform, which connects the stand for the glass vial and the two

micromotors (one for the polymer tube and one for the cargo tube translation), will be

necessary. To find the meeting point of two injection tubes, which are connected to the

micromotors, the angle between the micromotors and the platform should be fixed. This section described the structure of the platform and how the angle of the micromotors was quantified.

3.7.2   Materials and Methods

3.7.2.1 Materials

The goniometer (**Figure 31a)** with a 1/2inch virtual point (Thorlabs) was purchased to control the angle of the drug injection tube which will need to be determined and fixed for the rest of the microbubbles to be subsequently similar. The control range is ±15º for the goniometer.

Micromotors (CONEX-AG-LS25-27P) were purchased from Newport (**Figure 31b**) and both tubes for the polymer and drug injection were attached to these micomotors. The control range for the micromotor is ±27 mm.

1 dram of borosilicate glass vial (VWR) was used for the primary microbubble container, and a 1.8 cm thick wood panel was purchased from Home Depot.

3.7.2.2 Finding the micromotor angle
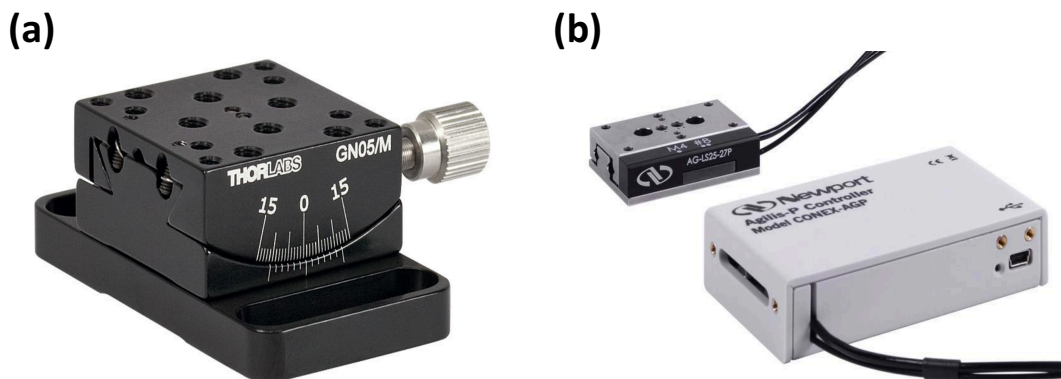
Figure 31 (a) a goniometer for controlling the angle that the cargo tube is inserted into the microbubble and (b) a micromotor which is used to move the polymer- and cargo-carrying tubes translationally. Adapted from [60, 61].

The wood panel was cut in 5 pieces; two 10x5 inches^2, one 5x7 inches^2, and two 1.97x2.75 inches^2 to prepare the stand which fits inside the container which will house the entire system. First three wood panels were adhered together via glue and became a stand with a base (**Figure 32a** and **32b**), which the glass vial is placed in (**Figure 32f**). The sides of the stand enable the micromotors to be attached at an angle (**Figure 32e**). The goniometer and one micromotor for the drug injection were attached via screws. Then, both tubes for the polymer and cargo were attached to the each micromotor. These two micromotors were placed on the micromotor holders. The glass vial was fixed on the base of the stand by its insertion into a hole. Its exact location is not critical as its purpose is to simply hold the 10% CMC which will be used to suspend the microbubble

in a precise location in space relative to the micromotors and independent of the glass vial.

Clay was used to quantify the required angles to have the polymer- and cargo-carrying tubes meet at the same location in space (this will be finely tuned based on the goniometer and micromotors). The micromotor supporters (**Figure 32e**) were cut to match the defined angles indicated by the clay.

3.7.3   Results and discussion

The measured angles of clay were quantified via a protractor at 16.27° for the polymer-carrying tube and 11.51° for the cargo-carrying tube. The length of each side of the micromotor supporters (**Figure 32e**) were around 7.5cm. After we assembled every component both tubes met at the same location, irrespective of the exact placement of the glass vial. The goniometer operation was necessary to inject drug exactly into the middle of the microbubble. The glued stand was sturdy enough to hold the weight of both micromotors.

Figure 32. Assembly of the wood stand's (a) walls (b) base (c) micromotors to translationally move the polymer- and cargo-carrying tubes (d) a goniometer to control the precise injection of the cargo within the microbubble (e) angled wood stands for attaching the micromotors to the walls and (f) a sample of a glass vial.

3.7.4 Conclusion

For the repeatability of microbubble formation, it is crucial to have consistent and automated parameters, to the extent possible.

The flexibility of the clay facilitated the quantification of the angles needed for the micromotor supports (**Figure 32e**). We observed that both tubes met in the glass vial, and the drug injection could be in the middle of the microbubble because the proper drug injection position was within the range of the goniometer.

3.8   ENGINEERING A SELF-CONTAINED LYOPHILIZATION-CAPABLE SYSTEM FOR THE MICROBUBBLES

3.8.1   Introduction

The automated apparatus is a self-contained system which includes (i) 2 syringe pumps, (ii) 2 micromotors, (iii) a goniometer, (iv) a UV bulb and (v) a vacuum pump. The syringe pump controls the injection rates and the timing (controlled by a library within Python) which will dictate the volume of the microbubbles' shell and the cargo contained therein. The mass of the cargo will be mainly controlled by the concentration used and not the volume. The cargo solution will have the pre-determined cryo-protectant ratios in preparation for the automated lyophilization. In order to create a

complete system for microbubble formation, it was necessary to combine the injection and UV curing systems to the lyophilization chamber. Therefore, a freeze-drying system was designed to accommodate both the polymer and cargo injections and the UV curing system.

The ideal condition for the microbubble lyophilization requires (i) a flash-freezing reservoir of liquid nitrogen to help retain the cargo within the center of the microbubble during the initial stages when the inner cargo bubble could float upwards while UV curing is taking place and(ii) and continued overnight lyophilization. In this section, we show the design of the vacuum chamber thus far to be used for lyophilization of the microbubbles.

3.8.2   Materials and Methods

3.8.2.1 Materials

A 3.5 gallons HDPE round pail were purchased from Grainger. 250 μL Glass barrels (Hamilton) are used for forming the microbubble and the cargo. A P-662 female luer to microtight assembly (Idex) is the total female part used to connect the tubes to the syringe pump barrels. The cargo tube is 12" in length and is a 30 gauge (inner diameter) tube (Hamilton). Clear Acetoxy curing RTV Silicone Sealant (Surebond®) was used for sealing the plastic container for sufficiently low pressures for lyophilization (the plastic container was cut and attached to a metal pot because the vacuum ended up collapsing

the bucket and we needed to strengthen the container). Legato 100 syringe pumps (KD Scientific) were used for controlling microbubble and drug injection rates. 0.5 dram borosilicate glass vial (VWR) was used for the primary microbubble container.

3.8.2.2 A self-contained lyophilizing system

The HDPE pail was used for the container which contained the stand, which holds two micromotors and the glass vial. The container was cut and glued to a stainless-steel pot to withstand the low temperature of liquid nitrogen and low pressures required for lyophilization. The already functioning lid from the plastic container which contains a transparent window, as well as an attachment point for the vacuum was a sturdy enough lid that we wanted to use it for the metal pot. We severed the portion that the lid attaches to and attached the metal pot thus the original lid and its plastic attachment portion was on the metal pot. Every leaking hold, which air could pass through, in the bucket and the lid was sealed using silicone sealant.

The stand, which was described in section 3.7, is able to be placed within this hybridized plastic-metal container.

3.8.3 Results and discussion

By applying the lyophilizing-capable vacuum (**Figure 33**), it was confirmed that the bucket was completely sealed using silicone sealant. Epoxy glue was intended to be

used for the sealing of the container initially but was found to be insufficient. The epoxy glue, however, was sufficient in attaching luer locks and tubes due to the epoxy glue resistance to chloroform. Both tubes for forming the microbubble and injecting the cargo can now be theoretically injected into the glass vial, which can contain 10% CMC.
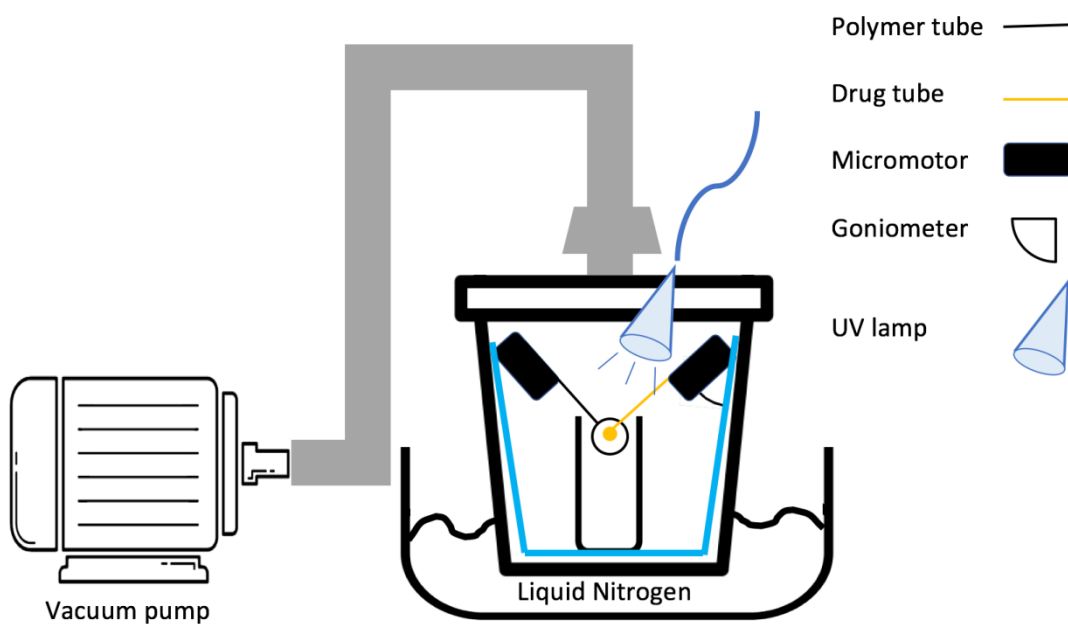
Figure 33. The design of the self-contained lyophilization system for microbubble formation.

This system has not been fully tested and we expect there to be a great deal of troubleshooting left for ensuring that this setup is kinetically controlled via LabView. The user interface is being built and automated by Whitney Souery, an undergraduate in

our lab. Whether this is actually capable of lyophilizing the microbubbles has not been able to be tested to date.

3.8.4   Conclusion

The container size is sufficiently large to contain every component needed for this system. How the liquid nitrogen flow into a secondary container is still yet to be determined. Furthermore, it is likely that we may need to have the glass vial protrude (yet still be sealed for lyophilization purposes) through the bottom of the container and into the liquid nitrogen. We are hoping this will not be required and have chosen a low-pressure-withstanding pot that will also facilitate thermal conduction for faster freezing times of the microbubble. If we need to slow down the process of freezing to not break internal components, this will be accomplished. We have confirmed that the hybridized pot is capable of withstanding the lyophilizing-capable vacuum. We need to have wires coming through the container, while still being sealed off to ensure the pressure is low enough for the sublimation process during lyophilization. All of this needs to be further investigated. Our goal is controlling every operation, such as microbubble and cargo injection, UV curing, and lyophilization using Labview and Python.

Through this automation system, we believe that microbubble fabrication will be more accurate and precise, and the microbubble physicochemical properties will be reliable and repeatable.

4 ENGINEERING CARGO RELEASE TIME OF THE MICROBUBBLES

4.1 QUANTIFY HOW DIFFERING MOLECULAR WEIGHTS OF PCL AFFECT RELEASE TIME OF THE MICROBUBBLES

4.1.1 Introduction

The release from PCL microparticle depends on the molecular weight, molecular weight distribution, and crystallinity. Such parameters affect the cargo entrapment and the structural stability of the microparticle. The kinetics of the cargo release can be controlled by not only hydrophobicity but also molecular weight of these polymers.

He, et al. produced microparticles with mPEG (MW 5kDa) and PCL (MW 20kDa) microparticles by double emulsion evaporation method and achieved approximately 20% more drug release when compared to plain PCL (MW 25kDa) after 42 days [62]. Considering this experiment, release of cargo is mainly due to erosion of polymers within the aqueous phase. However, Jeong, et al. reported that the main reason which dictates the release profile for the cargo is the cargo diffusion from amorphous regions of the microparticle [63]. Here we investigate the role of molecular weight of PCL within our microbubbles.

4.1.2 Materials and Methods

4.1.2.1 Materials

Synthesized PCLTA, PCL (average Mn 14 kDa and 45 kDa) (Sigma Aldrich), and 2hHydroxy-2-methylpropiophenone (photoinitiator) (TCI AMERICA) were used for PCL/PCLTA microbubbles. Legato 100 Syringe Pump (KD Scientific) was used for the microbubble injection. 0.5 dram borosilicate glass vials (VWR) were used for microbubble container. BSA-CF488 dye conjugates (Biotium) was used as the cargo.

4.1.2.2 Fabrication of different molecular weights of PCL/PCLTA microbubbles

14 kDa and 45 kDa PCL was dissolved in chloroform and the concentration was held at 800 mg/mL for forming the microbubble. This PCL solution was mixed with PCLTA as 1:3 volume ratio in order to solidify the PCL microbubble shell using chain entanglements with lower molecular weight PCL which had terminal acrylate groups, enabling UV curing. 1 μL of photoinitiator was added (0.05% final concentration). The polymer was loaded within the 250 mL glass barrel and the microbubble injection rate was controlled by the syringe pump at 0.5 μL/sec for 10 seconds.

250 μL of PBS was added to BSA-CF488 stock, and the concentration was 4 mg/mL. 12.5 mg of CMC was added to this cargo solution, so 5% (w/v) CMC BSA-CF488 cargo solution was prepared. This cargo was injected into the formed

microbubble using 34 G needle, then the microbubble was cured under UV light for 10 minutes. After confirming the microbubble was cured by confirming the hardness with pipette tips, the microbubbles were frozen in liquid nitrogen for 20 minutes and lyophilized overnight.

After lyophilizing, microbubbles were washed and soaked in 500 µL of PBS. The PBS solution was collected and analyzed for the fluorescence intensity every 2 days.

4.1.3   Results and discussion

14 kDa PCL/PCLTA microbubbles resulted in two separate bolus releases on day 2 and day 6 (**Figure 34**). The day 2 bolus is likely due to the presence of the fluorophore on the outer surface which has a greater propensity to partition into the organic phase (the cargo escaped as the cargo injecting tube was removed from the liquid shell of the microbubble. There were several failures involving premature release of the cargo by the temporary conduit created when removing the cargo injecting tube. This escaped cargo was dissolved in the outer 10% CMC solution and adsorped and partially was absorbed into the shell of the microbubble, according to confocal microscopy. The first release was the cargo from the microbubble surface which escaped. After degradation of the microbubbles over 6 days, microbubbles showed a second release from the internal cargo bubble. The released amount of the second bolus was less than the first release amount because the amount of drug in the 10% CMC was more than was actually injected into the microbubble. We will be optimizing this further.
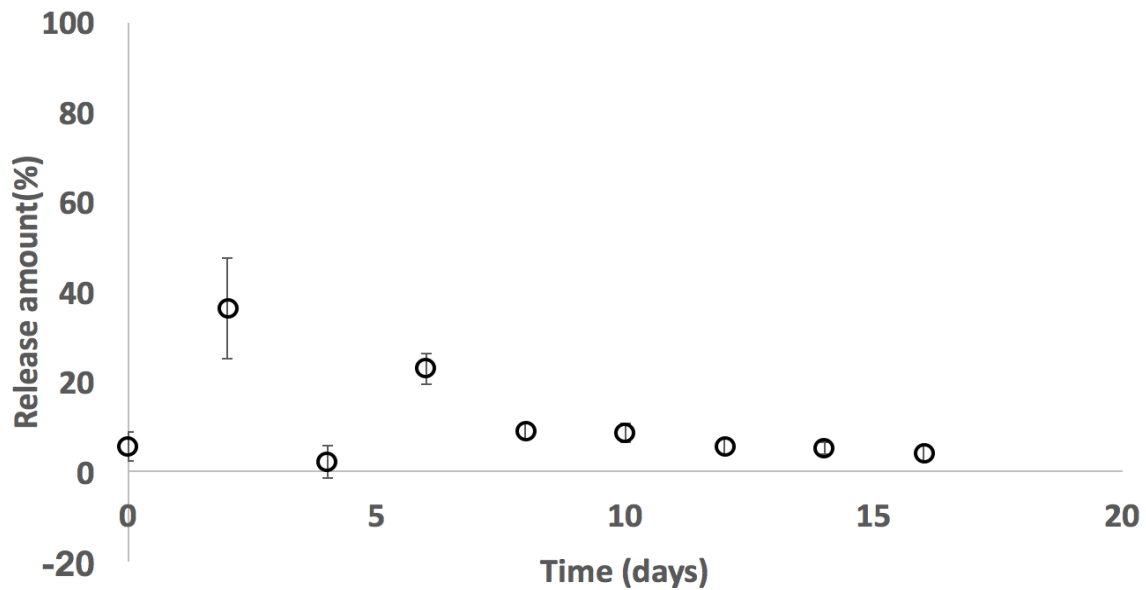
Figure 34 BSA-CF488 Release Profile from 14 kDa PCL/PCLTA.

45 kDa PCL/PCLTA microbubble also showed an initial bolus release on day 2, similar to the previous microbubbles, confirming this is likely independent of the wall thickness of the microbubble (**Figure 35**). The release of the cargo on day 2 was for the same reason as the 14 kDa PCL/PCLTA microbubbles. The second bolus was later than 14 kDa PCL/PCLTA microbubbles. Higher molecular weight polymers have longer chains, and thus can entrap the cargo longer than lower molecular weight microbubbles due to chain entanglement.
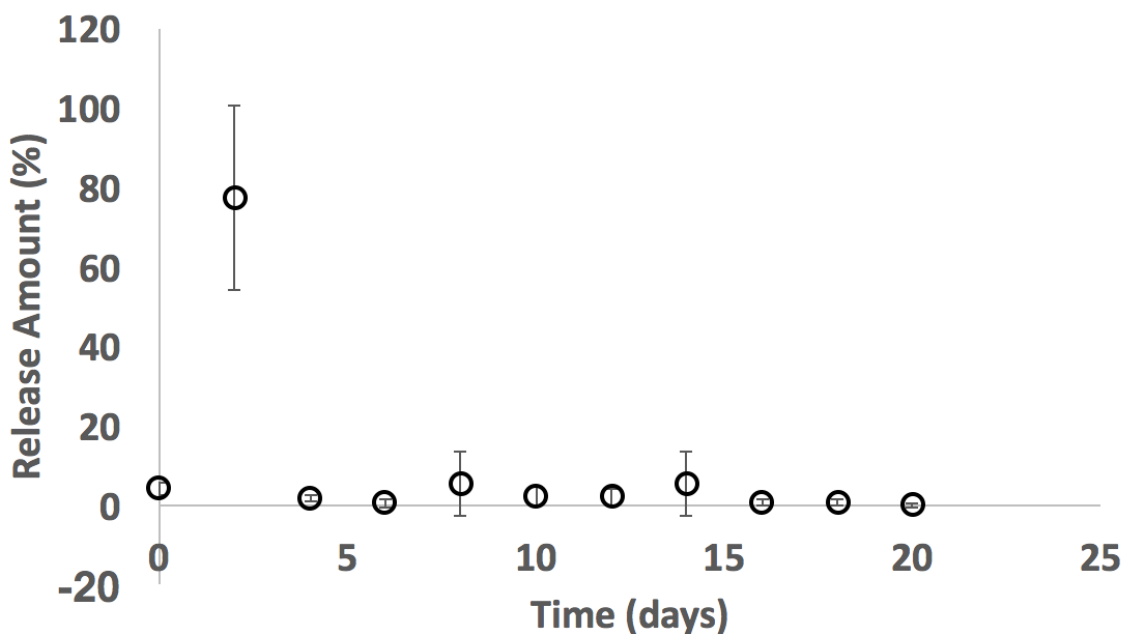
Figure 35 BSA-CF488 Release Profile from 45 kDa PCL/PCLTA.

4.1.4 Conclusion

Two different molecular weight of microbubbles showed different release
profiles. Both microbubbles burst twice, and the first burst was on day 2. However, the
second burst was on day 6 for 14 kDa PCL/PCLTA and on day 14 for 45 kDa
PCL/PCLTA (release profile is ongoing). The first burst of the drug, which was
dissolved in 10% CMC solution, was released from the surface of microbubbles. The
second burst of the drug was from the inside of the microbubble. 45 kDa PCL/PCLTA
has longer chain and erosion takes more time than 14 kDa PCL/PCLTA. Due to their
molecular weight difference, they have different release profile for the second release.

Through this work, we observed that increased molecular weights result in longer release profiles. Generally, there is a period from one week to a few months or a year between vaccine administrations. For the single injection vaccine, we can control the burst time by controlling the molecular weight of the microbubbles, we could use surface eroding polymers, and we could use thicker shells. The next chapter describes the correlation between the shell thickness of the microbubble and the release time.

4.2 QUANTIFYING HOW VARYING THE MICROBUBBLES' THICKNESS OF THE SHELL CONTROLS THE RELEASE TIME

4.2.1   Introduction

The release kinetics is highly dependent on the cargo encapsulation method. Single/double emulsion solvent evaporation technique distributes the cargo throughout the microparticles. Therefore, the diffusion of the cargo through the polymeric bulk have a greater contribution to the release kinetics than the polymer degradation/erosion [63]. It is highly probably that there are many diameters within a microparticle itself, in the context of double-emulsion-based microparticles. Thus, the conventional encapsulation method leads to a continuous release of cargo instead of bolus release, unless the catastrophic failure of the microparticles can be taken advantage of in order to achieve a secondary burst as was discussed earlier.

Since the cargo was encapsulated into the microbubble by injection, a bolus release profile was expected. Therefore, the release kinetics depends on the degradation/erosion of this shell and the cargo diffusion through the polymeric shell as well. In this chapter, the influence of microbubble's shell thickness on the release time was analyzed. Different cargo amounts were injected to the PCL/PCLTA microbubbles, so the polymeric shell is thicker to a smaller cargo volume and thinner with a bigger cargo volume.

4.2.2   Materials and Methods

4.2.2.1 Materials

Synthesized PCLTA, PCL (average Mn 45 kDa) (Sigma Aldrich), and 2-hydroxy-2-methylpropiophenone (photoinitiator) (TCI AMERICA) were used for PCL/PCLTA microbubbles. Legato 100 Syringe Pump (KD Scientific) was used for the microbubble injection. 0.5 dram borosilicate glass vials (VWR) were used as the primary microbubble container. BSA-CF488 dye conjugates (Biotium) was used as the model antigen for detection purposes.

4.2.2.2 Fabrication of PCL/PCLTA microbubbles with different shell thickness

45 kDa PCL was dissolved in chloroform and the concentration was held at 800 mg/mL. This PCL solution was mixed with PCLTA as 1:3 volume ratio to enable curing. 1 µL (0.05% final concentration) of the photoinitiator was added. The polymer was loaded to the 250 µL glass barrel and the microbubble injection rate was controlled by the syringe pump at 0.5 µL/sec for 10 seconds.

250 µL of PBS was added to BSA-CF488 stock, and the concentration is 4 mg/mL. 12.5 mg of CMC was added to this cargo solution, so 5% (w/v) CMC BSA-CF488 cargo solution was prepared.

The microbubbles were divided into two groups depends on the injected cargo volume. The cargo volume was controlled by the syringe pump. The smaller cargo volume would thus result in a thicker microbubble shell, and a larger cargo volume would result in a thinning of the microbubble shell.

The smaller cargo volume was injected for 2 seconds at a 0.5 µL/sec rate. The large cargo volume was injected for 5 seconds at the same rate. The microbubble was cured under UV light for 10 minutes. After confirming the microbubble was cured (similarly to the way we described previously), the microbubble was frozen in liquid nitrogen for 20 minutes and lyophilized overnight.

After lyophilization, the microbubble was washed and soaked in 500 µL of PBS. The PBS solution was collected and the fluorescence was analyzed every 2 days.

4.2.3   Results and discussion

The release of the cargo on day 2 was for the same reason as the different molecular weight release study (**Figure 36**). Since the microbubble for the release study with different shell thickness is formed with 45 kDa PCL/PCLTA, the second burst will be later than 14 kDa PCL/PCLTA microbubbles of the different molecular weight release study.
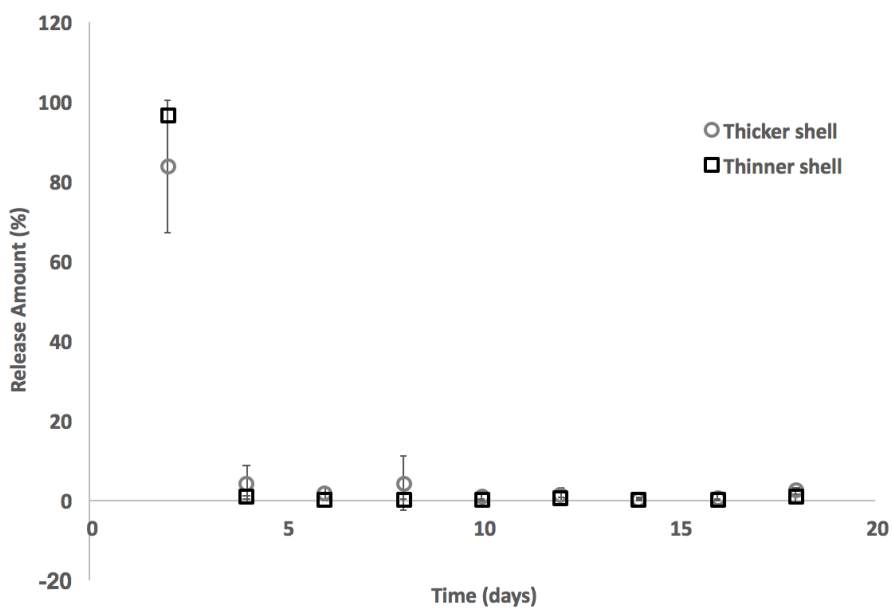
Figure 36 BSA-CF488 Release Profile two from different shell thickness PCL/PCLTA microbubbles.

4.2.4   Conclusion

Thicker shell microbubble causes more time to degrade the shell, and thus can entrap the cargo longer than thinner shell microbubbles. We expect to observe later second burst from thick shell microbubble.

5   QUANTIFY STABILITY OF HIV AND HEPATITIS B ANTIGENS

5.1 QUANTIFY HOW THE HIV GP120/41 AND HBSAG AYW ANTIGENS ARE STABLE IN TIME IN AN AQUEOUS ENVIRONMENT VERSUS IN A CRYO-PROTECTANT CONTEXT AT VARYING TEMPERATURES

5.1.1   Introduction

Among many factors, temperature, alongside with hydrolysis, is a crucial factor which affects protein stability. Fatunmbi, et al. showed that the avian influenza virus maintained its stability without any loss for 42 hours at -20 ℃ and -196 ℃ [64].

The function of cryo-protectants is also critical for stabilizing the structure and, hence the function, of the protein. Trehalose is one of a number of saccharides which can be used as a cryo-protectant and is arguably the most used cryo-protectant amongst the saccharides (other examples include, sucrose). The exact mechanism as to what degree saccharides absorb water which is retained even throughout the lyophilization process [65]. It is for this reason, that the saccharides help protect the function of the protein. Also, the protein is more likely to be denatured if the proteins interact with themselves; hence having many saccharides present causes the protein to mainly interact with the less-denaturing saccharides (in comparison to other proteins. Generally speaking, cryo-protectants are commonly used in high molar ratios in comparison to the antigen being

protected; the excess molar ratio is on the order of 100s to 1000s of times more than the antigen.

To evaluate the protein stability in the microbubble, the functionality of the antigen is analyzed using an enzyme-linked immunosorbent assay (ELISA). This data is compared to the control antigen which has been stored properly and is considered to be non-degraded; in this way percent functionality retained is able to be quantified. Using a calibration curve, the mass of the remaining functional antigen in time can also be quantified.

In this section, the control antigen was analyzed in various conditions so that we are able to know how well our microbubbles are capable of protecting antigen (in the presence and in the absence of a cryo-protectant) at differing temperatures and time points. To examine the effects of temperature, the antigen, functioning as a negative control was placed at three different temperatures in PBS; 4 ℃, room temperature and 37 ℃, in aqueous environment. Also, to identify the role of the cryo-protectants, trehalose was added to antigens, and subsequently lyophilized. The functionality of the mixture was analyzed at various time points and these results are considered the best-case scenario, or in other words the positive control. By varying the trehalose concentration, optimized concentrations for the enhancement of the antigen functionality was identified.

5.1.2 Materials and Methods

5.1.2.1 Materials

Coating buffer (ab210899), Recombinant HIV-1 gp120 + gp41 protein (ab49054), Anti-HIV-1 gp120 antibody conjugated to horseradish peroxidase (HRP) (ab53840), Anti-Hepatitis B Virus Surface Antigen (Ad/Ay) antibody-HRP (ab34553), and 450 nm Stop Solution for Tetramethylbezidine (TMB) Substrate (ab171529) were purchased from Abcam. HBsAg preS2 recombinant protein (HBS-870-005P) (eEnzyme), Non-fat dry milk (Andwin Scientific), and 1-Step™ Ultra TMB-ELISA Substrate Solution (Thermo scientific) were other material for ELISA. Trehalose (Acros Organics) was used for cyro-protectant.

5.1.2.2 ELISA protocols

HBsAg ayw antigen was diluted in a coating buffer as 10 μg/mL and loaded on the 96 well plate. Serial dilution of half concentration occurred, so each well has 50 μL of antigen solution. The plate was incubated for 2 hours at room temperature on the 400rpm plate shaker. After incubation, the plate was washed three times using 300 μL PBS for 5 minutes on the 400 rpm plate shaker. 300 μL of 5%(w/v) nonfat dry milk solution was loaded and incubated overnight at 4 ℃ for preventing non-specific binding of the antibody. Blocking solution washed twice with same methods of antigen washing.

97

Anti-Hepatitis B Virus Surface Antigen (Ad/Ay) antibody-HRP conjugates was diluted as 1:400 and loaded 100 µL. After 2 hours incubation at room temperature, the plate was washed three times with same methods of antigen washing. 100 µL of TMB solution was loaded and incubated for 15 minutes at room temperature by covering with foil. 100 µL of stop solution was added and the absorbance was read at 450 nm after 10 minutes from stop solution loading.

The same protocol was applied for HIV-1 gp120/41 ELISA except 1:800 dilution (1.25 µg/mL) of antigen and 2 hours of blocking.

5.1.2.3 Antigen stability without trehalose

Both HIV-1 gp120/41 and HBsAg ayw antigens were diluted in coating buffer as 80 µg/mL. The antigen solution was aliquoted as the same volume in nine microtubes. Microtubes were placed at 4 ℃, room temperature, and 37 ℃. Antigen samples were collected and frozen on days 4, 7, 14 and 21. After collecting day 21's samples, the functionality of every antigen was analyzed by ELISA.

5.1.2.4 Find optimized trehalose concentration

0.5 M of trehalose solution was prepared by adding 0.1797 g of trehalose to 1050 µL of coating buffer. Six different concentration of trehalose solutions were prepared

from 5×10^{-1} M to 5×10^5 M solution using a 10x serial dilution. 10 µg/mL of both antigen solutions were prepared by diluting the antigen stock using various trehalose solutions. Antigen solutions were placed at 37 ºC oven after aliquoting. The functionalities of both antigens (HIV-1 gp120/41 and HBsAg ayw) were analyzed on day 4 using ELISA.

5.1.2.5 Antigen stability with Trehalose

80 µg/mL of 625 µL of antigen solutions were prepared by diluting antigen stock using coating buffer. 17.11 g of trehalose was added to the antigen solutions for creating a 0.5 M trehalose solution. The antigen within the trehalose solution was aliquoted to 36 microtubes and lyophilized overnight. Microtubes were placed at 4 ºC, room temperature, and at 37 ºC. Antigen samples were collected and frozen on days 4, 7, 14 and 21. After collecting day 21 samples, the functionality remaining of the antigens with varying conditions were analyzed by ELISA.

5.1.3   Results and discussion

5.1.3.1 ELISA

After many trials, the ELISA protocol was finalized. Casein, 1%, 3%, 5% BSA, and 1%, 3% nonfat dry milk solutions were not sufficient in terms of preventing non-

specific binding. The blank wells which only coated with PBS indicated a high background even after blocking with casein, BSA, and low concentrations of nonfat dry milk solutions. Also, the incubation time of the blocking buffer appeared to not affect the results. 2 hours at room temperature and overnight at 4 ºC blocking with 5%(w/v) nonfat dry milk solution did not show any difference in decreasing the excessively high background as well. When loaded solutions were removed from the plate at each step, tapping the plate was preferred as it helped avoid disrupting the results by mechanical disruption caused by the pipette during the aspiration process.

Among 1:200 to 1:1000 antibody dilutions, 1:400 dilution for HBsAg ayw antibody and 1:800 dilution for HIV-1 gp120/41 antibody was sufficient in decreasing the excessively high background which could then be used as the calibration curve. Absorbance showed a linear trend between 2 and 10 µg/mL of antigen concentrations (**Figure 37**).
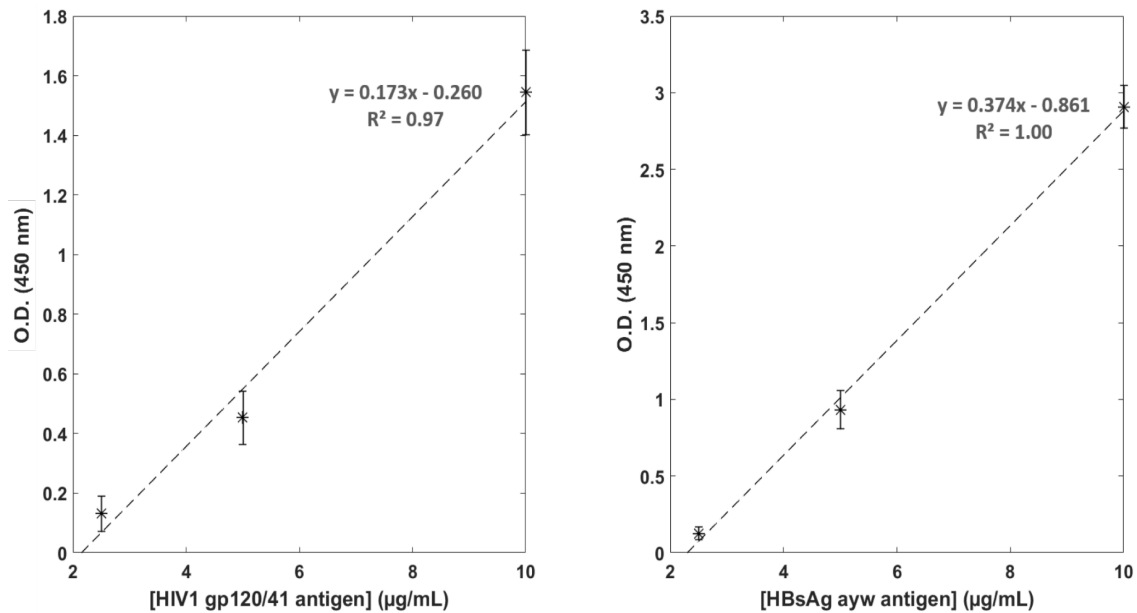
Figure 37. ELISA calibration curve of (a) HIV-1 gp120/41 (b) HBsAg ayw.
5.1.3.2 Antigen stability without Trehalose

HIV-1 gp120/41 antigen samples were collected and analyzed at weeks 1, week 2, and week 3 via ELISA. HIV-1 gp120/41 underwent loss of functionality as the weeks progressed. Also, the antigen formulations which were stored at higher temperatures indicated an enhanced loss of functionality due to thermal degradation (and also an increase in the hydrolysis due to an increase in water molecules' thermal energy levels. After 3 weeks, the functionality of HIV-1 gp120/41 reduced approximately 70% for all the conditions, regardless of the storage temperature. This means that HIV-1 gp120/41 antigens are susceptible to fast thermal degradation, even at 4 ºC. After 3 weeks, the functionality at 37 ºC, room temperature, and 4 ºC was reduced to 37%, 44%, and 48%, respectively.

The remaining mass of antigen which its percent functionality remaining was quantified, compared to the control (zero degradation – stored at -20 ºC) on days 4 and day 7. This indicated that there was a continual decrease in the HBsAg ayw antigen functionality as a function of time, according to the **figure 38**. Also, the degree to which higher storage temperatures resulted in faster decrease in functionality was quantified; this shows the high influence of thermal conditions on antigens' stabilities. On day 4, the samples which were maintained at 4 ºC retained 90% of function, whereas samples at 37 ºC retained only 41% of its functionality. After 3 weeks, the functionalities at 37 ºC, room temperature, and 4 ºC were reduced to 29%, 54%, and 80%, respectively.
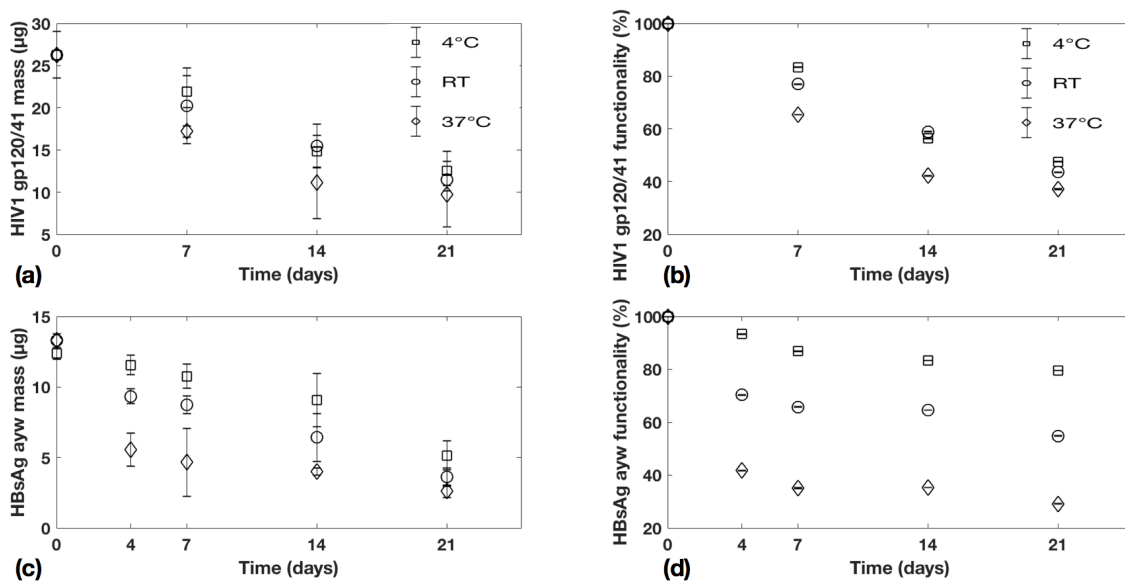
Figure 38. Antigen stability without trehalose. (a) mass of HIV-1 gp120/41, (b) functionality of HIV-1 gp120/41, (c) mass of HBsAg ayw, and (d) functionality of HBsAg ayw.

The functionality seems to be directly related to the amount of antigen available, since the less degraded samples present higher functionality signals (i.e. samples kept at 4 ºC had a lower functional loss). The upcoming results with trehalose in the context of the microbubble (these endeavors are currently ongoing within the lab) are expected to show attenuated loss of functionality due to the cryo-protectant effect.

5.1.3.3 Quantify optimized trehalose concentrations

The functionality of both antigens, HBsAg ayw and HIV-1 gp120/41, were increased with increasing trehalose concentrations (**Figure 39**). Even though it is apparent from these two graphs that there is a significant increase of functionality between 5×10^{-3} M and 5×10^{-4} M trehalose, both antigens' HBsAg ayw and HIV-1 gp120/41 functionalities kept increasing and reached 99.05% and 99.78% at 0.5 M trehalose, respectively. Because both antigens demonstrated almost 100% of functionality on day 4, trehalose concentrations of 0.5 M were used as the best-case scenario, or positive control (which is our gold standard of comparison).
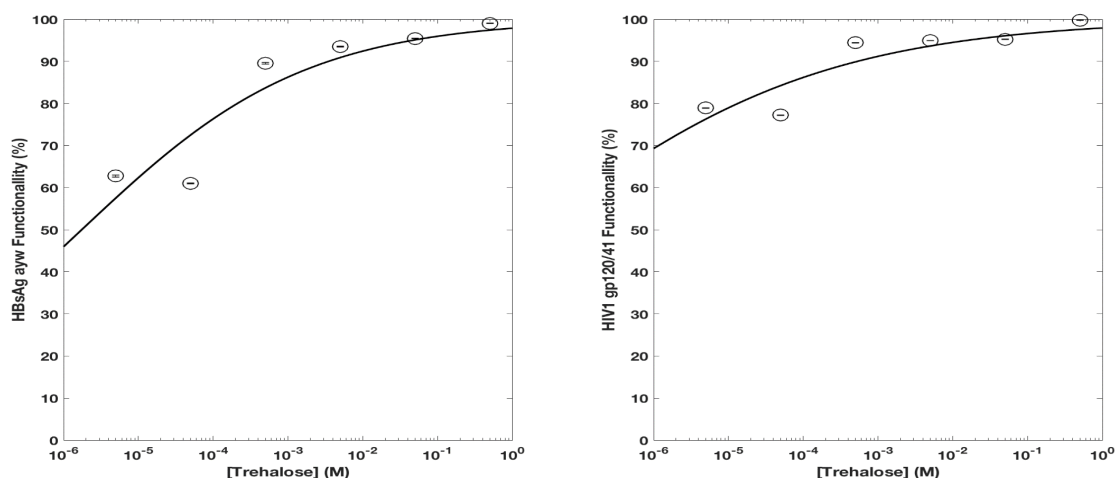
Figure 39. Correlation between antigens functionality and trehalose concentrations (a)HBsAg ayw (b) HIV-1 gp120/41.

5.1.3.4 Antigen stability with Trehalose at 0.5 M

In the presence of trehalose, HIV-1 gp120/41 antigens were more stable (**Figure 40a and b**). After 3 weeks, the functionality at 37 ºC, room temperature, and 4 ºC was reduced to 39%, 46%, and 51% in presence of trehalose, respectively. 2-3% of functionality was increased when it was compared to the functionality in the absence of trehalose.

The functionality of HBsAg ayw with trehalose was better than the functionality of HIV-1 gp120/41 (**Figure 40c and d**). After 3 weeks, the functionality at 37 ºC, room temperature, and 4 ºC was reduced to 59%, 60%, and 82%, respectively. Thus, trehalose was shown to have a thermal protective or thermal stabilizing effect for our antigens.
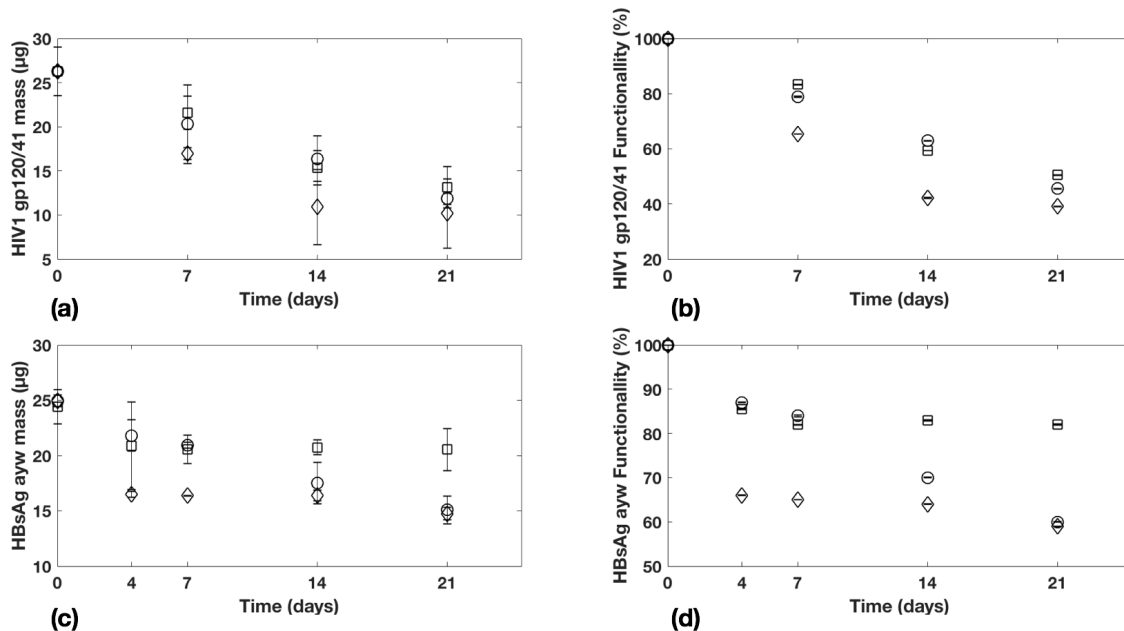
Figure 40 Antigen stability with trehalose. (a) mass of HIV-1 gp120/41, (b) functionality of HIV-1 gp120/41, (c) mass of HBsAg ayw, and (d) functionality of HBsAg ayw.

5.1.4   Conclusion

The ELISA protocols for each antigen was optimized after many trials. The high background was resolved using 5% non-fat dry milk solution, and the blocking time did not affect the results after 2 hours. The proper antibody dilution ratios were 1:400 for HBsAg ayw and 1:800 for HIV-1 gp120/41, respectively. From 2 μg/mL to 10 μg/mL the results showed a linear calibration curve.

The extent to which both antigens lost their functionality with increasing temperature as time proceeds was quantified. The loss of functionality was significantly

lower at 37 ℃ compared to the colder temperatures. After three weeks, HBsAg ayw lost 63% of the functionality and HIV-1 gp120/41 lost 71% of the functionality at 37 ℃. Trehalose enhanced the stability of both antigens. The stability of antigens increased with the trehalose concentration. On day 4, HBsAg ayw and HIV-1 gp120/41 showed 99.05% and 99.78% of stability with 0.5 M trehalose, respectively. Therefore, 0.5 M of trehalose was used to examine the antigen stability with the cryo-protectant.

While holding the temperature constant while varying trehalose, both antigens showed better functionality than without trehalose. HIV-1 gp120/41 lost 61% of the functionality and HBsAg lost 41% of it at 37 ℃. Even though both antigens' stabilities were enhanced, HBsAg ayw showed a greater enhancement than the HIV-1 gp120/41 antigen. This result may be explained by the fact that HIV-1 gp120/41 antigens mutate too fast, in comparison to when they are stabilized with trehalose.

The stability of antigens and the function of trehalose as a cryo-protectant were described in this work and will serve as the positive and negative controls or the gold standards for our microbubble application to delivery these specific antigens. In future work, we can apply trehalose also in the microbubbles and compare to this stability data but there will be a tradeoff between how many microbubbles will need to be delivered as the trehalose concentrations are increased because space that the antigen within the microbubbles will decrease due to the presence of more trehalose cryo-protectant.

6   DNA- AND AMINO ACID-BASED VACCINE DELIVERY SYSTEM

AGAINST INFECTIOUS DISEASES*

6.1 INTRODUCTION

With the continual improvement of DNA sequencing technology, we can better understand key conserved sequences which can be transcribed and translated into antigens and discover or engineer sequences which may be used for protection (i.e., TSOL18[66-68]). Via DNA recombinant technology we are able to mass produce nucleic acid code which can be directly delivered and can be subsequently processed and displayed by antigen presenting cells (APC)s for eventual seroconversion by the vaccinee's own transcription and translation machinery. Furthermore, via DNA recombinant technology peptides or proteins or subunits thereof can be mass produced in cells (i.e., E. coli and yeast) for vaccine manufacturing.

Many peptide and protein vaccines require a cold chain delivery (i.e., Recombivax HB®, Engerix-B®), whereas DNA vaccines are considered more thermostable (**Figure 41:(1)**). The vaccine may be uptaken intracellularly via endocytosis (**Figure 41:(2)**) [69]

or interact extracellularly via the toll-like receptor (TLR)2/4 pathway, resulting in the expression of pro-inflammatory cytokines and chemokines (interleukin (IL)-8/10, TNFα) (**Figure 41:(3)**). Plasmid DNA can either be randomly encapsulated by the nuclear envelope during mitosis or actively transported to the nucleus via nuclear localization signals (i.e. DNA-targeted sequences – SV40 [70]) (**Figure 41:(4)**).The proton sponge effect plays an important role for the plasmid DNA to escape the endolysosomal degradation pathway (**Figure 41:(5)**). Via the cytosolic degradation pathway, the amino acid-based antigen is degraded into peptides and presented by MHC II extracellularly to CD4$^+$ T cells (**Figure 41:(6)**) [71]. Via the proteasome degradation pathway (ubiquitin-proteasome pathway), antigens become peptides, which interact with CD8$^+$ T cell recptors (TCR)s via MHC I extracellularly, post-maturation which takes place mainly within the Golgi apparatus (**Figure 41:(7)**). DNA vaccines may contain unmethylated CpG sequences which function as a pathogen-associated molecular pattern (PAMP) and can activate TLR9 in the endosome, eventually releasing IL-4 and IFNα (**Figure 41:(8)**). The immune response can be Th2-biased (antibody-mediated) or Th1-biased (cell-mediated), depending on the cargo, the delivery vector, the adjuvant, and the context of antigen presentation (**Figure 41:(9)**) [72].

This article will discuss DNA- and amino acid-based vaccine delivery systems against infectious diseases, with an emphasis on polymeric-based applications. More specifically we will discuss: a brief historical perspective of vaccines and vaccine classifications; the engineering of kinetics for vaccine delivery; enhancing the duration of protection via non-kinetic approaches; enhancing the stability of cargo; the state of the

art in DNA-based vaccines; manufacturing and engineering DNA; the stability and safety of DNA vaccines; plasmid delivery; controlling gene expression via plasmid engineering and gene circuits; overcoming immunogenic issues of DNA-based vaccines; examples of DNA-based vaccine commercial successes; as well as give a summary of the state of the field, and report our perspective on future directions.
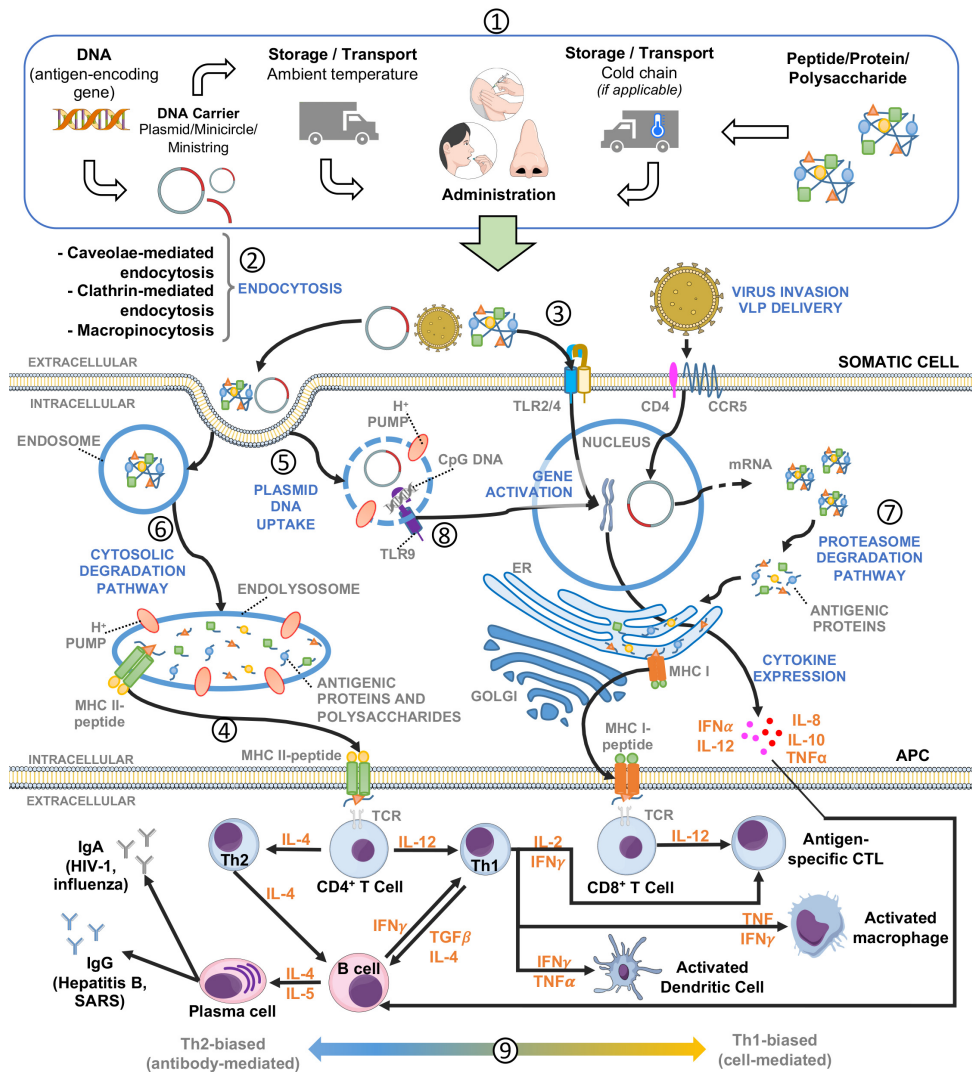
Figure 41 DNA- and amino acid-based vaccines. (1) Storage/transport via cold chain for amino acid-based vaccines versus more thermostable DNA-based vaccines; (2) endocytosis; (3) extracellular activation, through TLR2/4, resulting in the expression of pro-inflammatory cytokines and chemokines (IL-8/10, TNFα); (4) plasmid DNA uptake; (5) Proton sponge effect for DNA-based vaccines (6) the cytosolic degradation pathway, resulting in MHC II antigen presentation to CD4+ T cells; (7) the proteasome degradation pathway and the eventual MHC I antigen presentation to CD8+ T cells; (8) CpG sequences activating TLR9 and the resulting in IL-4 and IFNα release; (9) Th2-biased (antibody-mediated) and Th1-biased (cell-mediated) responses, depending on the context of antigen presentation.[72] (APC, antigen-presenting cell; CCR5, C-C chemokine receptor type 5; CpG DNA, DNA fragment containing cytosine nucleotide followed by guanine nucleotide; CTL, cytotoxic T lymphocyte; ER, endoplasmic reticulum; IFN, interferon; Ig, immunoglubulin; IL, interleukin; MHC, major histocomppatibility complex; TCR, T cell receptor; Th, T helper cell; TNF, tumor necrosis factor; TRL, toll-like receptor; VLP, virus-like particle).

110

6.1.1 From variation to vaccine: a historical perspective

Variolation itself is a crude method for introducing the variola virus intentionally by often simply scratching the scabs and pus of an infected individual into another to provide future protection. The variola virus, also known as smallpox, causes symptoms of fever, papules, and pustules. The Greek historian Thucydides reported a protective effect in smallpox survivors around 400 B.C.[73] Around 900 A.D., historical records describe nostril inoculation with the dry matter of smallpox pustules in China [74]. The Chinese book, "Great Herbal" describes the use of "powdered cow ice into child's nose" in 1597. According to historical records, variolation was commonly practiced in India, Africa, and China before the 17th century. Variolation inevitably led to many fatal infections but also provided protection against smallpox in many cases [75]. In Europe, the first records show that variolation was first used in Denmark, and then started spreading from Turkey in the 18th century. The development of variolation in Europe allowed conquistadors to use smallpox as a biological weapon to reduce the population of Native Americans during conquests, as variolation practices in the New World were less common [73].

The variola virus by many is considered the first infectious disease eradicated by a first-generation vaccine. Edward Jenner observed that a dairy maid had cowpox lesions on her finger and inoculated it into an 8-year-old neighbor boy, James Phipps who subsequently contracted cowpox and recovered in just a few days. Latter Jenner then exposed James Phipps to smallpox and the young boy was protected due to cross-

111

reactivity. Jenner published the result in the book "An Inquiry into the Causes and Effects of the Variolae vaccinae, a disease discovered in some of the western counties of England, particularly Gloucestershire and known by the name of Cow Pox". Vacca means cow, and vaccinia means cowpox in Latin, from which the word vaccine originates. According to the statistics of Jurin, the average mortality rate by smallpox was at one point 16.5% [76, 77]. Smallpox spread throughout European countries in the 18th century, and caused more than 1/3 of all blindness cases and killed around 400,000 people every year [78]. Smallpox was officially declared eradicated in 1980. Another historical example of greatly reducing rates of infection is poliomyelitis, which was spurred by the beginnings of cleaner water, as people were exposed to a lesser degree; thus they were no longer naturally immune [79]. Jonas Salk`s inactivated poliovirus vaccine (IPV) exhibited 80-90% effectiveness in preventing paralytic poliomyelitis supported by a large-scale clinical trial, comprising 1.8 million elementary school-aged children (1st to 3rd graders) [80]. Meanwhile, Herald Rea Cox and Albert Sabin were describing an effective and safe live-attenuated Oral Poliovirus Vaccine (OPV) between 1957 and 1959, following the guidelines established by the WHO Expert Committee on Poliomyelitis [81, 82]. By the year of 1961, Sabin's OPV type 3 vaccine was officially recommended by the U.S. Surgeon General and more than 50 million were immunized [82]. In 1988, prior to the World Health Organization (WHO) announced the resolution to eradicate Poliomyelitis [83]. In September 2015, OPV type 2 was removed from the trivalent vaccine, given how rare OPV type 2 infections occur. The type 2 serotype of OPV will now solely be used for outbreaks [84]. Recently, several countries

have started using Salk`s IPV vaccine (type 2 strain) as a means to further protect

children born after April 2016 [85].

6.2   AN OVERVIEW OF VACCINE CLASSIFICATIONS

	Whole-cell vaccines		Inactivated toxoid vaccines	Subunit vaccines			
	Live attenuated vaccines	Killed or Inactivated vaccines		Polysaccharide vaccines	Conjugate polysaccharide vaccines	Recombinant protein vaccines	DNA vaccines
Administration	*i.e.*, subcutaneous, percutaneous, oral, intranasal	*i.e.*, intramuscular, intradermal, subcutaneous	*i.e.*, intramuscular	*i.e.*, intramuscular, subcutaneous		*i.e.*, intramuscular	*i.e.*, intramuscular Mucosal
Production	**-** Bacteria applications **+** Virus culture **+** Large-scale production **-** Biocontainment	**+** Low-cost production **+** Large-scale production	**-** Toxin purification procedures **-** High-cost production	**+** Bacterial capsule components **-** Biocontainment		**-** Protein folding **-** Protein degradation **+** Encapsulation	**+** Molecular stability **+** Low-cost production **+** Encapsulation
Immunogenicity	**+** Natural infection **+** Immunization efficiency **+** Single or few doses **+** Life-long protection	**+** Natural infection **-** Multiple doses **-** Adjuvant use **+** Long-term protection	**-** Multiple doses **-** Adjuvant use	**+** Molecular pathogen - Multiple doses - Adjuvant use	**+** Stimulus by Conjugation - Multiple doses - Adjuvant use	**+** Particle design - Multiple doses - Adjuvant use	**+** Animal applications **-** Human applications **+** Particle design
Biosafety	**-** Risk of infection **-** Risk of reversion **-** Risk for the immuno-incompetent	**+** Safer than LAVs	**+** Fewer side effects (*i.e.*, local and systemic)	**+** No live pathogenic components **+** Fewer side effects			**+** No live components **+** Fewer side effects **-** Autoimmune response **-** Integration to genome **-** Indel mutations
Storage and Transportation	**-** Cold chain delivery	**-** Cold chain delivery	**+** No need for cold chain delivery	**+** No need for cold chain delivery	**+** No need for cold chain delivery	**+** No need for cold chain delivery	**+** No need for cold chain delivery
Licensed vaccines (trade names)	M-M-R II, OPV, FluMist, Rotarix, ProQuad, Adenovirus, Zostavax	Pediarix, Ipol, BioThrax, Infanrix, Daptacel, Gardasil, Cervarix, Flublok	Decavac, Tenivac	Menomune, Pneumovax 23	PedvaxHIB, Hiberix, Comvax, Prevnar 13	Engerix-B, Rcombivax HB	-

Table 1 Generalized qualitative comparisons of vaccine classifications. Please note that a few exceptions may contradict the generalized qualitative comparisons. Administration routes, advantages and disadvantages in the contexts of production, immunogenicity, biosafety, transportation/storage, and also examples of commercialized DNA- and amino acid-based vaccines for each vaccine classification are tabulated.

113

For convenience to the readers, a brief overview of vaccine classifications is discussed (**Table 1**).

6.2.1 Live attenuated vaccines

Live attenuated vaccines (LAV)s are a weakened form of the wild viruses or bacteria, which have a near zero probability of causing an infection. Although weakened, the structural integrity of pathogenic patterns is sufficiently preserved, enabling the efficient production of neutralizing antibodies. In particular cases, a virulent strain may be continually cultured until a non-pathogenic version arises through genomic mutations, reducing virulence. With increasing attenuation, however, seroconversion becomes more unlikely as the attenuated version becomes increasingly dissimilar in comparison to the wild-type antigen. Commercially available examples of LAVs are Attenuvax® (measles), Mumpsvax® (mumps), Meruvax-II® (rubella), Rotateq® and Rotarix® (rotavirus), and FluMist® (influenza) (**Table 1**) [86, 87].

Despite the biosafety risks, LAVs are easier to prepare and provide effective immunization by eliciting strong and long-lasting humoral and cellular immune responses. The good immunogenicity of LAVs is related to a simultaneous recognition of multiple pathogen patterns. Hence, there is an increasing interest for adjuvants and novel delivery systems (e.g., virus-like particle, polymeric microparticles), which are attempts of mimicking the immunostimulation provide by LAVs [88-90]. The LAVs may have exogenous material due to the production process, such as egg protein, hence

the use of a LAV may be contraindicated in cases when the vaccinee may have an allergic response.

6.2.2   Killed or inactivated vaccines

Killed or inactivated vaccines (IV)s consist of pathogenic microorganisms which are partially or completely incapacitated through exposure to heat, high-energy radiation (e.g., gamma radiation) or chemicals (e.g., formaldehyde). These treatments can be used to induce minor changes in the structure of the antigen, preserving sufficient immunostimulatory capacity, and preventing pathogenic reversion. Safety-wise, the IVs are safer than LAVs. Moreover, IVs may require a greater amount of antigen and higher numbers of booster doses for life-long immune protection when compared to LAVs (**Table 1**).

Currently, IVs, in conjunction with adjuvants such as polysaccharides (PS) and TLR ligands, are intensely studied [91, 92]. IVs are used worldwide for immunizations against influenza serotypes. The production capacity achieved 6.372 billion/year in 2005 [93]. Examples of IVs available on the market include Ipol® (poliovirus), Fluarix®, Flublock®, Fluzone® (influenza), Imovax® (rabies) (**Table 1**) [94-98].

6.2.3 Toxoid vaccines

Toxoid vaccines are usually obtained from exotoxins released by a toxigenic bacterial strain. The toxin undergoes a heat or chemical treatment (e.g., formaldehyde treatment to produce the Tetanus toxin) in order to achieve a toxoid form with an acceptable toxic level for vaccine utility (**Table 1**). Therefore, the toxoid cannot induce a pathogenic condition within the patient, yet must improve the capacity of eliciting the antibody-mediated immune response. Generally, therapies against toxoids are antibody-mediated, which can be provided to the patient through passive immune therapy (e.g., administration of engineered antibodies, maternal antibodies to the fetus during pregnancy) [99, 100].

Toxoid vaccines can be mass-produced via bioreactors. A semi-continuous reactor maintains the toxigenicity of the pathogenic bacteria [101]. Tetanus and diphtheria toxoid vaccines are commercially available as a single-toxoid or a combined toxoid vaccine. Diphtheria and Tetanus vaccines are commonly combined with other types of vaccines such as DTaP (Infanrix®, Daptacel®), which includes acellular Pertussis as a constituent (Table 1) [102]. Toxoid vaccines present a low risk for infection and side effects but also are associated with immunogenicity. Recent studies report enhanced immunogenicity of toxoid vaccines combined with adjuvants such as the TLR4 agonist [103].

116

6.2.4 Unconjugated polysaccharide vaccines

Unconjugated or plain polysaccharide vaccines are a specific type of subunit vaccine (refer to the following section and **Table 1**) composed by polysaccharides from bacterial capsules. Bacterial capsules' polysaccharides which are highly antigenic can serve as the immune target within the vaccine. The risks of contamination and reversion are drastically reduced due to the vaccine composition. Polysaccharide vaccines are largely used in the immunization against pneumococcal, meningococcal, and typhoid diseases. Pneumococcal (PNEUMOVAX®23) meningococcal (Menomune®; Sanofi Pasteur, however, recently reported they will discontinue production of their Menomune vaccine; they are moving towards a conjugate vaccine replacement which is in phase III clinical trials) [104], and typhoid (Typhim Vi®) are examples of polysaccharides vaccines (**Table 1**) [105]. After vaccine administration, polysaccharide fragments interact with MHC II, which leads to a predominantly cellular immune response and limited humoral and memory IgG responses [106]. Particularly in infants there is an increased risk of infection due to their immature immune system [107].

6.2.5 Subunit vaccine

Subunit vaccines present superior safety profiles in comparison to whole-cell vaccines since there is no risk of infection or reversion of the microorganism to the pathogenic form. Thus, subunit vaccines can be ideal for immunocompromised patients

[108]. Despite subunit vaccines having several safety and stability advantages, the immunogenicity is often lower than ideal and requires adjuvants and booster doses to achieve adequate prophylactic immune responses, providing protection against future exposures. Subunit vaccines comprise a sub-portion of the antigen, as opposed to the whole microorganism employed for LAV and IV (**Table 1**). Subunit vaccines are generally more stable and more easily stored and transported. For example, Flood, et al. [109] reported the development of an H1N1 influenza subunit vaccine stabilized by freeze-drying process, which remained stable for 3 years at room temperature and 37 ºC.

6.2.6   Subunit vaccine - Conjugate polysaccharide

Because obtaining protective immunity using solely polysaccharides is challenging, more potent antigens (commonly a subunit) are commonly conjugated to the polysaccharides. For example, it was reported that the 13-valent pneumococcal conjugate vaccine elicited a greater functional response in pneumococcal vaccine-naïve adults, when comparing the specific antigens within the 23-valent pneumococcal polysaccharide vaccine [110]. Haemophilus influenzae type b vaccine (Hib) was the first protein-conjugate polysaccharide vaccine produced (1980) [111]. Hib is not given in sequential boosters, however, unless patients have had a splenectomy or are hematopoietic stem cell transplant recipients. The subsequent success of protein-conjugated polysaccharides vaccines against meningococcal and pneumococcal infections were in 1994 and 1996, respectively [112, 113].

In 2011, Avci, et al. [114] reported that T cells are not only capable of interacting with peptides on major histocompatibility complexes but also are capable of directly detecting the polysaccharide portion of the glycoconjugate. This discovery elucidates, in part, the mechanism behind unconjugated polysaccharide vaccines discussed above (glycovaccines) and will certainly impact the development of this type of vaccine.

6.2.7   Subunit vaccine – Non-recombinant

Regarding the production of non-recombinant subunit vaccines, the pathogenic microbes are cultured, disrupted, and the antigen of interest is extracted, purified into subunits through a combination of physical separation techniques (i.e., chromatography) [115], or chemical modifications, such as base extraction, disulfide reduction (i.e., via dithiothreitol or glutathione) [116]. For recombinant DNA-based subunit vaccines, a replicating vector (e.g., yeast or bacteria) is transformed with an engineered DNA sequence for transcription and translation into a recombinant protein vaccine which can then be administered to the vaccinee.

6.2.8   Subunit – Recombinant: amino acid based-vaccines

Recombinant protein vaccines are antigen-based synthetic proteins produced by recombinant DNA technology. For instance, Hepatitis B recombinant protein vaccine (HEPLISAV-B®, FENDrix®) is based on hepatitis B virus surface antigen (HBsAg) and

several HIV-1 recombinant protein vaccines are based on surface glycoproteins (gp140) [92, 117, 118]. In both cases, recombinant proteins were produced to mimic antigenic molecules and used them as immunostimulatory agents for prophylactic therapy. Because there is no pathogenic whole-cell or subunit in the recombinant protein vaccine formulation, the risk of reversion to virulence is minimized but the immunogenicity is inferior [119].

DNA and protein vaccines share a major part of the production process but vary in the immune system eliciting mechanisms (**Figure 41**). The first step consists in inserting the gene of interest (GOI) into the plasmid vector, which follows the transformation into the replicating bacteria or yeast. After the replication, the recombinant protein is extracted, purified, and prepared as a vaccine. In the case of DNA vaccines, commonly the replicating prokaryotic vector is disrupted, the engineered DNA is extracted, and purified to produce the final vaccine. After the administration to the patient, recombinant protein vaccines are internalized within the host cells, processed to antigenic peptides, which elicit the immune system. DNA vaccine must achieve the nucleus in order to use the host molecular machinery to promote the transient expression of the GOI. After the transcription and translation of the GOI, it is processed to antigenic peptides and elicits immune responses.

6.2.9   Subunit – Recombinant: DNA vaccines

In the case of a "DNA vaccine", the engineered DNA is directly administered to the patient and usually with a carrier, where transient gene expression provides the antigen of interest. DNA vaccines were introduced in the late 90s, when Wolff, et al. [120] injected plasmid DNA intramuscularly in mice. Afterward, Jiao, et al. [121] proposed the delivery of DNA plasmid to non-human primates, and Ulmer, et al. [122] described a vaccine against influenza using plasmid DNA in mice. The following sections will cover: the manufacturing and the engineering of DNA vaccines; the stability and safety of DNA vaccines; the kinetics controls for DNA vaccine release; the delivery barriers for DNA vaccines; the active nuclear transport for nuclear uptake of DNA; the control of gene expression via plasmid engineering and gene circuits; the techniques to overcome immunogenic issues of DNA vaccines; and the delivery methods of DNA vaccines in pre-clinical and clinical trials.

6.3   ENGINEERING KINETICS OF VACCINES VIA POLYMERIC METHODS

Although some LAVs and IVs are known for their favorable immunogenic properties and the induction of long-term protection with a single or a small number of doses, other vaccines such as toxoid and subunit vaccines generally require a greater number of exposures to the antigen compared to LAVs and IVs. However, the administration of multiple doses increases the vaccination cost, reduces the coverage

capacity, and creates additional obstacles to accomplishing long-term vaccination schedules, particularly in developing countries [123]. In this context, the vaccine research field is increasingly interested in the development of formulations that require fewer numbers of injections or employ delivery systems capable of auto-boosting.

Polymeric delivery systems' physicochemical properties can be fine-tuned to kinetically control antigen release profiles in order to improve the seroconversion of vaccines. The variety of polymers and structural modifications creates a plethora of possibilities in designing sustained release systems intended for multiple and long-term boost as a single injection. Understanding the structure-activity relationships aids the researchers in designing superior drug delivery systems based on rationale, as opposed to high-throughput screening.

The effective generation of memory T cells depends on several stimuli: the antigen presentation, co-stimulation, and the presence of inflammatory/danger signals [124]. Nolz, et al. [60] demonstrated how the history of antigen exposure can affect the number, phenotype, and function of T cells. Multiple vaccine doses (intermittent antigen release) can improve the immunogenicity but methodical studies are necessary to optimize the immune response for varying the kinetics of prime and/or boosting series, in conjunction with the use of adjuvants. On the one hand, the excessive exposure to the antigen can lead to a T-cell exhaustion state, in which the effector and memory capacities are reduced. In the case of a defective stimulation (i.e. lack of adequate co-stimulatory/co-inhibitory signals), a T-cell unresponsive state can be observed (T cell anergy) [125]. In the case of vaccines that require multiple boosts, T cell anergy

induction is a possibility. It is critical to fully elucidate how the kinetics of antigen release affects seroconversion for full optimization.

In terms of engineering kinetics, several studies have developed delivery systems for sustained release of the compound of interest [126]. As for vaccines, such systems are intended to provide long-term immunization with a single-shot administration, especially for toxoid and subunit vaccines. The most common method to control drug kinetics involves polymeric systems such as: polyacrylic acid (PAA) [127], poly(β-amino ester) (PBAE) [128], poly(lactic-co-glycolic acid) (PLGA) [129], poly(methyl methacrylate) (PMMA) [130], polycaprolactone (PCL) [131], ethylene vinyl acetate polymers [132], chitosan[133], and layer-by-layer (LbL) delivery of various combinations of polyelectrolytes [134]. A non-exhaustive list of non-polymeric systems include: microchips [135], layered double hydroxide nanoparticles [136], and silica particles [137].

Polymer-based drug delivery systems have been studied for decades and mainly employ biocompatible and biodegradable polymers. For example, Zarrati, et al. [130] described the use of a DNA vaccine prepared with PMMA for Leishmania immunization. The plasmid DNA vector was encapsulated within the PMMA and administered through intramuscular injection, which induced the production of cytokines and elicited an antibody response in mice. Titti, et al. [138] employed PMMA-based microspheres to deliver the HIV-1 Tat protein and alum as an adjuvant in Rhesus macaques. This vaccine design led to a balanced Th1/Th2 response and strong anti-Tat humoral response.

123

PLGA is a hydrophobic, relatively biocompatible (has had approved indications by the Food and Drug Administration (FDA)) and biodegradable co-polymer which is widely employed as a biomaterial for medical use. In the vaccine field, PLGA-based systems have been mainly studied with respect to antigen encapsulation and delivery as nano- and microparticles due to PLGA's ability to control degradation, achieved by monomeric ratio modulation of the lactides (less hydrophilic) and glycolides (more hydrophilic) [139-143]. McHugh, et al. [123] discussed several studies involving polymeric single-particle or reservoir boosting systems for vaccine delivery. McHugh, et al. also discussed vaccine administration by (1) repetitive injections via boluses, (2) single-injections of microparticles that release antigen continuously, and (3) single injections of microparticles with programmable pulsatile antigen release.

DeMuth, et al. [127] described a vaccine design based on silk-tipped and PAA pedestal composite microneedles for the transcutaneous delivery of antigen (ovalbumin, OVA). The composite microneedle (**Fig. 42A**) allowed different antigen release regimens in a single-administration vaccine. Five minutes after priming, the antigen was completely released from the PAA pedestal of the microneedle (**Fig. 42B**, MN-PAA), while the antigen released from the silk tip (MN-silk) took 4 days to to reach completion. Moreover, a continuous antigen release was detected up to 14 days from a methanol-treated silk tip (MN-MeOH-silk), which demonstrated an improved cross-linked silk structure. This approach avoided the use of needles, enhanced the inflammatory response, and enabled the modulation of the release kinetics of antigens by
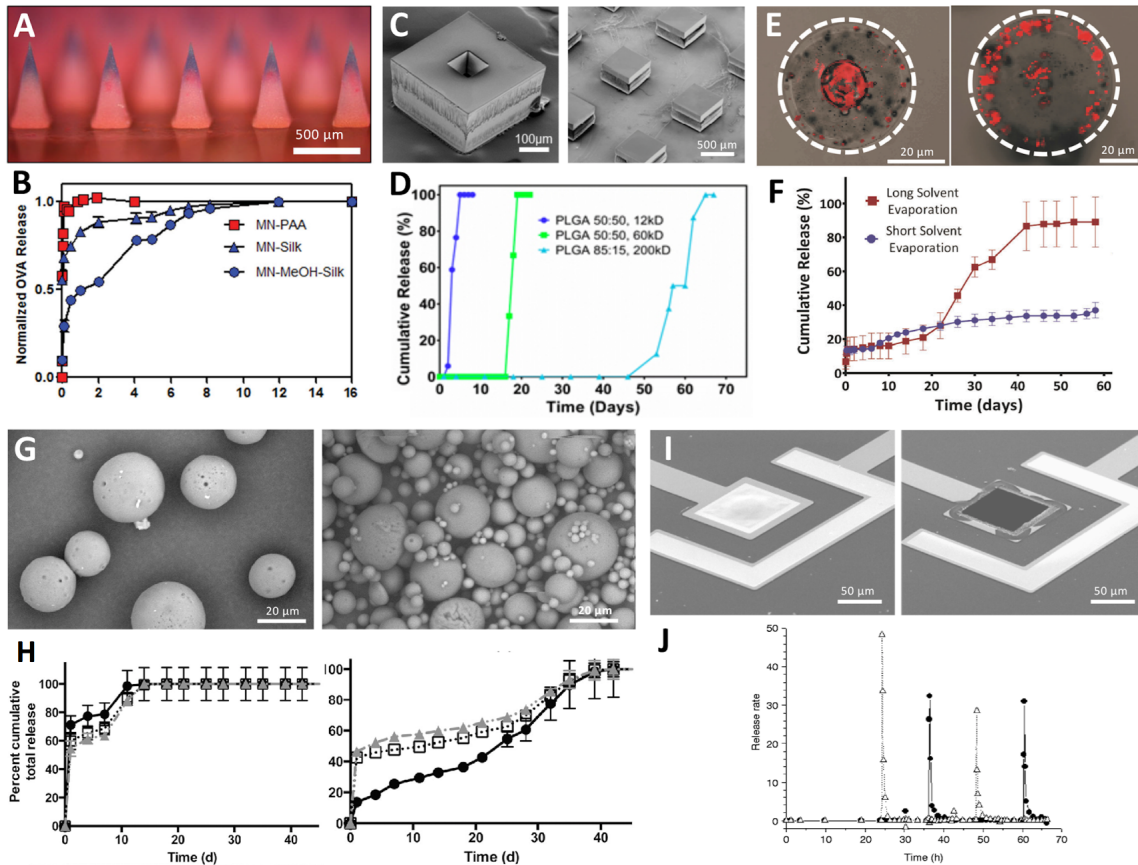
Figure 42 Polymer-based delivery systems. (A) Silk/PAA composite microneedle micrograph (scale bar: 500 μm); (B) OVA release from silk/PAA microneedles measured by fluorescence; (C) microfabricated PLGA microparticle before antigen dispensing (left, scale bar: 100 μm) and after thermal sealing (right, scale bar: 500 μm); (D) antigen release in pulsatile kinetics measured by fluorescence; (E) antigen distribution in PLGA microspheres submitted to a short (left) and long solvent evaporation (right, scale bar: 20 μm) on the evaporation time; (F) different antigen release profiles obtained for short and long solvent evaporation; (G) IPV antigen-containing PLGA microspheres with 7.5% EPO (left) and 5% EPO/0.4% L-arginine (right, scale bar: 20 μm); (H) IPV antigen release profile change drastically with the microparticle composition; (I) micrograph of the wirelessly controlled implantable PLGA microchip before (left) and after (right, scale bar: 50 μm) the triggering the antigen release; (J) antigen release rate release show well defined pulsatile release. Adapted with permission from [5, 127, 144, 145]. Adapter from [25]

chemically altering the microneedle structure. The antigen-specific T cell and humoral responses presented 10-fold increases in comparison to parenteral needle administration.

McHugh, et al. [144] designed an injectable PLGA-based microparticle using computer chip-based microfabrication techniques, a picoliter dispenser, in addition to a novel cap sealing method using a mask aligner (which is generally used for photolithography. With this technology they obtained highly controlled antigen releasing profiles (**Fig. 42C**). The microparticles presented a greatly tunable and sharp antigen bolus release observed from four to seventy days (**Fig. 42D**). The different release kinetics were achieved by varying the polymeric chain size (12-200 kDa) and lactide:glycolide ratios . Predicting which microparticles were properly sealed, however, was a major challenge.

Dutta, et al. [5] described a dichloromethane and ethanol procedure to control antigen distribution in microparticles and how the distribution of antigen throughout the particle modified the release profile. However, such solvents are known to denature proteins used as antigens which limits the potential applications of the technology. In **Fig. 42E,** the authors show that a short period of ethanol evaporation (left) leads to antigen concentrated in the core of the particle. In the case of a long period of ethanol solvent evaporation (right), the antigen was found in both the core and the peripheral area of the microsphere. With the particles obtained by long solvent evaporation demonstrated a greater release rate during days 22 to 42 which is likely due to catastrophic failure of the microparticles. Other groups have also demonstrated a second burst due to catastrophic failure of PLGA-based microparticles [25]. After the observed

126

release rate increased from days 22 to 42, the cumulative release reached almost 90% after 2 months (**Fig. 42F**).

Tzeng, et al. [25] achieved a stable and long-term IPV antigen release from PLGA microspheres produced with thermostabilizing molecules (e.g., maltodextrin, trehalose, sucrose, monosodium glutamate) and Eudragit® E PO (EPO), which likely served as a buffer for the acidifying degradation byproducts of PLGA. In **Fig. 42G**, the scanning electron microscope images depict PLGA microspheres with 7.5% EPO (left) and 5% EPO with 0.4% L-arginine. The release profiles for IPV serotypes 1, 2, and 3 drastically change with the addition of L-arginine, which likely helps buffer the internal acidification process during the degradation of PLGA microspheres. Furthermore, the buffering process was likely responsible for enabling stability and a slower release profile (**Fig. 42H**). Catastrophic breakdown of the microparticles later in the degradation process enabled the microparticles to have an additional boosting effect which was apparent in a number of the formulations.

In 2012, Farra, et al. [135] performed the first clinical trial of an implantable microchip system for drug delivery controlled by wireless communication which is a promising delivery system for sustained release of vaccines. The experiment tested the release of anabolic hormones used in the treatment of osteoporosis. The implanted device was found to be well-tolerated by the patients. The initial development of the controlled microchip delivery system (**Fig. 42I** (microchip), **42J** (release profile)) was first reported by Santini, et al. in 1999 [145].

DeMuth, et al. [146] developed a PLGA microneedle vaccine coated with an erodible multilayer, which contained protein vaccine (OVA) and an adjuvant, monophosphoryl lipid A. Interbilayer-crosslinked multilamellar lipid vesicles (ICMV)s produced with dioleoylphosphatidylcholine were used to encapsulate the protein vaccine and adjuvant. The anionic ICMVs were intercalated with cationic and biodegradable PBAE. The OVA release qualitatively increased from 6 to 24 hours according to confocal microscopy, demonstrating the kinetic behavior of the PBAE and ICMV degradation.

The LbL is a surface deposition technique based on electrostatic interactions that allow the fabrication of diverse wafer-like drug delivery systems [147]. Using LbL for vaccine design holds great potential to produce long-term immunization with controllable release profiles. A variety of charged entities have been used for LbL including: polymers, charged lipids, polysaccharides for the cationic/anionic combination. In the study performed by van der Maaden, et al. [148] inactivated poliovirus fragments which were deposited atop microneedles and subsequently covered by a cationic polymeric layer made of N-trimethyl chitosan chloride (TMC). This bilayer was repeated 10 times to deposit sufficient levels of antigen on the microneedle array, which contained 585 ng of viral protein and 700 ng of TMC. The immunization process included a prime, followed by a booster at three weeks. The authors demonstrated they successfully induced an IPV-specific antibody response.

A couple of other PLGA-based vaccine developments include a vaccine for autoimmune encephalitis, as well as a hydrogel-based OVA vaccine platform. PLGA

nanoparticles were employed to deliver the subcutaneous vaccine for encephalomyelitis autoimmune disease. The PLGA-containing myelin oligodendrocyte glycoprotein functioned as the antigen and IL-10 as an adjuvant showed sustained release for 31 days [149]. Bobbala, et al. [131] recently described the development of the pentablock hydrogel-based vaccine delivery system which employed a pentablock copolymer depot loaded with PLGA nanoparticles and an alum adjuvant. They demonstrated control over the hydrogel release time by the ratio of PCL and polylactic acid content. Both cellular and humoral immune responses were detected in mice and a specific OVA-IgG antibody response was observed for 49 days after the injection.

6.4 ENHANCING THE DURATION OF IMMUNE PROTECTION USING NON-KINETIC APPROACHES

Adjuvant	Composition	Disease	Vaccine Type (comercial name)	Immune response	Research stage	Year
Alum	Alum, 3-O-desacyl-4'-monophosphoryl lipid A (AS04®) (GSK MPL®)	Influenza A	Virus-like particle (M2eVLP)	improved cross-protection	mice	2014
		Human Papilomavirus	Protein vaccine (HPV-16 L1/HPV-18 L1) [GSK Cervarix®]	enhanced antibody response	clinical study (girls 9-14 years)	2015
		Toxoplasmosis	DNA vaccine (toxifilin gene)	enhanced humoral response and switched from Th2 to Th1	mice	2016
		Hepatitis B	Protein vaccine (HBsAg) [GSK FENDrix®]	enhanced humoral and cell-mediated immune reponses	clinical study (renal-transplanted patients)	2017
Squalene oil-in-water emulsions	Squalene, montane 80, eumugin B1 PH (AF03®)	Influenza	Protein vaccine (haemagluttinin)	enhanced humoral immune response	mice	2014
	Squalene, MPL®, saponin (QS21®) (AS02®)	Pneumonia	Protein vaccine (PhtD)	increased frequency of CD4$^+$ T cells and memory B cells	Phase I	2015
	Squalene, tween 80, sorbitan triolate (MF59®)	HIV-1C	Protein vaccine (gp140)	enhanced humoral and cell-mediated immune reponses	Phase I	2016
	Squalene, glycerol, egg phosphatidylcholine, poloxamer, ammonium phosphate buffer (Stable Emulsion, SE)	Influenza A/H5	Protein vaccine (rHA) [Panblock®]	met criterion for seroconversion rate	Phase II	2017
	Squalene, tween 80, α-tocopherol (AS03®)	Influenza A/H5N1	Inactivated virus vaccine (SV)	increased levels of IL-6 and IP-10 within 24 hours after vaccination	Phase I	2017
Liposomes	MPL®, saponin (QS21®) (AS01®)	Malaria	Protein vaccine (RTS,S) [Mosquirix®]	immunoprotection for 3-4 year infants, enhanced efficiency with booster	Phase III	2015
		Varicella-zoster virus	Subunit vaccine (HZ/su) [GSK Shingrix®]	significant immune protection in adults ≥50 years	Phase III	2015
	DDA®, TDB® (CAF01®)	Tuberculosis	Subunit vaccine (H56/CAF01®)	longlasting immunoprotection and enhanced CD4$^+$ T cell response	Phase I	2016
TLR ligand	GLA-AF (TRL4 ligand)	HIV clade C	DNA vaccine/Attenuated vaccine/Protein vaccine (HIV env/gag-pol-nef, MVA-C, HIV CN54dp140)	enhanced T and B cell immune responses	mice	2014
	dsRNA analog Poly(I:C) (TRL3 ligand)	Seasonal influenza	Inactivated vaccine (TIV)	enhanced humoral response	mice	2014
		Human Papilomavirus	Subunit vaccine (HIV-1 gp140)	longlasting IgG/IgA response	mice	2016
	CpG 1018 (TLR9 ligand) (Dynavax HEPLISAV-B®)	Hepatitis B	Protein vaccine (HBsAg) [Dynavax HEPLISAV-B®]	enhanced superior seroprotection	Phase III	2015
	CpG 7909 (TLR9 ligand)	Meningococcal infection	Subunit vaccine (dLPS/OMP)	early and increased IgG/IgM response	Phase I	2015
	Cationic antimicrobial polypeptide/IC31® (TLR9 ligand)	Tuberculosis	Protein vaccine (H4:IC31®)	high frequency CD4$^+$ T cells and longlasting memory response	Phase I	2015
	Alum-absorbed GLA/SLA (TRL4 ligand)	Malaria	Protein vaccine (GMZ2.6C)	enhanced parasite-specific antibody and induced Th1 response	mice	2016
	Lipopolypeptide Pam2/Pam3 (TLR2/6, TLR2/1 ligand)	Parasitic helminths	Autoclaved vaccine (ALM+Pam2/Pam3)	Th2 polarization	mice, parasite	2016
	dsRNA analog Poly(I:C) (TRL3 ligand)	Cancer	Protein vaccine (Db126 WT-1)	infiltration of CD8$^+$ T cells in tumor	mice	2016
		Human Papilomavirus	Subunit vaccine (HIV-1 gp140/HSV-2 gD)	longlasting IgG/IgA response	mice	2016
	Alum-absorbed GLA/SLA (TRL4 ligand)	Malaria	Protein vaccine (GMZ2.6C)	enhanced parasite-specific antibody and induced Th1 response	mice	2016
	Alum-absorbed SMIP7.10 (TRL7 ligand)	Meningococcal infection	Conjugated polysaccharide vaccine (MenC-CRM197)	Th1 polarization	mice	2016
	Imidazoquinolines (TLR7/TLR8 ligand)	various	various	Th1 polarization	clinical study (newborn)	2016

Table 2 Examples of adjuvants. [91, 92, 117, 118, 150-187]

Polysaccharide	Inulin (Advax®)	Hepatitis B	Protein vaccine (HBsAg)	enhanced humoral and cell-mediated immune reponses	Phase I	2014
		Seasonal influenza	Inactivated vaccine (TIV)	low-dose TIV/Advax® induced efficient immune response	Phase I	2016
	Chitosan	Tetanus	Toxoid vaccine (TT)	enhanced mucosal immune response	-	2014
		Influenza	Subunit vaccine (HA-split)	enhanced humoral and cell-mediated immune reponses	-	2014
		various	various	Th1 polarization	-	2015
Genetic Adjuvant	IL-12/IL-15 plasmid		DNA vaccine	no enhanced immune response, tolerable adjuvanted-vaccine	Phase I	2012
	Il-12 plasmid	HIV-1	DNA vaccine	induction of CD4+/CD8+ T cell response	Phase I	2013
	NF-κB subunit p65/RelA, Type-1 transactivator T-bet		DNA vaccine (HIV pGag, pEnv)	enhanced T, B cell, and antibody responses	mice	2014
	PPE44/pCI-OVA	Tuberculosis	Live attenuated vaccine/pDNA (BCG)	enhanced T and B cell immune responses	mice	2014
	CTA	Cholera	DNA vaccine (HIV-1 Tat-Rev-Vif-Integrase-Nef)	upregulation of IL-6, IL-1β	mice	2014
	C-terminal HSP70	Infectious bursal disease (chicken)	DNA vaccine (VP2 gene of IBDV)	enhanced humoral and cell-mediated immune reponses	chicken	2015
	GM-CDF	Cancer	DNA vaccine (MUC1-VEGFR2)	inhibition of tumorigenic cell growth	mice	2016

Table 2 Continued.

Long-term protection provided by a single-shot vaccine may be achieved by regulating the vaccine kinetics (refer to Engineering kinetics of vaccines via polymeric methods section) or by non-kinetic approaches which may be achieved by: (1) molecular immunostimulants (e.g., nucleic acids, polysaccharides, proteins, polymers) and (2) advanced vaccine particles (e.g., nanoparticles, microparticles, virus-like particles) (**Table 2**) [188, 189].

6.4.1 Pathogen-associated molecular patterns

PAMPs are key signatures that healthy innate immune systems are able to recognize and build an immune response against. PAMPs can be recognized by both specific TLRs as well as NOD-like receptors. For example, each of the following are recognized by specific TLRs to enhance immunogenicity: lipopolysaccharides (LPS)s (TLR2/4), flagellin (TLR5), unmethylated CpG DNA sequences (TLR9 within

endolysosomes) [190], double- (dsRNA; TLR3) and single-stranded RNA (ssRNA; TLR7). Of note, unmethylated CpG motifs are known to activate innate immunity by triggering the expression of Th1 and pro-inflammatory cytokines [191]. A phase I clinical study showed that CpG 7909 (TLR9 ligand) was capable of inducing early and intense IgG/IgM responses against meningococcal infection. In another clinical study (phase III), the CpG 1018-adjuvanted hepatitis B vaccine (HEPLISAV-B®) induced seroprotection [117, 167].

6.4.2   Adjuvant action – alum, lipids, and polymers

Alum has been used since 1926. With the aluminum salt (AS), enhanced antibody titres are commonly observed. For example, Leung, et al. reported a 1.8-fold increase in the antibody titers after the administration of AS04-adjuvanted (monophosphoryl lipid A adsorped onto aluminum salt) bivalent recombinantprotein vaccine against human papillomavirus (HPV-16/18, Cervarix®) in comparison to the tetravalent HPV-6/11/16/18 vaccine (Gardasil®). Lindemann, et al. showed the licensed vaccine FENDrix® (alum-adjuvanted vaccine against Hepatitis B) to improve both humoral antibody levels from 10 to264 IU/L) and cell-mediated immune responses (**Table 2**) [118, 151]. Additionally, other adjuvant constructions utilized alum-adsorbed TLR ligands, which stimulates the expression of co-stimulatory molecules and inflammatory mediators and consequently enhances the immune response. For instance, the TLR4 ligand glucopyranosyl lipid/synthetic second-generation lipid (GLA/SLA) was

used in the treatment against malaria and induced high IFN-gama response in CD4+ Th1 cells [169, 171]. Although alum is commonly employed for adjuvanticity, limitations for intracellular pathogens have been observed (i.e., Mycobacterium tuberculosis (TB)). Furthermore, alum may promote IgE antibody production, thereby sensitizing against alum.

Liposome-adjuvanting examples include: the AS01®-adjuvanted RTS,S (Mosquirix®; anti-malaria) and the CAF01®-adjuvanted subunit vaccine H56. Greenwood, et al. demonstrated Mosquirix® induced effective immune protection within infants and children during a phase III clinical trial. In the screening stage, the seropositivity rates for anti-circumsporozoite antibodies was 12.8% and it reached 99.9% after the 3 doses of the RTS,S/AS01 vaccine [192]. Woodworth, et al. described long-lasting immune protection elicited by a fusion protein vaccine adjuvanted with CAF01 liposome. Such vaccine methodologies have demonstrated tuberculosis immunization by enhancing a specific $CD4^+$ T cell population that localizes within the TB-infected lung parenchyma cells [159, 162]. Emulsions have also been commercialized as MF59®, AS02®, AS03®, AF03®. The general composition comprises triterpenes/triterpenoids, phospholipids, and other surfactants. A recent phase I clinical trial for HIV-1 vaccination revealed that subjects that received a gp150 priming followed by an antigen-expressing modified vaccinia Ankara (MVA) as a boost induced binding antibody responses for 40.5% of all subjects, whereas the gp140/MF59® boost induced binding antibody responses in 100% of the subjects [156].

Biopolymers are widely used for medical applications and have been reported to have adjuvant action in specific applications. For example, polysaccharide-based adjuvants can also improve the immunogenicity of vaccines. Chitosan (CS) is known as a mucoadhesive molecule and may have important role in mucosal immunization [82]. Sawaengsak, et al. [176, 178] reported nanoparticles of CS combined with tri-polyphosphate and hemagglutinin (HA) to induce a 2-fold increase in the number of splenocytes that secrete IFNγ in mice infected with influenza virus when compared with an un-adjuvanted HA vaccine. Also, Gordon, et al. [91, 175] reported the inulin-based adjuvants (Advax®) to elicit efficient immune response against hepatitis B immunization during phase I clinical trial. At least a 4-fold increase in the seroprotection and the CD4 T-cell responsiveness was observed for subjects immunized with Advax when compared to HBsAg alone. Despite of these example, biopolymer has difficulties to control drug release due to its solubility in water. The drug carrier which has higher pectin proportion in pectin: high amylose portion ratio as 1:1 shows faster drug release than lower pectin portion, 4:1. In 4 hours, higher pectin proportion carrier released 59.07% of Nimesulide and lower pectin proportion carrier released 79.42% [193]. Relatively non-toxic and degradable (i.e., via hydrolysis of esters or amidolysis of amides) polymers such as poly(anhydride) (PA), poly-N-isopropyl acrylamide (PNIPAAm), and PLGA also find application in vaccines. Tamayo, et al. [194] reported the recognition of PA nanoparticles by TLR2/4/5, eliciting CD8+ T cell responses, and Th1 polarization in mice. Wafa, et al. [195] showed the polymeric structure affecting the intensity of the CD8+ T cell response and was also observed to increase the protective

duration. PA nanoparticle-based vaccines were recently employed for immunizing against swine influenza within pigs [196] and against H5N1 influenza [197]. Shakya, et al. [198] discussed the use of PNiPAAm combined with collagen type II as a polymeric adjuvant to reduce the risk of triggering autoimmune responses.

Several studies describe the enhanced immunogenicity due to the adjuvant properties of PLGA in comparison to non-adjuvanted antigen priming for subunit vaccines (recommended review article [199]). The size of PLGA particles (i.e. nano or microparticle), as well as the monomeric lactide:glycolide ratio played a crucial role in modulating immunogenicity [200]. Li, et al. [201] described an increase of Th1 cytokine expression (IFNγ, IL-17) to their pertussis toxoid vaccine by employing dual-range sized particles ranging from 200 to 300 nm and 5 μm with a monomeric ratio of 50:50. Cruz, et al. [202] reported an increased T-cell response by employing PLGA nanoparticles (50:50 L:G) for encapsulating and delivering a protein vaccine.

6.5 MANUFACTURING AND ENGINEERING DNA

Engineering and manufacturing DNA vaccines involves multidisciplinary fields such as molecular biology/biochemistry, separation techniques, and material science. A GOI can be inserted into a self-replicating organism (bacteria or yeast). A circular plasmid DNA (pDNA) is usually used as the DNA cloning vector, which can then be extracted from the replicating organism, and can be chemically purified [203]. The pDNA can be engineered to be expressed in bacteria (i.e. Escherichia coli (E. coli))

[204] or yeast (i.e. Pichia pastoris) [205, 206] for amplification purposes in bioreactors and can also able expressed in mammalian cells for a therapeutic purpose. The major components involved within an engineered DNA plasmid are the origin of replication, a promoter, and the GOI, and also commonly an antibiotic resistance gene for selection [207]. As for E. coli-based plasmid production, the composition of the culture media can vary from mineral-containing media to complex mixtures supplemented with yeast extracts. After the replication in thebioreactor, bacteria can undergo a lysing process through alkaline or thermal treatment, followed by plasmid purification via centrifugation and precipitation [208, 209]. This large-scale pDNA production is cost-effective in comparison to LAV and IV manufacturing processes. A relatively more recent advent of minicircles (episomal DNA)/miniplasmids (i.e., P1, P7, F)/ministrings [210-215] can potentially be transported more easily through cellular barriers to improve bioavailability [211].

6.6 SAFETY OF DNA VACCINES

The scientific community has high expectations for DNA vaccine use because of 1) the ability to control the transcribed and translated product, thereby controlling the ability of the antigen to not revert to a virulent pathogenic form; 2) the relatively low production cost of DNA vaccines; 3) the innate stability of DNA vaccines for storage and transportation [216, 217] purposes.

Despite the positive outlook, DNA vaccines have low immunogenicity and hence require immunostimulants and adjuvants. Also, DNA vaccines could potentially trigger autoimmune diseases by eliciting anti-DNA antibody production due to the use of prokaryotic DNA vectors (e.g. plasmid DNA). Such vectors may contain unmethylated CpG sequences and are recognized as a PAMP by TLR9 [121, 218]. CpG repeats for this reason can and have been avoided in a number of commercially available plasmids. Minicircle DNA [211, 213, 214, 219, 220] and ministring DNA [221, 222], have been reported to have less risk of insertional mutagenesis, since major bacterial DNA is removed.

DNA vaccines may cause indel mutations, and incorporation to the host genome depending on the mechanism of delivery. Despite non-viral gene delivery systems being safer than viral vectors, insertional mutagenesis risks are not zero, although the risks are believed to be lower than everyday random mutations. Today, there is still no licensed DNA vaccine for human use [223, 224].

In 1989, Gilkeson, et al. [225] associated prokaryotic double-stranded DNA (dsDNA) immunization to the development of anti-dsDNA antibodies in mice. In 1994, Lilic, et al. [226] described the induction of anti-DNA antibodies after the administration of a subunit vaccine against hepatitis B virus (HBV) and more recently Zafrir, et al. [227] reported that the HBV vaccine induced an autoimmune syndrome induced by the required adjuvants. On the other hand, other studies suggested no direct effect of vaccinations to triggering autoimmune diseases [228].

The administration of a DNA vaccine exposes the patient to foreign DNA or its fragments that could insert into the host's chromosomal DNA [229]. In the case of incorporation into an exon, an insertional mutation or frameshift mutation to occur. Such mutations can cause a gene to malfunction or inactivate (i.e. a tumor suppressor gene). The insertion of foreign genes in the host genome could lead to constituent expression of previously silent bacterial/parasite genes that have been inserted as well. The insertion may also increase the probability of rearrangements or breaking. The guidelines for industrial production of DNA vaccines published by the FDA recommends that the pDNA is more than 80% supercoiled in order to help prevent insertional mutagenesis. It has been reported that the FDA recommends integration studies, regardless of the delivery method, if there are greater than 10,000 copies of foreign DNA per μg of host DNA [230].

6.7 STABILITY OF DNA VACCINES

6.7.1 Environmental stability (non-biological)

DNA vaccines benefit from not needing such rigorous temperature control, as do protein-based vaccines. However, the stability of nucleic acid-based vaccines in dry conditions (i.e. storage and transportation) or in aqueous conditions are highly dependent on stabilization techniques. Crine, et al. [231] reported the stability of apurinic sequence sites to remain undamaged for about 288 to 335 hours at 37 ºC, pH 7.21, and a buffer

solution close to physiological media. Karni, et al. [232] investigated the thermal degradation rates of pDNA (0.75 µg of pUC19) and found that at 170 ºC in aqueous solution, there was complete degradation after 9 minutes. When the pDNA was incubated at 200 ºC in aqueous conditions, no intact pDNA could be found after 20 seconds. In the case of dried pDNA, the degradation temperature was reported to have a lower threshold. They incubated pDNA, pUC19, at every 10 ºC for 5 minutes and degradation is started from at 130 ºC and completed around 190 ºC. Also, of note, prokaryotic DNA was reported to be more thermally stable than eukaryotic DNA [233].

6.7.2   Biologically-relevant stability

The stability of nucleic acids in the physiological environment depends on specific conditions in the intracellular, tissue, and systemic levels. In an in vivo environment there is variation in pH (~5-7.45), exposure to various enzymes (i.e., nucleases) and reactive oxygen species, as well as the possibility of being epigenetically modified or modified by host DNA repair mechanisms [234].

The development of delivery systems for nucleic acids (e.g. polymeric and lipid vectors) which control the nucleic acid's microenvironment helps maintain the molecular stability, as there is a decrease in the degradation rate when in a complexed state (i.e. polyplex, lipoplex) versus a free state [235]. For example, the in vivo half-life for a non-ionically-complexed DNA is approximately 10 minutes in the extracellular environment while the intracellular half-life is longer, close to for 1-4 hours. While

139

being in a complexed state is advantageous in terms of its structural stability, if the DNA is excessively complexed then successful transcription will not be as efficient, as the plasmid will not be accessible to the transcription machinery [236].

Evans et.al. [237] described the relevance of controlling the main mechanisms of the DNA degradation (e.g. depurination/β-elimination and free radical oxidation by employing chelators and hydroxyl radical scavengers). The use of ethanol and EDTA (ethylenediamine tetra-acetic acid) or DTPA (diethylenetriaminepentaacetic acid) in DNA-based formulations are associated with enhancing the remaining DNA amount from approximately 30% to 70% after a 1-month incubation at 50 ºC.

Peptide nucleic acid (PNA) are uncharged molecules that demonstrate increased resistance against nucleases and RNases in comparison to endogenous nucleic acid, which can have benefits for specific gene delivery and DNA vaccine applications. The conjugation of PNAs with cell-penetrating peptides (CPP)s can enhance the molecular stability and facilitate transfection [238]. In addition to being highly stable, CPP-conjugated PNAs have improved DNA sequence recognition and induces a higher affinity with the lipid membranes because of the peptide backbone [239].

Epigenetic modification affects the molecular stability and the genetic expression of DNA. Modifications such as DNA methylation are more likely to occur in CpG-enriched regions [240] and the methylated regions may subsequently recruit DNA methylated-binding proteins and histone deacetylases (HDAC)s, which downregulate gene expression [241] as the transcriptional machinery cannot access the DNA.

6.8 PLASMID DELIVERY

On a cellular level, transporting highly charged macromolecules, such as DNA, across a negatively charged phospholipid bilayer membrane and subsequently through the restrictive nuclear enveloped is challenging. More specifically, the main delivery barriers of plasmid DNA are as follows: stability (described in the previous section), cellular uptake, endolysosomal escape, decomplexation from the carrier, and nuclear envelope translocation. The cellular uptake of non-viral gene delivery carriers can be uptaken via clathrin-, caveolae-mediated endocytosis, or macropinocytosis (endocytic pathways) [242, 243]. Plasmids can be internalized within the nucleus via intranuclear injection, direct/indirect nuclear localization signals (i.e. DNA-targeted sequences), and encapsulation by the nuclear envelope upon reformation post-mitosis [244]. Plasmids can be internalized within the nucleus via intranuclear injection, direct/indirect nuclear localization signals (i.e. DNA-targeted sequences), and encapsulation by the nuclear envelope upon reformation post-mitosis.

On a systemic level, eliciting specific antibody subtype responses depends on the context of the delivery method. For instance, the Lactobacillus vector against the influenza A virus induces a higher survival rate in a murine model through intranasal vaccine administration than oral administration [245]. Increased IgA titers were measured for the intranasal route for an anti-HIV DNA vaccine, in comparison to the intramuscular route after DNA vaccination [246]. IgG2a can be induced greater via an

intramuscular vaccine administration; whereas a gene gun method could elicit a greater IgG1 antibody response [247].

6.8.1 Physical DNA delivery methods

Electroporation was intended to create transient pores in the plasma membrane of host cells to increase the kinetics of plasmid DNA under an electrical field. In a recent clinical trial, a DNA vaccine was injected intramuscularly with subsequent electroporation [248].

Another physical method developed by delivering plasmid DNA-adsorbed gold nanoparticles using gas-pressurized guns, which also improved the cellular uptake. A gene gun has been recently used in preclinical trial in non-human primates to deliver DNA vaccine against dengue virus [249]. Choi, et al. [250] compared three different delivery methods (intramuscular, intradermal, epidermal inoculation) using plasmid-coated gold beads through particle-pressurized bombardment Intradermal injection and gene-gun show specific IgG antibody responses but not IgA. Despite the induction of IgG responses, both the gene gun and intradermal administration methods failed to protect mice from a rotavirus infection in this specific example.

Davtyan, et al. [251] investigated the efficiency of a gene gun-delivery method for a DNA epitope vaccine (DepVac) versus an electroporated method (intramuscularly) for immunizing against Alzheimer's disease. They found similar antibody and T cell responses in both methods for this specific application.

Other physical methods have included physical puncturing of the cells via microneedles (impalefection), hydrostatic pressure, squeezing cells in a microfluidic chamber (in addition to electroporation) [252], and sonoporation [253].

6.8.2 Non-viral methods

Lipids or cationic, amine-containing polymers are often used to complex with anionic plasmid macromolecules into nano-sized carriers, which facilitates the cellular uptake and inhibits the degradation of the plasmid during trafficking. The number of free carriers in the solution is critical to the delivery efficiency and it is typically administered in many fold excess. The main challenges for non-viral methods are increasing the cellular uptake efficiency, avoiding the endolysosomal degradation, and preventing protein unfolding or denaturation during carrier encapsulation [254].

Tang, et al. [255] described the delivery of a protein cargo by fusion protein-containing gold nanoparticle-stabilized capsules directly to the cytosol by membrane fusion, which prevented protein degradation in the endolysosome. In the comparison of caspase-3 delivery with and without nanoparticle-stabilized capsules(NPSC) to HeLa cells, caspase-3 with NPSC shows 72.0% apoptosis of HeLa cells after 1 hour incubation while without NPSC shows around 2%.

Analysis of the cell membrane's interaction with amphiphilic materials has demonstrated that adsorption of hydrophobic moieties (i.e. Lipofectamine 2000®/3000®, lipid-based or a greater number of carbons in the polymer backbone or

sidechain) can cause disruption or deformation of the outer layer of the cell membrane, and that this disruption can induce endosomal uptake [128, 256, 257]. Therefore, promoting cellular uptake is often accomplished using polymers designed to increase the interaction between nanoparticles and the cell membrane.[6]

In regards to the cell specificity, surface modifications can be employed for enhancement and structures of the carriers can be screened via high throughput methods to discover cell specificity (i.e. healthy versus cancerous using PBAEs) [258].

After internalization via an endocytic pathway, the plasmid DNA or vaccine carrier should efficiently escape from the endolysosome into the cytoplasm in order to avoid degradation. Several authors describe a greater endosomal escape using polyethyleneimine (PEI) conjugated to the plasmid DNA in order to further enhance the "proton sponge effect", which provoke the endosome to swell and then disrupt **[259]**. This effect occurs due to the buffering capacity of the unprotonated amine groups of the PEI structure, creating an imbalance in charge and osmotic pressure across the membrane. Thus, there is an influx of Cl^- ions and water molecules into the endosome **[260]**. Other escape mechanisms have involved fusogenic peptides, For example, Nakase and Futaki **[261]** suggested the association between PEI and the fusogenic peptide GALA on the cationic lipid-coated exosomes, which increased endosomal escape of exosomes. Hu, et al. **[262-264]** developed a DNA vaccine against malignant melanoma employing Tat-based fusogenic peptide with PEI-mannose nanoparticles adsorbed in microneedles. The use of the Tat-based fusogenic peptide resulted in stronger T-cell

responses and enhanced expression of IFNγ e IL-12. This kind of approach can potentially be applied for plasmid DNA delivery [151].

A nuclear localization sequence can also be indirectly incorporated in plasmid DNA-polymer complexes by using DNA targeting sequence (DTS) [265]. DTS is a DNA sequence that can be incorporated in the plasmid DNA and is a binding site for transcription factors. After the DNA is separated from the complex, this sequence containing the sequence for NLS can be transcribed and translated to allow for improved nuclear delivery of the plasmid DNA. A well-known example of DTS is simian virus 40 (SV40) which has a binding site for NLS-containing transcription factors [235, 266]. Thus when SV40 promoter sequence is incorporated in the plasmid DNA of interest, improved gene transfection can be observed.

Extensive reviews recommended for non-viral gene delivery barriers: [267, 268].

6.8.3   Viral-like particles

The viral invasion efficiency can also be achieved through virus-like particles (VLP)s, which consist of self-assembled structures of proteins that mimic the viral capsid but carry no viral genetic material as well [269]. This approach enables the presentation of PAMPs similarly to what a viral pathogen would elicit in the patient's immune system but without risk of contamination, infection, or reversion. The licensed vaccines Engerix®, Recombivax®, Gardasil® are examples of successful VLPs available in the market. Akache, et al. [270] described the Qb-VLP produced from Qb

capsid protein subunits, self-assembled using bacterial RNA, and conjugated with IgE peptides for the treatment of asthma and rhinitis. Experiments in mice showed increased levels of anti-IgE antibodies, which was enhanced by the TLR7 activation (RNA as an intrinsic adjuvant). This approach enables the presentation of PAMPs similarly to what a viral pathogen would elicit in the patient's immune system but without risk of contamination, infection, or reversion. The licensed vaccines Engerix®, Recombivax®, Gardasil® are examples of successful VLPs available in the market. Akache, et al. described the Qb-VLP produced from Qb capsid protein subunits, self-assembled using bacterial RNA, and conjugated with IgE peptides for the treatment of asthma and rhinitis. Experiments in mice showed increased levels of anti-IgE antibodies, which was enhanced by the TLR7 activation (RNA as an intrinsic adjuvant).

Recent clinical trials employed VLP for the immunization against HIV-1 (phase II, modified vaccinia Ankara expressing HIV-1 VLPs) [271], Chikungunya virus (phase I, recombinant E1/E2 structural proteins) [272, 273], influenza A virus (phase I, a Qb-VLP containing gH1/HA) [274], human papillomavirus L1 (phase III, HPV16/18) [275].

6.8.4 Viral methods

Viruses have been adapting over eons to efficiently delivery nucleic acids. Although, there have been many concerns over insertional mutagenesis and the safety profile of viral vectors, particular concerns for certain viruses have been alleviated to varying degrees; for example, viruses can be engineered to have greater control over

tropism [276]. We recommend the following extensive review for further information regarding viral gene delivery by Thomas, et al [277].

Another cellular uptake pathway for delivery particle is by mimicking the conditions of a viral invasion. The viral membrane fusion to the host plasma membrane depends on the envelope glycoproteins to overcome the unfavorable energetic barrier [278]. Virosomes are produced from the pathogenic virus itself devoid of genetic material. The advantage is that the virosomes can easily cross the host plasma membrane and deliver the DNA vaccine cargo into the host cell [279]. Leroux-Roels, et al. [280] described a phase I clinical trial employing gp41-derived peptide vaccine against HIV-1 using virosomes.

6.8.5 Clinical trials

The research conducted in animal models indicated good immunogenicity to DNA vaccine, but the clinical trials indicate a non-trivial translation to human [281]. Research has led to several licensed DNA vaccines for veterinary use only (West Nile Innovator®, Apex-IHN®, Life Tide-SW5®) [282] while DNA vaccines for human use has remained in various phases of clinical trials.

According to Gene Therapy Clinical Trials Worldwide website by Wiley, the majority of gene therapy clinical trials are still in the beginning stages. 57.3% (1409 out of 2463) of clinical trials are in phase 1 and this number expectedly decreases with each stage; phase 2 and phase 3 are 17.3% and 3.8%, respectively.

The greatest indication for gene therapy clinical trials is for cancer (64.5%), followed by monogenic diseases (10.3%) (i.e., cystic fibrosis and hemophilia) and infectious diseases (7.5%). The most common vector used in gene therapy clinical trials was the adenovirus, which accounted for 21.4%. Retrovirus and naked/plasmid DNA accounted for 18.2% and 17.2%, respectively.

6.9   CONTROLLING GENE EXPRESSION VIA PLASMID ENGINEERING AND GENE CIRCUITS

The design of the plasmid includes the selection of the DNA insert (gene of interest, GOI), the DNA vector, the transformation protocol, and the host organism. The GOI chosen must be related to the expression of molecules from pathogenic organism that can elicit effective immunoprotective, such as surface bacterial proteins (HBsAg for Hepatitis B disease and envelope viral glycoproteins (gp120 for HIV-1 disease) [283-285]. The replication of plasmid DNA in E. coli-replicated is common for several DNA vaccines [286, 287]. Recent technologies suggest that the use of minicircle DNA as non-viral DNA vehicle may increase therapy biosafety, since bacterial DNA is removed from parental plasmid, remaining only the GOI and promoter/terminator sequences [288]. Moreover, studies about gene transfer shows that minicircle induce 10-1000-fold increase in long-term transgene expression in vivo and in vitro, which can impact improve the immunogenicity of the DNA vaccines [289].

In this sense, Deans, et al. proposed a novel mechanism which allows gene expression control through inducers attached to genetic circuits [290]. Through the optics of the DNA vaccine technology, it would be possible to accurately switch on/off the expression of GOIs through molecular controllers, enabling the regulation of the immune response intensity and type (cell-mediated/humoral).

The genetic expression profile depends on stimuli from sources other than the prime DNA vaccine, and can be understood by means of the Th1/Th2 balance, enabling the fine control of cell-mediated and humoral immune responses. CpG ODNs are synthetic oligodeoxynucleotides with great similarity to DNA sequences found in prokaryotic genome (unmethylated CpG sites in bacterial genome) and can be recognized by TLR9 in the endolysosomes of the host immune cells, inducing Th1-biased immune response [291, 292]. Recent DNA vaccine studies successfully enhanced immunogenicity by including CpG ODNs as booster [293-295].

Early studies about the improvement of pDNA transient gene expression (TGE) efficiency investigated different combinations of promoter/enhancer for gene expression, as well as the TGE efficiency for HIV-1 vaccination [296, 297]. Sun, et al. [298] and Li, et al. [299] reported use of posttranslational regulatory elements to improve the efficiency of DNA vaccine.

Codon optimization consists in adapting the DNA sequences between different species intending to augment the expression of the GOI. During the plasmid design, low frequency eukaryotic codons in the foreigner DNA backbone are identified and replaced for high frequency codons, but maintaining the same the respective coded amino acids

[300-302]. Recent progresses enhanced immunogenicity in mice and chicken primed with codon-optimized DNA vaccine [303-305].

Synthetic gene circuits provide tools for accurately controlling gene expression, which can be relevant in the development of DNA vaccine [290].

Recently synthetic biology has been widely used for developing genetic engineering to conduct various developmental and functional studies. As discussed previously, gene networks are often used in E.coli and other simple organisms but gene networks are increasingly being designed for mammalian cells. Lac operon, for example, has been widely used in many gene expression studies where isopropyl β-D-1-thiogalactopyranoside (IPTG) is used as an inducer to promote gene transcription. The timing of the addition of this inducer controls the transcription [306]. Similarly, biomaterials have been proposed to be used along with synthetic biology for improved control in gene expression in mammalian cells [290]. While biomaterials provide a 3D microenvironment for the cells, synthetic biology can be combined with biomaterials to have better control over gene expression. Gene circuits in the cells can be incorporated in the biomaterial of choice for more control over the inducer. Various biomaterials can be designed such that the release of inducers can be controlled. Biomaterials like polyethylene glycol (PEG) and PLGA can be used for various applications in the study of soft tissues and bone structures, respectively. Gene circuits are designed for different applications and to improve transfection efficiency before incorporating the cells with gene circuits in the biomaterials.

Synthetic biology is used to design gene circuits which is applicable for many processes, such as cancer. For example, gene circuit was designed to be used with CRISPR technology where two single-nucleotide polymorphisms related to the occurrence of colon cancer is detected and cas9 enzyme is used to control the expression of target genes [307]. Brophy and Voigt [308] built a gene circuit in E.coli with an anti-sense promoter placed next to the terminator to study the function of anti-sense promoter as a regulator. The same group has also worked on designing computation tools like the "DNAplotlib" to visualize the gene circuit outline [309]. Another application in gene circuit and synthetic biology is the orthogonal polymerases to independently controlling multiple pathways in the same cell [310]. Using multiple activator-chaperone pairs have also been observed to improve the orthogonality in gene circuits [311]. Moon, et al. [311] used a 4-input AND gate that can control the gene expression of multiple pathways at the same time independent of each other employing E.coli.

6.10 OVERCOMING IMMUNOGENIC ISSUES OF DNA-BASED VACCINES

One of the suggested solutions is to integrate the plasmid, genes for those cytokines such as IL-4 or granulocyte-macrophage colony-stimulating factor (GM-CSF) that enhances immune responses or for C3d oligomers as an adjuvant for B-lymphocyte cells. Other likely approach may include an ensuing booster immunization with the relating antigen as a protein. Concomitantly, several studies assessed the immunogenicity of adjuvants inserted in the antigen vector (genetic adjuvant) and expressed by the host

151

organism, prompting a more complex DNA vaccination strategy and merging with the gene therapy field. Some studies assessed the immunogenicity of DNA vaccines containing chemokine expressing sequences for HIV-1 immunization [180-182]. Kalams, et al. [180] reported IL-12 and/or IL-15 to produce safe and immunogenic HIV-1 Gag DNA vaccine and 2013 the same author evaluated the positive impact of the electroporation (EP) delivery methodology for the HIV-1 Gag antigen/IL-12 adjuvant plasmid vector both as phase I clinical trial. More recently, there have been studies exploring genetic adjuvants against cholera (murine) [184], infectious bursal disease (chicken) [186], as well as cancer (murine) [187].

6.11 EXAMPLES OF DNA-BASED VACCINE COMMERCIAL SUCCESSES

According to the DNA vaccine database DNAVaxDB [312], there have been over 20,000 articles by 2017 indexed in PubMed and google scholar that have been taken to study DNA vaccines. However, there has not yet been a licensed DNA vaccine for human use so far. Since the gene-based formulation required more safety evaluations compared to conventional vaccines (e.g. nucleic acid integration into host chromosomal genome), the processes of DNA vaccines for human applications are relatively time consuming. While many human DNA vaccines are still being evaluated in clinical trials, there have been 4 studies of DNA vaccines that are approved for veterinary applications. An overview of approved DNA vaccines for animal models has been reported in several articles [313-315]. These vaccines target to different animal species, including horse,

salmon, swine and dog model. The earliest approvals were in 2005, West Nile–Innovator® and Apex-IHN®. These two are prophylactic vaccines for infectious diseases, encoding parts of protein of viruses, against West Nile Virus and infectious haematopoietic necrosis virus, respectively. In 2008, a single dose of vaccine expressing the growth hormone releasing hormone, LifeTide® SW5, was licensed for gene therapy. The latest approved one was in 2010, Oncept^{TM}, used for cancer immunotherapy against oral melanoma.

The success of vaccine tests in animal models boosts the investigation and investment of human clinical trials. To date, there are currently at least 40 clinical interventional trials evaluating human DNA vaccines, according to a quick search with "DNA Gene plasmid vaccine" on the Clinical Trials website. Studies under unknown status/withdrawn were excluded and studies have been patented/sponsored were then summarized in **Table 3**. The majority of these trials are investigating for infectious diseases as prophylactic vaccines, including HIV infection, virus infection, influenza, hepatitis B, etc. A variety of trials for potential therapeutic usage as immunotherapy for cancer, immunomodulator for asthma/allergy, and gene therapy for chronic infection are being evaluated as well. A detailed analysis of clinical trials of gene based prophylactic vaccines (including virus vaccine) was reported by Nakayama, et al. in 2015 [316].

	Product name	Vector name	Clinical status	Trial number	Sponser
Infectious disease (prevention)					
HIV infection	GOVX-B11	pGA2/JS7	Phase II	NCT00820846	GeoVax
HIV infection (prevention and treatment)	PENNVAX® -B		Phase I	NCT01082692	Inovio Pharmaceuticals
	PENNVAX® -G		Phase I	NCT01260727	Inovio Pharmaceuticals
	PENNVAX® -GP		Phase I	NCT02431767	Inovio Pharmaceuticals
Hepatitis B	INO-1800		Phase I	NCT02431312	Inovio Pharmaceuticals
Zika virus infections	GLS-5700		Phase I	NCT02809443 NCT02887482	GeneOne Life Science Inovio Pharmaceuticals
Middle East respiratory syndrome coronavirus (MERS CoV)	GLS-5300		Phase I	NCT02670187	GeneOne Life Science Inovio Pharmaceuticals
Influenza A H5N1 and H1N1 subtypes	INO-3510		Phase I	NCT01405885	Inovio Pharmaceuticals
Viral hemorrhagic fever with renal syndrome	HTNV/PUUV DNA Vaccine	pWRG/HTN-M(co)/pWRG /PUUV-M(s2)	Phase II	NCT02116205	Ichor Medical Systems US Army Medical Research and Materiel Command
Cytomegalovirus infection in hematopoietic cell transplantation/ solid organ (kidney) transplantation	ASP0113	TransVax	Phase III/Phase II	NCT01877655 NCT01974206	Astellas Pharma Vical
Cancer immunotherapy					
Pancreatic Cancer	MVI-118	pTVG-AR	Phase I	NCT02411786 NCT00849121	Madison Vaccines
	MVI-816	pTVG-HP	Phase II	NCT01706458 NCT02499835	Madison Vaccines
Allergy immunotherapy					
Japanese red cedar allergy, pollen allergy, peanut allergy	ASP-4070	LAMP-Vax	Phase I	NCT02469688	Astellas Pharma Immunomic Therapeutics
Gene therapy for chronic infection					
HSV-2 infection	herpes simplex bivalent DNA vaccine	VCL-HB01	Phase II	NCT02837575	Vical

Table 3 Selected current DNA vaccines in the progress of Phase I to III clinical trials.

Up to date, most of clinical trials showed no evidence of DNA integration into host chromosome and immunologic tolerance. However, poor DNA plasmids transfection efficiency resulting in insufficient induction of immune response is possibly one of the greatest challenges in current trials. As a result, more trials utilized hybridized formulations or higher DNA doses for greater immunogenicity [317]. GOVX-B11, are

two components vaccine. It consists of a DNA vaccine used to prime a person's immune response and a recombinant MVA (modified vaccinia Ankara, attenuated vaccine) used to boost the primed responses. Their studies were undertaken in HIV infected participants on antiretroviral treatment and have been demonstrated that GOVX-B11 is capable of eliciting antibodies and T cell response against a heterologous challenge [318]. On the other hand, PENNVAX DNA vaccines developed by Inovio Pharmaceuticals, currently in phase I progress, utilize the same prime-boost strategy as GOVX-B11 by combining a viral vector vaccine. Further, Inovio demonstrated that the immune response can be enhanced when delivered via in vivo intradermal electroporation of PENNVAX compared to syringe injection [319, 320]. These results reveal that the modification of DNA vaccine formulation or delivery approach can improve the potency and efficacy of the DNA vaccines in human trials.

As of 2016, a great deal of second generation vaccines have been licensed and released on the market. Some of DNA vaccines have been approved for sale in animal health as well (summarized in **Table 4**). These reports provide evidence on the potential and growth of worldwide market for new vaccine technologies. Regarding the feasibility of current trials of DNA vaccines, further advancement of the plasmid formulation and delivery approaches will be the necessary work for the continued improvement of DNA platform.

Vaccine Type	Vaccine Target	Product Name	Administration	Date of Approval	Company involved
Live attenuated vaccine	Cholera	Vaxchora	Oral	2016	PaxVax
	Influenza	FluMist	Intranasal	2003	MedImmune
Inactivated vaccine	Influenza virus subtypes A and type B	Flucelvax	Intramuscular	2012	Novartis
	Influenza	Fluzone Preservative-free	Intradermal	2002	Sanofi Pasteur
inactivated Hepatitis A and recombinant protein	Hepatitis A and B	Twinrix	Intramuscular	2001	GlaxoSmithKline
Toxoid conjugated vaccine	Invasive meningococcal disease	Menveo	Intramuscular	2010	Novartis
	Haemophilus influenzae type b	Hiberix	Intramuscular	2009	GlaxoSmithKline
	Diphtheria, Tetanus, Acellular Pertussis, Hepatitis B, Polio	Pediarix	Intramuscular	2002	GlaxoSmithKline
Polysaccharide vaccine	Streptococcus pneumoniae	Prevnar 13	Intramuscular	2010	Wyeth
Recombinant proteins	Meningococcal Group B	Bexsero	Intramuscular	2015	Novartis
	Influenza viru subtypes A and type B	Flublok	Intramuscular	2013	Protein Science

Vaccine Type	Vaccine Target	Product Name	Species	Date of Approval	Company involved
DNA vaccine	West Nile virus	West Nile-Innovator®	Horses	2005	Fort Dodge
	Infectious haematopoietic necrosis virus (IHNV)	Apex-IHN®	Salmon	2005	Novartis
	Growth hormone releasing hormone (GHRH)	LifeTide® SW5	Swine	2008	VGX™ Animal Health
	Melanoma	Oncept™	Dogs	2010	Merial

Table 4 Recent licensed protein and DNA vaccine therapies. (data extracted from 2001 to 2017)

6.12 CONCLUSION AND FUTURE DIRECTIONS

The present article compiled recent advancements on nucleic acid- and protein-based vaccines from the point of view of the biomedical engineering by bringing together basic, applied, and translational knowledge in order to point future trends to addressing global vaccinology challenges. First of all, the challenges are present in several categories such as logistics (i.e. molecular stability, storage and transportation conditions, global coverage rates), in vivo barriers (i.e. administration pathways,

156

intracellular/nuclear uptake rates, endosomal escape), and immunological issues (i.e. Th1/Th2 balance, effective seroconversion, adjuvancity, gene expression).

In this sense, the development of nuclei acid-based vaccines combined with the encapsulation with biocompatible and biodegradable polymers can enable a sophisticated solution in short-term. Even though there still no DNA vaccine for human use in the market, this scenario may change. The development of gene circuits creates a new horizon for developing novel DNA constructs with enhanced gene stability and precise expression control. Furthermore, personalized drugs designed to fit the patient's specific genetic characteristics could be also developed.

Regarding the protein-based vaccines, there is an immediate need for long-term single injection vaccines for both bolus and sustained antigen release kinetics. Such technology can reduce the number of administration necessary to accomplish a multiple vaccination regimen (e.g. hepatitis B require three doses at 0, 3, and 6 months) [321] and can dramatically change the vaccination scenario for both developed and developing countries. Thus, it is necessary to develop a protective carrier to prevent the antigen to degrade in the in vivo hydrolytic and enzymatic environment. The development of PLGA-, PCL-, PBAE-based microparticles for antigen delivery will continue promising solutions in the next few years. However, further studies are needed about the antigen stabilization inside the carrier.

Freeze-drying or lyophilization is a well-known technique to improve storage and transportation properties of vaccines by removing water from the delivery nano/microparticle but maintaining the bioactivity and the conformation of encapsulated

antigens. In major antigen encapsulation methods (e.g. single-, double-emulsion, spray drying, solvent extraction), water remains inside the particle core even after the lyophilization, which continually exposes the antigen to hydrolytic degradation [322, 323]. Some studies reported the effect of time and thermal conditions of the secondary drying step of lyophilization over the antigen stability [324, 325].

Another way to improve water control for antigen stability is by using cryo-protectants, which are already widely used in the food and drug industry to enhance the lifespan of the products. In vaccinology, sugar cryo-protectants are essential to preserve the antigen structure due to hygroscopic properties, avoiding protein aggregation and degradation during lyophilization [25, 326, 327]. A recent study showed trehalose to consistently preserve the structure and function of protein in exosome after several freeze-thaw cycles [328]. Also, the adequate antigen/cryo-protectant proportion can optimize the antigen preservation for long-term delivery, even though the correlation between the cryo-protectant concentration and the stability is not yet completely understood [329].

Another challenge for the current vaccinology is to overcome the poor immunogenicity of subunit vaccine, especially for DNA-based vaccines. Despite the commercial successes of DNA vaccines for veterinary use, no version has been licensed for human use. A deeper knowledge about the immune system and the development of technologies that offer accurate gene expression control can overcome the immunogenicity and biosafety problems regarding DNA vaccines.

Studies of Deans, et al. [290] advanced to the control of transgene expression by the construction of gene circuits with a precise switch on/off mechanism. The production of a gene circuit employed suppressors to inhibiting the expression of the GOI. The precise control of gene expression considerably reduces the risks of (1) expression of prokaryotic genes from the GOI, (2) eliciting anti-DNA antibodies, (3) foreign DNA integration to the host genome, (4) indel mutations.

Equally important to the need for precise gene expression is the choice for the adequate GOI in the plasmid construction to efficiently elicit the immune system. Mutations in pathogenic microorganisms leads a constantly renewing pool of circulating PAMPs, which creates an enormous challenge to the immune systems to recognize and elicit an immune response. Conserved sequences are reliable targets for DNA vaccine applications since it allows the expression of more recognizable PAMPs by the host immune system regardless of the evolutionary virus or bacterial mutation. Zheng, et al. described influenza virus matrix protein M1/M2 and nucleoprotein to be highly conserved and important for developing a universal influenza antigen. Yang, et al. [330] showed HIV-1 short conserved sequences of Nef, Gag, and Env (i.e. from 43 to 86 amino acids) to be highly immunogenic [18].

Addressing the current challenges of vaccination demands the knowledge of diverse fields such as physics, chemistry, physiology, immunology, microbiology, computer science. In this context, biomedical engineering has a crucial role in enabling efficient interdisciplinary communication for streamlining technology translation from advancements from the basic sciences.

7 CONCLUSIONS AND FUTURE WORK

7.1 ENCAPSULATION OF ANTIGEN WITHIN THE CONTEXT OF THE MICROBUBBLES

We quantified antigen stability in aqueous solutions as the positive control (gold standard of what we could potentially achieve; dry environment with optimized cryo-protectant concentration, 0.5 M trehalose, at three different temperatures in section 5.1) and also the negative control (in PBS at varying temperatures) and also. Since the microbubble is fabricated mainly for vaccine depots (subcutaneous injection or possibly intranasal embedding for mucosal delivery), the stability of both antigens HIV-1 gp120/41 and HBsAg ayw in the microbubble need to be quantified in the presence of various trehalose concentrations at temperature in time.

Antigen wi injected into the microbubble as same method that we inject BSA-dye conjugates. Because we analyzed the optimized trehalose concentrations, according to our experiment on day 4, the microbubble can be opened on day 4 and day 14 we can subsequently analyze the remaining functionality using ELISA to understand the decrease in functionality of the antigens within the microbubbbles in time.

We expect the antigen functionality will be better than in the aqueous solution without trehalose, but less than dry phase with trehalose. Because we suspect that aqueous phase in the drug is not fully evaporated during the lyophilization process. To avoid this, we will vent the inside of microbubble by connecting the venting tube

directly to the microbubble (**Figure 43**) and subsequently anneal the polymer in a

localized manner post-lyophilization. This venting system allows to improve the antigen

stability. This stability is critical for successfully immunize our bodies.
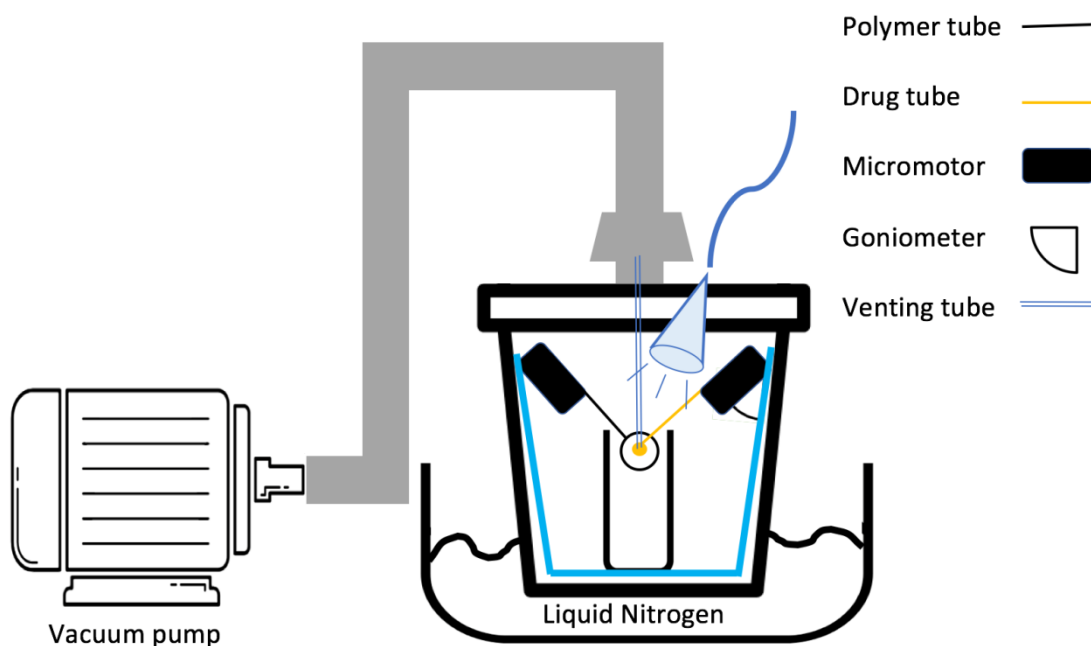
Figure 43. The automated system of microbubble formating using a venting will further improve the prevention of hydrolysis within our microbubbles.

7.2   MULTI-LAYERED MICROBUBBLES

As a vaccine depot, the microbubbles are required to release drug at different dates

for the auto-boosting application. To enable different release times, the microbubbles

161

were formed using different MW and different shell thicknesses. The bolus released at different time points as was confirmed by the release study of BSA-dye conjugates.
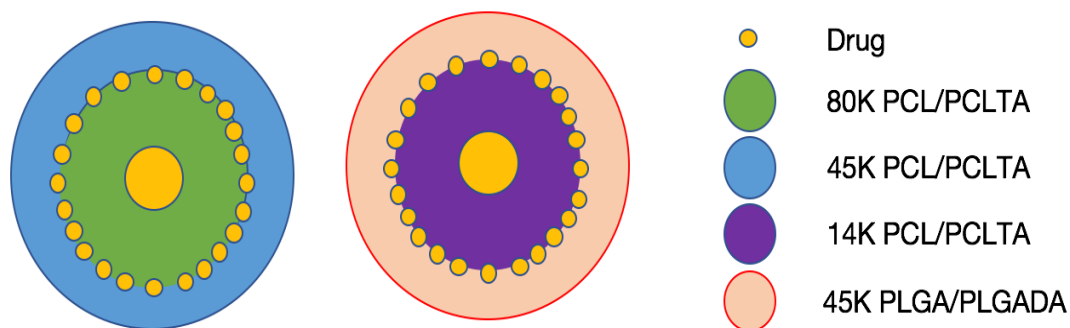
Figure 44 Multi-layered microbubbles which be formed by multiple injections of phase-separating polymers in the middle of the microbubble before curing.

The major drawback of this microbubble is that patients need to inject same number of microbubbles that would result in a human dose to complete the vaccination regimen. We may need a few or even dozens of microbubbles which will be painful (we are endeavoring to miniaturize the microbubbles to the extent possible). Perhaps a topical pain reliever could be applied prior to injection of the microbubbles but this would increase the cost of the therapy which is not ideal from a translational standpoint. Future work will explore multi-layered microbubbles. Each layer has different MW or different polymers which will help catering the microbubbles to required vaccines schedules. This could be accomplished by injecting multiple phase separating polymers (within organic solvents, **Figure 44**) in the middle of the microbubble sequentially

before curing. Using phase-separating polymers to achieve a wall with multiple degradation properties would be useful for modulating the release kinetics so that we can target any vaccine schedule required.

The release study (section 4.2) has shown the drug attached on the surface of microbubble released on day 2. This drug was dissolved in 10% CMC due to the failure of injection and it was adsorbed to the microbubble surface due to a partitioning effect during the curing stage and the likely the initial phases of lyophilization. These surface coating entities could be used for combinatorial therapies (likely not applicable for protein-based antigen) involving various small molecules. The reason why the model antigen had favorable partitioning effect into the organic solvent was likely because of the conjugated fluorescence dye. This would need to be further investigated as to what entities will be able to partition into the outer portion of the microbubbles, if we decide to use this as a tool (i.e., an initial bolus of vaccine rather than within the fluid (i.e., 3% CMC) that would be helping push the microbubble through the needle during the subcutaneous injection phase (or possibly intramuscular if required, or intranasal embedding).

We could also in the future deliver multiple types of microbubbles which would collectively result in the vaccine schedule required if there are limitations in obtaining more than 1 auto-boosting dose per microbubble.

7.3   MINIMIZING THE DIAMETER OF THE MICROBUBBLES FOR IMPROVING INJECTABILITY

In section 3.6, we controlled the size of the microbubble by controlling the syringe pump rate. The minimum size was 325 µm with 0.005 µL/sec. For intramuscular injection, 22-25 G needles are used for viscous solutions. It means only less than 711 µm of microbubble can be delivered through intramuscular injection. For subcutaneous applications, it would be ideal to be able to achieve injection via a 24 G needle. Therefore, further optimization of the microbubble diameter is necessary to deliver the microbubble and also reduce pain or required pain analgesics prior to microbubble injection.

In this work, the microbubble diameter was close to 1 mm as the SEM images indicated. The reason for this bigger microbubble diameters is because injection of the drug cannot be visualized with bare eyes. As the automation of this system is realized, we will be able to miniaturize the diameter without the need for visualization as we are no longer would be manually inserting the cargo within the microbubbles. We could observe the drug injection, however, by installing a camera inside of the system's container used for lyophilization. To make smaller size of microbubbles, we would likely need to use the syringe pump rate which is slower than 0.5 µL/sec or be able to cause the micromotors to move translationally faster than the manufacturer's set rate.

REFERENCES

[1] The top 10 causes of death. <http://www.who.int/mediacentre/factsheets/fs310/en/>, 2017 (accessed 17th Nov 2017.).

[2] Progress and Challenges with Achieving Universal Immunization Coverage 2015 Estimates of Immunization Coverage. <http://www.who.int/immunization/monitoring_surveillance/who-immuniz.pdf>, (accessed 17th Nov 2017.).

[3] WHO | Hepatitis B. <http://www.who.int/mediacentre/factsheets/fs204/en/>, 2017 (accessed 17th Nov 2017.).

[4] Countries Compared by Health > Physicians > Per 1,000 people. International Statistics at NationMaster.com. <http://www.nationmaster.com/country-info/stats/Health/Physicians/Per-1,000-people>, (accessed 17th Nov 2017.).

[5] D. Dutta, C. Fauer, K. Hickey, M. Salifu, S.E. Stabenfeldt, Tunable delayed controlled release profile from layered polymeric microparticles, J Mater Chem B Mater Biol Med 5(23) (2017) 4487-4498.

[6] C.J. Bishop, K.L. Kozielski, J.J. Green, Exploring the role of polymer structure on intracellular nucleic acid delivery via polymeric nanoparticles, J Control Release 219 (2015) 488-99.

[7] C.J. Bishop, R.L. Majewski, T.R. Guiriba, D.R. Wilson, N.S. Bhise, A. Quinones-Hinojosa, J.J. Green, Quantification of cellular and nuclear uptake rates of polymeric gene delivery nanoparticles and DNA plasmids via flow cytometry, Acta Biomater 37 (2016) 120-30.

[8] K.J. McHugh, T.D. Nguyen, A.R. Linehan, D. Yang, A.M. Behrens, S. Rose, Z.L. Tochka, S.Y. Tzeng, J.J. Norman, A.C. Anselmo, X. Xu, S. Tomasic, M.A. Taylor, J. Lu, R. Guarecuco, R. Langer, A. Jaklenec, Fabrication of fillable microparticles and other complex 3D microstructures, Science 357(6356) (2017) 1138-1142.

[9] C. Berkland, E. Pollauf, C. Raman, R. Silverman, K. Kim, D.W. Pack, Macromolecule release from monodisperse PLG microspheres: control of release rates and investigation of release mechanism, J Pharm Sci 96(5) (2007) 1176-91.

[10] J.F. Perz, G.L. Armstrong, L.A. Farrington, Y.J. Hutin, B.P. Bell, The contributions of hepatitis B virus and hepatitis C virus infections to cirrhosis and primary liver cancer worldwide, J Hepatol 45(4) (2006) 529-38.

[11] A. Schweitzer, J. Horn, R.T. Mikolajczyk, G. Krause, J.J. Ott, Estimations of worldwide prevalence of chronic hepatitis B virus infection: a systematic review of data published between 1965 and 2013, Lancet 386(10003) (2015) 1546-55.

[12] Z. Qian, W. Jianqiong, L. Hongmei, Z. Rong, L. Li, Z. Jinping, S. Tao, Distribution and epidemiologic trends of HBV genotypes and subtypes in 14 countries neighboring china, Hepat Mon 15(5) (2015) e24422.

[13] R. Liu, Y. Li, K.R. Wangen, E. Maitland, S. Nicholas, J. Wang, Analysis of hepatitis B vaccination behavior and vaccination willingness among migrant workers from rural China based on protection motivation theory, Hum Vaccin Immunother 12(5) (2016) 1155-63.

[14] S. Nayagam, M. Thursz, E. Sicuri, L. Conteh, S. Wiktor, D. Low-Beer, T.B. Hallett, Requirements for global elimination of hepatitis B: a modelling study, Lancet Infect Dis 16(12) (2016) 1399-1408.

[15] M.M. Santoro, C.F. Perno, HIV-1 Genetic Variability and Clinical Implications, ISRN Microbiol 2013 (2013) 481314.

[16] A.F. Santos, M.A. Soares, HIV Genetic Diversity and Drug Resistance, Viruses 2(2) (2010) 503-31.

[17] M. Rolland, S. Manocheewa, J.V. Swain, E.C. Lanxon-Cookson, M. Kim, D.H. Westfall, B.B. Larsen, P.B. Gilbert, J.I. Mullins, HIV-1 conserved-element vaccines: relationship between sequence conservation and replicative capacity, J Virol 87(10) (2013) 5461-7.

[18] O.O. Yang, A. Ali, N. Kasahara, E. Faure-Kumar, J.Y. Bae, L.J. Picker, H. Park, Short conserved sequences of HIV-1 are highly immunogenic and shift immunodominance, J. Virol. 89(2) (2015) 1195-204.

[19] M. Caskey, F. Klein, J.C. Lorenzi, M.S. Seaman, A.P. West, Jr., N. Buckley, G. Kremer, L. Nogueira, M. Braunschweig, J.F. Scheid, J.A. Horwitz, I. Shimeliovich, S. Ben-Avraham, M. Witmer-Pack, M. Platten, C. Lehmann, L.A. Burke, T. Hawthorne, R.J. Gorelick, B.D. Walker, T. Keler, R.M. Gulick, G. Fatkenheuer, S.J. Schlesinger, M.C. Nussenzweig, Viraemia suppressed in HIV-1-infected humans by broadly neutralizing antibody 3BNC117, Nature 522(7557) (2015) 487-91.

[20] G.J. Nabel, Challenges and opportunities for development of an AIDS vaccine, Nature 410(6831) (2001) 1002-7.

[21] M. Chojnacky, W. Miller, D. Ripple, G. Strouse, Nistir, G. Locke, P.D. Gallagher, Thermal Analysis of Refrigeration Systems Used for Vaccine Storage, (2009).

[22] D.D. Kristensen, T. Lorenson, K. Bartholomew, S. Villadiego, Can thermostable vaccines help address cold-chain challenges? Results from stakeholder interviews in six low- and middle-income countries, Vaccine 34(7) (2016) 899-904.

[23] R.D. Vaishya, A. Mandal, M. Gokulgandhi, S. Patel, A.K. Mitra, Reversible hydrophobic ion-paring complex strategy to minimize acylation of octreotide during long-term delivery from PLGA microparticles, Int J Pharm 489(1-2) (2015) 237-45.

[24] D. Manickavasagam, M.O. Oyewumi, Critical assessment of implantable drug delivery devices in glaucoma management, J Drug Deliv 2013 (2013) 895013.

[25] S.Y. Tzeng, R. Guarecuco, K.J. McHugh, S. Rose, E.M. Rosenberg, Y. Zeng, R. Langer, A. Jaklenec, Thermostabilization of inactivated polio vaccine in PLGA-based microspheres for pulsatile release, J. Control. Release 233 (2016) 101-13.

[26] S. Guo, C.M. Lin, Z. Xu, L. Miao, Y. Wang, L. Huang, Co-delivery of cisplatin and rapamycin for enhanced anticancer therapy through synergistic effects and microenvironment modulation, ACS Nano 8(5) (2014) 4996-5009.

[27] K.G. Desai, S.P. Schwendeman, Active self-healing encapsulation of vaccine antigens in PLGA microspheres, J Control Release 165(1) (2013) 62-74.

[28] K. Zhao, W. Li, T. Huang, X. Luo, G. Chen, Y. Zhang, C. Guo, C. Dai, Z. Jin, Y. Zhao, H. Cui, Y. Wang, Preparation and efficacy of Newcastle disease virus DNA vaccine encapsulated in PLGA nanoparticles, PLoS One 8(12) (2013) e82648.

[29] Y. Patil, J. Panyam, Polymeric nanoparticles for siRNA delivery and gene silencing, Int J Pharm 367(1-2) (2009) 195-203.

[30] P. Gentile, V. Chiono, I. Carmagnola, P.V. Hatton, An overview of poly(lactic-co-glycolic) acid (PLGA)-based biomaterials for bone tissue engineering, Int J Mol Sci 15(3) (2014) 3640-59.

[31] M.V. Balashanmugam, S. Nagarethinam, H. Jagani, V.R. Josyula, A. Alrohaimi, N. Udupa, Preparation and characterization of novel PBAE/PLGA polymer blend microparticles for DNA vaccine delivery, ScientificWorldJournal 2014 (2014) 385135.

[32] A. Taluja, Y.S. Youn, Y.H. Bae, Novel approaches in microparticulate PLGA delivery systems encapsulating proteins, Journal of Materials Chemistry 17(38) (2007) 4002.

[33] R. Kulkarni, G. Sapkal, M. Gore, Evaluation of Japanese encephalitis virus polytope DNA vaccine candidate in BALB/c mice, Virus Res 170(1-2) (2012) 118-25.

[34] L. Polo-Corrales, M. Latorre-Esteves, J.E. Ramirez-Vick, Scaffold design for bone regeneration, J Nanosci Nanotechnol 14(1) (2014) 15-56.

[35] J.J. Sinikumpu, W. Serlo, Biodegradable poly-L-lactide-co-glycolide copolymer pin fixation of a traumatic patellar osteochondral fragment in an 11-year-old child: A novel surgical approach, Exp Ther Med 13(1) (2017) 242-246.

[36] R.A. Maldonado, R.A. LaMothe, J.D. Ferrari, A.H. Zhang, R.J. Rossi, P.N. Kolte, A.P. Griset, C. O'Neil, D.H. Altreuter, E. Browning, L. Johnston, O.C. Farokhzad, R.

Langer, D.W. Scott, U.H. von Andrian, T.K. Kishimoto, Polymeric synthetic nanoparticles for the induction of antigen-specific immunological tolerance, Proc Natl Acad Sci U S A 112(2) (2015) E156-65.

[37] S.Y. Lee, H. Hyun, J.Y. Youn, B.S. Kim, I.B. Song, M.S. Kim, B. Lee, G. Khang, H.B. Lee, Preparation of nano-emulsified paclitaxel using MPEG-PLGA diblock copolymers, Colloids and Surfaces A: Physicochemical and Engineering Aspects 313-314 (2008) 126-130.

[38] Y.Q. Wang, Y.; Choi, S. H., FDA's Regulatory Science Program for Generic PLA/PLGA-Based Drug Products, American Pharmaceutical Review (2016).

[39] H. Sah, L.A. Thoma, H.R. Desu, E. Sah, G.C. Wood, Concepts and practices used to develop functional PLGA-based nanoparticulate systems, Int J Nanomedicine 8 (2013) 747-65.

[40] S. Manoochehri, B. Darvishi, G. Kamalinia, M. Amini, M. Fallah, S.N. Ostad, F. Atyabi, R. Dinarvand, Surface modification of PLGA nanoparticles via human serum albumin conjugation for controlled delivery of docetaxel, Daru 21(1) (2013) 58.

[41] X. Shen, T. Li, Z. Chen, Y. Geng, X. Xie, S. Li, H. Yang, C. Wu, Y. Liu, Luminescent/magnetic PLGA-based hybrid nanocomposites: a smart nanocarrier system for targeted codelivery and dual-modality imaging in cancer theranostics, Int J Nanomedicine 12 (2017) 4299-4322.

[42] R. Dinarvand, N. Sepehri, S. Manoochehri, H. Rouhani, F. Atyabi, Polylactide-co-glycolide nanoparticles for controlled delivery of anticancer agents, Int J Nanomedicine 6 (2011) 877-95.

[43] P. Fonte, S. Soares, A. Costa, J.C. Andrade, V. Seabra, S. Reis, B. Sarmento, Effect of cryoprotectants on the porosity and stability of insulin-loaded PLGA nanoparticles after freeze-drying, Biomatter 2(4) (2012) 329-39.

[44] J.Y. Kim, D.-W. Cho, Blended PCL/PLGA scaffold fabrication using multi-head deposition system, Microelectronic Engineering 86(4-6) (2009) 1447-1450.

[45] E. Diaz, I. Sandonis, M.B. Valle, M. Valle, A. Blanca, In Vitro Degradation of Poly(caprolactone)/nHA Composites, Journal of Nanomaterials 2014 (2014) 1-8.

[46] J.H. Byun, H.A. Lee, T.H. Kim, J.H. Lee, S.H. Oh, Effect of porous polycaprolactone beads on bone regeneration: preliminary in vitro and in vivo studies, Biomater Res 18 (2014) 18.

[47] J.-H. Shim, J.-Y. Won, S.-J. Sung, D.-H. Lim, W.-S. Yun, Y.-C. Jeon, J.-B. Huh, Comparative Efficacies of a 3D-Printed PCL/PLGA/β-TCP Membrane and a Titanium Membrane for Guided Bone Regeneration in Beagle Dogs, Polymers 7(10) (2015) 2061-2077.

[48] V. Agrahari, V. Agrahari, W.T. Hung, L.K. Christenson, A.K. Mitra, Composite Nanoformulation Therapeutics for Long-Term Ocular Delivery of Macromolecules, Mol Pharm 13(9) (2016) 2912-22.

[49] S.F. Chou, K.A. Woodrow, Relationships between mechanical properties and drug release from electrospun fibers of PCL and PLGA blends, J Mech Behav Biomed Mater 65 (2017) 724-733.

[50] <Advisory Committee on Immunization Practices, Center for Disease Control and Prevention - 2017 - 2017 Combined Recommended Immunization.pdf>.

[51] J.U.I. Higginbotham, L. Clement, Polymer Molecular Weight Analysis by 1H NMR Spectroscopy, (2011).

[52] C. Lei, S. Wang, Poly(ε-caprolactone) acrylates synthesized using a facile method for fabricating networks to achieve controllable physicochemical properties and tunable cell responses, Polymer 51(1) (2010) 164-177.

[53] H. Kweon, M.K. Yoo, I.K. Park, T.H. Kim, H.C. Lee, H.S. Lee, J.S. Oh, T. Akaike, C.S. Cho, A novel degradable polycaprolactone networks for tissue engineering, Biomaterials 24(5) (2003) 801-8.

[54] B.D. Ulery, L.S. Nair, C.T. Laurencin, Biomedical Applications of Biodegradable Polymers, J Polym Sci B Polym Phys 49(12) (2011) 832-864.

[55] S.M. Wilson, A. Bacic, Preparation of plant cells for transmission electron microscopy to optimize immunogold labeling of carbohydrate and protein epitopes, Nat Protoc 7(9) (2012) 1716-27.

[56] A. Karatas, O. Sonakin, M. Kilicarslan, T. Baykara, Poly (epsilon-caprolactone) microparticles containing Levobunolol HCl prepared by a multiple emulsion (W/O/W) solvent evaporation technique: effects of some formulation parameters on microparticle characteristics, J Microencapsul 26(1) (2009) 63-74.

[57] A. Imbrogno, E. Piacentini, E. Drioli, L. Giorno, Preparation of uniform poly-caprolactone Microparticles by membrane emulsification/solvent diffusion process, Journal of Membrane Science 467 (2014) 262-268.

[58] Y.S. Lee, P.J. Johnson, P.T. Robbins, R.H. Bridson, Production of nanoparticles-in-microparticles by a double emulsion method: a comprehensive study, Eur J Pharm Biopharm 83(2) (2013) 168-73.

[59] C.M. Baena-Aristizabal, H. Fessi, A. Elaissari, C.E. Mora-Huertas, Biodegradable microparticles preparation by double emulsification-Solvent extraction method: A Systematic study, Colloids and Surfaces A: Physicochemical and Engineering Aspects 492 (2016) 213-229.

[60] Thorlabs - GN05/M Small Goniometer with 12.7 mm Distance to Point of Rotation, ±15°. <https://www.thorlabs.com/thorproduct.cfm?partnumber=GN05/M>, (accessed 17th November 2017.).

[61] CONEX-AG-LS25-27P. <https://www.newport.com/p/CONEX-AG-LS25-27P>, (accessed 17th November 2017.).

[62] Y. He, P. Liu, C. Shi, Y. Liu, S. Liu, X. Feng, D. Fu, The influence of hydrophilic mPEG segment on formation, morphology, and properties of PCL-mPEG microspheres, Advances in Polymer Technology (2017).

[63] J.C. Jeong, J. Lee, K. Cho, Effects of crystalline microstructure on drug release behavior of poly(epsilon-caprolactone) microspheres, J Control Release 92(3) (2003) 249-58.

[64] O.O. Fatunmbi, J.A. Newman, D.A. Halvorson, V. Sivanandan, Effect of temperature on the stability of avian influenza virus antigens under different storage conditions, Avian Dis 37(3) (1993) 639-46.

[65] Y.F. Maa, M. Ameri, C. Shu, L.G. Payne, D. Chen, Influenza vaccine powder formulation development: spray-freeze-drying and stability evaluation, J Pharm Sci 93(7) (2004) 1912-23.

[66] G.B.L. Harrison, D.D. Heath, R.P. Dempster, C. Gauci, S.E. Newton, W.G. Cameron, C.M. Robinson, S.B. Lawrence, M.W. Lightowlers, M.D. Rickard, Identification and cDNA cloning of two novel low molecular weight host-protective antigens from Taenia ovis oncospheres, Int. J. Parasitol. 26(2) (1996) 195-204.

[67] K.S. Johnson, G.B.L. Harrison, M.W. Lightowlers, K.L. Ohoy, W.G. Cougle, R.P. Dempster, S.B. Lawrence, J.G. Vinton, D.D. Heath, M.D. Rickard, Vaccination against Ovine Cysticercosis Using a Defined Recombinant Antigen, Nature 338(6216) (1989) 585-587.

[68] M.W. Lightowlers, R. Rolfe, C.G. Gauci, Taenia saginata: Vaccination against cysticercosis in cattle with recombinant oncosphere antigens, Exp. Parasitol. 84(3) (1996) 330-338.

[69] M.A. Dobrovolskaia, S.E. McNeil, Immunological properties of engineered nanomaterials, Nat Nanotechnol 2(8) (2007) 469-78.

[70] Y. Xu, W. Liang, Y. Qiu, M. Cespi, G.F. Palmieri, A.J. Mason, J.K. Lam, Incorporation of a Nuclear Localization Signal in pH Responsive LAH4-L1 Peptide Enhances Transfection and Nuclear Uptake of Plasmid DNA, Mol Pharm 13(9) (2016) 3141-52.

[71] C. Watts, The endosome-lysosome pathway and information generation in the immune system, Biochim Biophys Acta 1824(1) (2012) 14-21.

[72] Y. Liu, H. Yin, M. Zhao, Q. Lu, TLR2 and TLR4 in autoimmune diseases: a comprehensive review, Clin Rev Allergy Immunol 47(2) (2014) 136-47.

[73] S. Riedel, Edward Jenner and the history of smallpox and vaccination, Proc (Bayl Univ Med Cent) 18(1) (2005) 21-5.

[74] A. Boylston, The origins of inoculation, J R Soc Med 105(7) (2012) 309-13.

[75] C.P. Gross, K.A. Sepkowitz, The myth of the medical breakthrough: smallpox, vaccination, and Jenner reconsidered, Int. J. Infect. Dis. 3(1) (1998) 54-60.

[76] C.E. Scudamore, Small-pox Mortality, British Medical Journal 2(3904) (1935) 879-879.

[77] N.J. Willis, Edward Jenner and the eradication of smallpox, Scott Med J 42(4) (1997) 118-21.

[78] A.M. Behbehani, The smallpox story: life and death of an old disease, Microbiol Rev 47(4) (1983) 455-509.

[79] A. Boylston, The origins of inoculation, J R Soc Med 105(7) (2012) 309-13.

[80] J.E. Juskewitch, C.J. Tapia, A.J. Windebank, Lessons from the Salk polio vaccine: methods for and risks of rapid translation, Clin Transl Sci 3(4) (2010) 182-5.

[81] A.B. Sabin, Oral poliovirus vaccine. History of its development and prospects for eradication of poliomyelitis, JAMA 194(8) (1965) 872-6.

[82] A.M. Payne, Oral immunization against poliomyelitis, Bull. World Health Organ. 23(6) (1960) 695-703.

[83] H. Jafari, J.M. Deshpande, R.W. Sutter, S. Bahl, H. Verma, M. Ahmad, A. Kunwar, R. Vishwakarma, A. Agarwal, S. Jain, C. Estivariz, R. Sethi, N.A. Molodecky, N.C.

Grassly, M.A. Pallansch, A. Chatterjee, R.B. Aylward, Polio eradication. Efficacy of inactivated poliovirus vaccine in India, Science 345(6199) (2014) 922-5.

[84] Introduction to inactivated polio vaccine and switch from trivalent to bivalent oral poliovirus vaccine worldwide, 2013-2016, Wkly Epidemiol Rec 90(27) (2015) 337-43.

[85] O. World Health, Polio vaccines: WHO position paper, March 2016-recommendations, Vaccine (2016).

[86] W.M. Switzer, H. Zheng, G. Simmons, Y. Zhou, S. Tang, A. Shankar, B. Kapusinszky, E.L. Delwart, W. Heneine, No evidence of murine leukemia virus-related viruses in live attenuated human vaccines, PLoS One 6(12) (2011) e29223.

[87] D.F. Hoft, K.R. Lottenbach, A. Blazevic, A. Turan, T.P. Blevins, T.P. Pacatte, Y. Yu, M.C. Mitchell, S.G. Hoft, R.B. Belshe, Comparisons of the Humoral and Cellular Immune Responses Induced by Live Attenuated Influenza Vaccine and Inactivated Influenza Vaccine in Adults, Clin Vaccine Immunol 24(1) (2017).

[88] N.K. Jain, N. Sahni, O.S. Kumru, S.B. Joshi, D.B. Volkin, C. Russell Middaugh, Formulation and stabilization of recombinant protein based virus-like particle vaccines, Adv Drug Deliv Rev 93 (2015) 42-55.

[89] N. Valero-Pacheco, M. Perez-Toledo, M.A. Villasis-Keever, A. Nunez-Valencia, I. Bosco-Garate, B. Lozano-Dubernard, H. Lara-Puente, C. Espitia, C. Alpuche-Aranda, L.C. Bonifaz, L. Arriaga-Pizano, R. Pastelin-Palacios, A. Isibasi, C. Lopez-Macias, Antibody Persistence in Adults Two Years after Vaccination with an H1N1

2009 Pandemic Influenza Virus-Like Particle Vaccine, PLoS ONE 11(2) (2016) e0150146.

[90] T. Vesikari, N. Brodszki, P. van Damme, J. Diez-Domingo, G. Icardi, L.K. Petersen, C. Tran, S. Thomas, A. Luxembourg, M. Baudin, A Randomized, Double-Blind, Phase III Study of the Immunogenicity and Safety of a 9-Valent Human Papillomavirus L1 Virus-Like Particle Vaccine (V503) Versus Gardasil(R) in 9-15-Year-Old Girls, Pediatr Infect Dis J 34(9) (2015) 992-8.

[91] D.L. Gordon, D. Sajkov, Y. Honda-Okubo, S.H. Wilks, M. Aban, I.G. Barr, N. Petrovsky, Human Phase 1 trial of low-dose inactivated seasonal influenza vaccine formulated with Advax delta inulin adjuvant, Vaccine 34(33) (2016) 3780-6.

[92] E. Bardel, R. Doucet-Ladeveze, C. Mathieu, A.M. Harandi, B. Dubois, D. Kaiserlian, Intradermal immunisation using the TLR3-ligand Poly (I:C) as adjuvant induces mucosal antibody responses and protects against genital HSV-2 infection, Npj Vaccines 1 (2016) 16010.

[93] K.A. McLean, S. Goldin, C. Nannei, E. Sparrow, G. Torelli, The 2015 global production capacity of seasonal and pandemic influenza vaccine, Vaccine 34(45) (2016) 5410-5413.

[94] J.F. Mosley, 2nd, L.L. Smith, C.K. Parke, J.A. Brown, J.M. LaFrance, P.K. Clark, Quadracel: Vaccination Against Diphtheria, Tetanus, Pertussis, and Poliomyelitis in Children, P T 41(4) (2016) 238-53.

[95] M.M. Cox, R. Izikson, P. Post, L. Dunkle, Safety, efficacy, and immunogenicity of Flublok in the prevention of seasonal influenza in adults, Ther Adv Vaccines 3(4) (2015) 97-108.

[96] C.A. Robertson, C.A. DiazGranados, M.D. Decker, A. Chit, M. Mercer, D.P. Greenberg, Fluzone(R) High-Dose Influenza Vaccine, Expert Rev Vaccines 15(12) (2016) 1495-1505.

[97] P.L. Moro, E.J. Woo, W. Paul, P. Lewis, B.W. Petersen, M. Cano, Post-Marketing Surveillance of Human Rabies Diploid Cell Vaccine (Imovax) in the Vaccine Adverse Event Reporting System (VAERS) in the United States, 19902015, PLoS Negl. Trop. Dis. 10(7) (2016) e0004846.

[98] F. Zhu, H. Deckx, R. Roten, B. Michiels, M. Sarnecki, Comparative Efficacy, Safety and Immunogenicity of Hepavax-Gene TF and Engerix-B Recombinant Hepatitis B Vaccines in Neonates in China, Pediatr Infect Dis J 36(1) (2017) 94-101.

[99] J.A. Englund, I.N. Mbawuike, H. Hammill, M.C. Holleman, B.D. Baxter, W.P. Glezen, Maternal immunization with influenza or tetanus toxoid vaccine for passive antibody protection in young infants, J Infect Dis 168(3) (1993) 647-56.

[100] S. Kurikka, H. Kayhty, H. Peltola, L. Saarinen, J. Eskola, P.H. Makela, Neonatal immunization: response to Haemophilus influenzae type b-tetanus toxoid conjugate vaccine, Pediatrics 95(6) (1995) 815-22.

[101] P.A. Nielsen, Large-scale production of tetanus toxoid, Appl Microbiol 15(2) (1967) 453-4.

[102] T. Vesikari, T. Becker, A.F. Vertruyen, K. Poschet, S.A. Flores, M.F. Pagnoni, J. Xu, G.F. Liu, J.E. Stek, F. Boisnard, S. Thomas, E. Ziani, A.W. Lee, A Phase III Randomized, Double-blind, Clinical Trial of an Investigational Hexavalent Vaccine Given at Two, Three, Four and Twelve Months, Pediatr. Infect. Dis. J. 36(2) (2017) 209-215.

[103] J. Bortolatto, L. Mirotti, D. Rodriguez, E. Gomes, M. Russo, Adsorption of Toll-Like Receptor 4 Agonist to Alum-Based Tetanus Toxoid Vaccine Dampens Pro-T Helper 2 Activities and Enhances Antibody Responses, J Immunol Res 2015 (2015) 280238.

[104] P. Sanofi, SANOFI PASTEUR STATEMENT ON THE DISCONTINUATION OF MENINGOCOCCAL POLYSACCHARIDE VACCINE, GROUPS A, C, Y AND W-135 COMBINED.

[105] S.A. Plotkin, Vaccines: past, present and future, Nat. Med. 11(4 Suppl) (2005) S5-11.

[106] C.M. Snapper, Differential regulation of polysaccharide-specific antibody responses to isolated polysaccharides, conjugate vaccines, and intact Gram-positive versus Gram-negative extracellular bacteria, Vaccine 34(30) (2016) 3542-8.

[107] M. Cadoz, Potential and limitations of polysaccharide vaccines in infancy, Vaccine 16(14-15) (1998) 1391-5.

[108] J. Cote-Daigneault, F. Peerani, E. MacMahon, E. Delaporte, J.F. Rahier, J.F. Colombel, Management and Prevention of Herpes Zoster in the

Immunocompromised Inflammatory Bowel Disease Patient: A Clinical Quandary, Inflamm Bowel Dis 22(10) (2016) 2538-47.

[109] A. Flood, M. Estrada, D. McAdams, Y. Ji, D. Chen, Development of a Freeze-Dried, Heat-Stable Influenza Subunit Vaccine Formulation, PLoS One 11(11) (2016) e0164692.

[110] L.A. Jackson, A. Gurtman, M. van Cleeff, K.U. Jansen, D. Jayawardene, C. Devlin, D.A. Scott, E.A. Emini, W.C. Gruber, B. Schmoele-Thoma, Immunogenicity and safety of a 13-valent pneumococcal conjugate vaccine compared to a 23-valent pneumococcal polysaccharide vaccine in pneumococcal vaccine-naive adults, Vaccine 31(35) (2013) 3577-84.

[111] S. Nishat, P.R. Andreana, Entirely Carbohydrate-Based Vaccines: An Emerging Field for Specific and Selective Immune Responses, Vaccines (Basel) 4(2) (2016).

[112] C. Mameli, V. Fabiano, L. Daprai, G. Bedogni, M. Faccini, M.L. Garlaschi, F. Penagini, D. Dilillo, E. Torresani, M. Gramegna, G.V. Zuccotti, A longitudinal study of streptococcus pneumoniae carriage in healthy children in the 13-valent pneumococcal conjugate vaccine era, Hum Vaccin Immunother 11(4) (2015) 811-7.

[113] E.L. Anderson, T. Bowers, C.M. Mink, D.J. Kennedy, R.B. Belshe, H. Harakeh, L. Pais, P. Holder, G.M. Carlone, Safety and immunogenicity of meningococcal A and C polysaccharide conjugate vaccine in adults, Infect. Immun. 62(8) (1994) 3391-5.

[114] F.Y. Avci, X.M. Li, M. Tsuji, D.L. Kasper, A mechanism for glycoconjugate vaccine activation of the adaptive immune system and its implications for vaccine design, Nat. Med. 17(12) (2011) 1602-U115.

[115] N. Ravenscroft, M.A. Haeuptle, M. Kowarik, F.S. Fernandez, P. Carranza, A. Brunner, M. Steffen, M. Wetter, S. Keller, C. Ruch, M. Wacker, Purification and characterization of a Shigella conjugate vaccine, produced by glycoengineering Escherichia coli, Glycobiology 26(1) (2016) 51-62.

[116] A. Rosler, G.W. Vandermeulen, H.A. Klok, Advanced drug delivery devices via self-assembly of amphiphilic block copolymers, Adv Drug Deliv Rev 53(1) (2001) 95-108.

[117] J.M. Janssen, S. Jackson, W.L. Heyward, R.S. Janssen, Immunogenicity of an investigational hepatitis B vaccine with a toll-like receptor 9 agonist adjuvant (HBsAg-1018) compared with a licensed hepatitis B vaccine in subpopulations of healthy adults 18-70 years of age, Vaccine 33(31) (2015) 3614-8.

[118] M. Lindemann, M. Zaslavskaya, M. Fiedler, B. Wilde, F.M. Heinemann, A. Heinold, P.A. Horn, O. Witzke, Humoral and Cellular Responses to a Single Dose of Fendrix in Renal Transplant Recipients with Non-response to Previous Hepatitis B Vaccination, Scand. J. Immunol. 85(1) (2017) 51-57.

[119] M. Hansson, P.A. Nygren, S. Stahl, Design and production of recombinant subunit vaccines, Biotechnol Appl Biochem 32 (Pt 2) (2000) 95-107.

[120] J.A. Wolff, R.W. Malone, P. Williams, W. Chong, G. Acsadi, A. Jani, P.L. Felgner, Direct gene transfer into mouse muscle in vivo, Science 247(4949 Pt 1) (1990) 1465-8.

[121] S. Jiao, P. Williams, R.K. Berg, B.A. Hodgeman, L. Liu, G. Repetto, J.A. Wolff, Direct gene transfer into nonhuman primate myofibers in vivo, Hum Gene Ther 3(1) (1992) 21-33.

[122] J.B. Ulmer, J.J. Donnelly, S.E. Parker, G.H. Rhodes, P.L. Felgner, V.J. Dwarki, S.H. Gromkowski, R.R. Deck, C.M. DeWitt, A. Friedman, et al., Heterologous protection against influenza by injection of DNA encoding a viral protein, Science 259(5102) (1993) 1745-9.

[123] K.J. McHugh, R. Guarecuco, R. Langer, A. Jaklenec, Single-injection vaccines: Progress, challenges, and opportunities, J Control Release 219 (2015) 596-609.

[124] N.S. Butler, J.C. Nolz, J.T. Harty, Immunologic considerations for generating memory CD8 T cells through vaccination, Cell Microbiol 13(7) (2011) 925-33.

[125] E.J. Wherry, M. Kurachi, Molecular and cellular insights into T cell exhaustion, Nat Rev Immunol 15(8) (2015) 486-99.

[126] J.J. Moon, B. Huang, D.J. Irvine, Engineering nano- and microparticles to tune immunity, Adv Mater 24(28) (2012) 3724-46.

[127] P.C. DeMuth, Y. Min, D.J. Irvine, P.T. Hammond, Implantable silk composite microneedles for programmable vaccine release kinetics and enhanced immunogenicity in transcutaneous immunization, Adv Healthc Mater 3(1) (2014) 47-58.

[128] C.J. Bishop, T.M. Ketola, S.Y. Tzeng, J.C. Sunshine, A. Urtti, H. Lemmetyinen, E. Vuorimaa-Laukkanen, M. Yliperttula, J.J. Green, The effect and role of carbon

atoms in poly(beta-amino ester)s for DNA binding and gene delivery, J Am Chem Soc 135(18) (2013) 6951-7.

[129] R.K. Gupta, M. Singh, D.T. O'Hagan, Poly(lactide-co-glycolide) microparticles for the development of single-dose controlled-release vaccines, Adv Drug Deliv Rev 32(3) (1998) 225-246.

[130] S. Zarrati, M. Mahdavi, F. Tabatabaie, Immune responses in DNA vaccine formulated with PMMA following immunization and after challenge with Leishmania major, J Parasit Dis 40(2) (2016) 427-35.

[131] S. Bobbala, V. Tamboli, A. McDowell, A.K. Mitra, S. Hook, Novel Injectable Pentablock Copolymer Based Thermoresponsive Hydrogels for Sustained Release Vaccines, AAPS J. 18(1) (2016) 261-9.

[132] S. Kalachandra, T. Takamata, D.M. Lin, E.A. Snyder, J. Webster-Cyriaque, Stability and release of antiviral drugs from ethylene vinyl acetate (EVA) copolymer, J Mater Sci Mater Med 17(12) (2006) 1227-36.

[133] J.A. Ko, H.J. Park, S.J. Hwang, J.B. Park, J.S. Lee, Preparation and characterization of chitosan microparticles intended for controlled drug delivery, Int J Pharm 249(1-2) (2002) 165-74.

[134] C. Wang, C. He, Z. Tong, X. Liu, B. Ren, F. Zeng, Combination of adsorption by porous CaCO3 microparticles and encapsulation by polyelectrolyte multilayer films for sustained drug delivery, Int J Pharm 308(1-2) (2006) 160-7.

[135] R. Farra, N.F. Sheppard, Jr., L. McCabe, R.M. Neer, J.M. Anderson, J.T. Santini, Jr., M.J. Cima, R. Langer, First-in-human testing of a wirelessly controlled drug delivery microchip, Sci Transl Med 4(122) (2012) 122ra21.

[136] H. Hu, K.M. Xiu, S.L. Xu, W.T. Yang, F.J. Xu, Functionalized layered double hydroxide nanoparticles conjugated with disulfide-linked polycation brushes for advanced gene delivery, Bioconjug Chem 24(6) (2013) 968-78.

[137] K.N. Yang, C.Q. Zhang, W. Wang, P.C. Wang, J.P. Zhou, X.J. Liang, pH-responsive mesoporous silica nanoparticles employed in controlled drug delivery systems for cancer treatment, Cancer Biol Med 11(1) (2014) 34-43.

[138] F. Titti, M.T. Maggiorella, F. Ferrantelli, L. Sernicola, S. Bellino, B. Collacchi, E. Fanales Belasio, S. Moretti, M.R. Pavone Cossut, R. Belli, E. Olivieri, S. Farcomeni, D. Compagnoni, Z. Michelini, M. Sabbatucci, K. Sparnacci, L. Tondelli, M. Laus, A. Cafaro, A. Caputo, B. Ensoli, Biocompatible anionic polymeric microspheres as priming delivery system for effetive HIV/AIDS Tat-based vaccines, PLoS One 9(10) (2014) e111360.

[139] E. Mathiowitz, J.S. Jacob, Y.S. Jong, G.P. Carino, D.E. Chickering, P. Chaturvedi, C.A. Santos, K. Vijayaraghavan, S. Montgomery, M. Bassett, C. Morrell, Biologically erodable microspheres as potential oral drug delivery systems, Nature 386(6623) (1997) 410-4.

[140] J. Cheng, B.A. Teply, I. Sherifi, J. Sung, G. Luther, F.X. Gu, E. Levy-Nissenbaum, A.F. Radovic-Moreno, R. Langer, O.C. Farokhzad, Formulation of

functionalized PLGA-PEG nanoparticles for in vivo targeted drug delivery, Biomaterials 28(5) (2007) 869-76.

[141] C.E. Astete, C.M. Sabliov, Synthesis and characterization of PLGA nanoparticles, J Biomater Sci Polym Ed 17(3) (2006) 247-89.

[142] C.L. Stevenson, J.T. Santini, Jr., R. Langer, Reservoir-based drug delivery systems utilizing microtechnology, Adv Drug Deliv Rev 64(14) (2012) 1590-602.

[143] R. Langer, New methods of drug delivery, Science 249(4976) (1990) 1527-33.

[144] K. McHugh, T. Nguyen, D. Yang, A. Linehan, J. Lu, S. Tzeng, A. Behrens, R. Langer, A. Jaklenec, Novel pulsatile-release microparticles for single-injection vaccination.

[145] J.T. Santini, Jr., M.J. Cima, R. Langer, A controlled-release microchip, Nature 397(6717) (1999) 335-8.

[146] P.C. DeMuth, J.J. Moon, H. Suh, P.T. Hammond, D.J. Irvine, Releasable layer-by-layer assembly of stabilized lipid nanocapsules on microneedles for enhanced transcutaneous vaccine delivery, ACS Nano 6(9) (2012) 8041-51.

[147] K. Ariga, Y.M. Lvov, K. Kawakami, Q. Ji, J.P. Hill, Layer-by-layer self-assembled shells for drug delivery, Adv Drug Deliv Rev 63(9) (2011) 762-71.

[148] K. van der Maaden, E. Sekerdag, P. Schipper, G. Kersten, W. Jiskoot, J. Bouwstra, Layer-by-Layer Assembly of Inactivated Poliovirus and N-Trimethyl Chitosan on pH-Sensitive Microneedles for Dermal Vaccination, Langmuir 31(31) (2015) 8654-60.

[149] R.A. Rosalia, L.J. Cruz, S. van Duikeren, A.T. Tromp, A.L. Silva, W. Jiskoot, T. de Gruijl, C. Lowik, J. Oostendorp, S.H. van der Burg, F. Ossendorp, CD40-targeted dendritic cell delivery of PLGA-nanoparticle vaccines induce potent anti-tumor responses, Biomaterials 40 (2015) 88-97.

[150] Y.N. Lee, M.C. Kim, Y.T. Lee, H.S. Hwang, M.K. Cho, J.S. Lee, E.J. Ko, Y.M. Kwon, S.M. Kang, AS04-adjuvanted virus-like particles containing multiple M2 extracellular domains of influenza virus confer improved protection, Vaccine 32(35) (2014) 4578-85.

[151] T.F. Leung, A.P. Liu, F.S. Lim, F. Thollot, H.M. Oh, B.W. Lee, L. Rombo, N.C. Tan, R. Rouzier, D. Friel, B. De Muynck, S. De Simoni, P. Suryakiran, M. Hezareh, N. Folschweiller, F. Thomas, F. Struyf, Comparative immunogenicity and safety of human papillomavirus (HPV)-16/18 AS04-adjuvanted vaccine and HPV-6/11/16/18 vaccine administered according to 2- and 3-dose schedules in girls aged 9-14 years: Results to month 12 from a randomized trial, Hum Vaccin Immunother 11(7) (2015) 1689-702.

[152] D. Apter, C.M. Wheeler, J. Paavonen, X. Castellsague, S.M. Garland, S.R. Skinner, P. Naud, J. Salmeron, S.N. Chow, H.C. Kitchener, J.C. Teixeira, U. Jaisamrarn, G. Limson, A. Szarewski, B. Romanowski, F.Y. Aoki, T.F. Schwarz, W.A. Poppe, F.X. Bosch, A. Mindel, P. de Sutter, K. Hardt, T. Zahaf, D. Descamps, F. Struyf, M. Lehtinen, G. Dubin, H.P.S. Group, Efficacy of human papillomavirus 16 and 18 (HPV-16/18) AS04-adjuvanted vaccine against cervical infection and

precancer in young women: final event-driven analysis of the randomized, double-blind PATRICIA trial, Clin Vaccine Immunol 22(4) (2015) 361-73.

[153] P. Song, S. He, A. Zhou, G. Lv, J. Guo, J. Zhou, Y. Han, H. Zhou, Z. Hao, H. Cong, Vaccination with toxofilin DNA in combination with an alum-monophosphoryl lipid A mixed adjuvant induces significant protective immunity against Toxoplasma gondii, BMC Infect Dis 17(1) (2017) 19.

[154] C. Pion, V. Courtois, S. Husson, M.C. Bernard, M.C. Nicolai, P. Talaga, E. Trannoy, C. Moste, R. Sodoyer, I. Legastelois, Characterization and immunogenicity in mice of recombinant influenza haemagglutinins produced in Leishmania tarentolae, Vaccine 32(43) (2014) 5570-6.

[155] I. Leroux-Roels, J.M. Devaster, G. Leroux-Roels, V. Verlant, I. Henckaerts, P. Moris, P. Hermand, P. Van Belle, J.T. Poolman, P. Vandepapeliere, Y. Horsmans, Adjuvant system AS02V enhances humoral and cellular immune responses to pneumococcal protein PhtD vaccine in healthy young and older adults: randomised, controlled trials, Vaccine 33(4) (2015) 577-84.

[156] G.E. Gray, K.H. Mayer, M.L. Elizaga, L.G. Bekker, M. Allen, L. Morris, D. Montefiori, S.C. De Rosa, A. Sato, N. Gu, G.D. Tomaras, T. Tucker, S.W. Barnett, N.N. Mkhize, X. Shen, K. Downing, C. Williamson, M. Pensiero, L. Corey, A.L. Williamson, Subtype C gp140 Vaccine Boosts Immune Responses Primed by the South African AIDS Vaccine Initiative DNA-C2 and MVA-C HIV Vaccines after More than a 2-Year Gap, Clin Vaccine Immunol 23(6) (2016) 496-506.

[157] J.J. Treanor, L. Chu, B. Essink, D. Muse, H.M. El Sahly, R. Izikson, K.L. Goldenthal, P. Patriarca, L.M. Dunkle, Stable emulsion (SE) alone is an effective adjuvant for a recombinant, baculovirus-expressed H5 influenza vaccine in healthy adults: A Phase 2 trial, Vaccine 35(6) (2017) 923-928.

[158] L.M. Howard, K.L. Hoek, J.B. Goll, P. Samir, A. Galassie, T.M. Allos, X. Niu, L.E. Gordy, C.B. Creech, N. Prasad, T.L. Jensen, H. Hill, S.E. Levy, S. Joyce, A.J. Link, K.M. Edwards, Cell-Based Systems Biology Analysis of Human AS03-Adjuvanted H5N1 Avian Influenza Vaccine Responses: A Phase I Randomized Controlled Trial, PLoS One 12(1) (2017) e0167488.

[159] S.C.T.P. Rts, Efficacy and safety of RTS,S/AS01 malaria vaccine with or without a booster dose in infants and children in Africa: final results of a phase 3, individually randomised, controlled trial, Lancet 386(9988) (2015) 31-45.

[160] A. Olotu, G. Fegan, J. Wambua, G. Nyangweso, A. Leach, M. Lievens, D.C. Kaslow, P. Njuguna, K. Marsh, P. Bejon, Seven-Year Efficacy of RTS,S/AS01 Malaria Vaccine among Young African Children, N Engl J Med 374(26) (2016) 2519-29.

[161] H. Lal, A.L. Cunningham, O. Godeaux, R. Chlibek, J. Diez-Domingo, S.J. Hwang, M.J. Levin, J.E. McElhaney, A. Poder, J. Puig-Barbera, T. Vesikari, D. Watanabe, L. Weckx, T. Zahaf, T.C. Heineman, Z.O.E.S. Group, Efficacy of an adjuvanted herpes zoster subunit vaccine in older adults, N Engl J Med 372(22) (2015) 2087-96.

[162] J.S. Woodworth, S.B. Cohen, A.O. Moguche, C.R. Plumlee, E.M. Agger, K.B. Urdahl, P. Andersen, Subunit vaccine H56/CAF01 induces a population of

circulating CD4 T cells that traffic into the Mycobacterium tuberculosis-infected lung, Mucosal Immunol (2016).

[163] M. Hamborg, R. Kramer, C.E. Schante, E.M. Agger, D. Christensen, L. Jorgensen, C. Foged, C.R. Middaugh, The physical stability of the recombinant tuberculosis fusion antigens h1 and h56, J Pharm Sci 102(10) (2013) 3567-78.

[164] P.F. McKay, A.V. Cope, J.F. Mann, S. Joseph, M. Esteban, R. Tatoud, D. Carter, S.G. Reed, J. Weber, R.J. Shattock, Glucopyranosyl lipid A adjuvant significantly enhances HIV specific T and B cell responses elicited by a DNA-MVA-protein vaccine regimen, PLoS One 9(1) (2014) e84707.

[165] J.Z. Oh, R. Ravindran, B. Chassaing, F.A. Carvalho, M.S. Maddur, M. Bower, P. Hakimpour, K.P. Gill, H.I. Nakaya, F. Yarovinsky, R.B. Sartor, A.T. Gewirtz, B. Pulendran, TLR5-mediated sensing of gut microbiota is necessary for antibody responses to seasonal influenza vaccination, Immunity 41(3) (2014) 478-92.

[166] M. Azuma, Y. Takeda, H. Nakajima, H. Sugiyama, T. Ebihara, H. Oshiumi, M. Matsumoto, T. Seya, Biphasic function of TLR3 adjuvant on tumor and spleen dendritic cells promotes tumor T cell infiltration and regression in a vaccine therapy, Oncoimmunology 5(8) (2016) e1188244.

[167] A.S. Cross, N. Greenberg, M. Billington, L. Zhang, C. DeFilippi, R.C. May, K.K. Bajwa, Phase 1 testing of detoxified LPS/group B meningococcal outer membrane protein vaccine with and without synthetic CPG 7909 adjuvant for the prevention and treatment of sepsis, Vaccine 33(48) (2015) 6719-26.

[168] H. Geldenhuys, H. Mearns, D.J. Miles, M. Tameris, D. Hokey, Z. Shi, S. Bennett, P. Andersen, I. Kromann, S.T. Hoff, W.A. Hanekom, H. Mahomed, M. Hatherill, T.J. Scriba, H.I.T.S. Group, M. van Rooyen, J. Bruce McClain, R. Ryall, G. de Bruyn, H.I.T.S. Groupa, The tuberculosis vaccine H4:IC31 is safe and induces a persistent polyfunctional CD4 T cell response in South African adults: A randomized controlled trial, Vaccine 33(30) (2015) 3592-9.

[169] S.L. Baldwin, W. Roeffen, S.K. Singh, R.W. Tiendrebeogo, M. Christiansen, E. Beebe, D. Carter, C.B. Fox, R.F. Howard, S.G. Reed, R. Sauerwein, M. Theisen, Synthetic TLR4 agonists enhance functional antibodies and CD4+ T-cell responses against the Plasmodium falciparum GMZ2.6C multi-stage vaccine antigen, Vaccine 34(19) (2016) 2207-15.

[170] A. Halliday, J.D. Turner, A. Guimaraes, P.A. Bates, M.J. Taylor, The TLR2/6 ligand PAM2CSK4 is a Th2 polarizing adjuvant in Leishmania major and Brugia malayi murine vaccine models, Parasit Vectors 9 (2016) 96.

[171] C. Buonsanti, C. Balocchi, C. Harfouche, F. Corrente, L. Galli Stampino, F. Mancini, M. Tontini, P. Malyala, S. Bufali, B. Baudner, E. De Gregorio, N.M. Valiante, D.T. O'Hagan, R. Rappuoli, U. D'Oro, Novel adjuvant Alum-TLR7 significantly potentiates immune response to glycoconjugate vaccines, Sci Rep 6 (2016) 29063.

[172] S.D. van Haren, D.J. Dowling, W. Foppen, D. Christensen, P. Andersen, S.G. Reed, R.M. Hershberg, L.R. Baden, O. Levy, Age-Specific Adjuvant Synergy: Dual

TLR7/8 and Mincle Activation of Human Newborn Dendritic Cells Enables Th1 Polarization, J Immunol 197(11) (2016) 4413-4424.

[173] A.J. Smith, Y. Li, H.G. Bazin, J.R. St-Jean, D. Larocque, J.T. Evans, J.R. Baldridge, Evaluation of novel synthetic TLR7/8 agonists as vaccine adjuvants, Vaccine 34(36) (2016) 4304-12.

[174] C.B. Fox, M.T. Orr, N. Van Hoeven, S.C. Parker, T.J. Mikasa, T. Phan, E.A. Beebe, G.I. Nana, S.W. Joshi, M.A. Tomai, J. Elvecrog, T.R. Fouts, S.G. Reed, Adsorption of a synthetic TLR7/8 ligand to aluminum oxyhydroxide for enhanced vaccine adjuvant activity: A formulation approach, J Control Release 244(Pt A) (2016) 98-107.

[175] D. Gordon, P. Kelley, S. Heinzel, P. Cooper, N. Petrovsky, Immunogenicity and safety of Advax, a novel polysaccharide adjuvant based on delta inulin, when formulated with hepatitis B surface antigen: a randomized controlled Phase 1 study, Vaccine 32(48) (2014) 6469-77.

[176] G. Barhate, M. Gautam, S. Gairola, S. Jadhav, V. Pokharkar, Enhanced mucosal immune responses against tetanus toxoid using novel delivery system comprised of chitosan-functionalized gold nanoparticles and botanical adjuvant: characterization, immunogenicity, and stability assessment, J Pharm Sci 103(11) (2014) 3448-56.

[177] S. Arthanari, G. Mani, M.M. Peng, H.T. Jang, Chitosan-HPMC-blended microspheres as a vaccine carrier for the delivery of tetanus toxoid, Artif Cells Nanomed Biotechnol 44(2) (2016) 517-23.

[178] C. Sawaengsak, Y. Mori, K. Yamanishi, A. Mitrevej, N. Sinchaipanid, Chitosan nanoparticle encapsulated hemagglutinin-split influenza virus mucosal vaccine, AAPS PharmSciTech 15(2) (2014) 317-25.

[179] E.C. Carroll, L. Jin, A. Mori, N. Munoz-Wolf, E. Oleszycka, H.B. Moran, S. Mansouri, C.P. McEntee, E. Lambe, E.M. Agger, P. Andersen, C. Cunningham, P. Hertzog, K.A. Fitzgerald, A.G. Bowie, E.C. Lavelle, The Vaccine Adjuvant Chitosan Promotes Cellular Immunity via DNA Sensor cGAS-STING-Dependent Induction of Type I Interferons, Immunity 44(3) (2016) 597-608.

[180] S.A. Kalams, S. Parker, X. Jin, M. Elizaga, B. Metch, M. Wang, J. Hural, M. Lubeck, J. Eldridge, M. Cardinali, W.A. Blattner, M. Sobieszczyk, V. Suriyanon, A. Kalichman, D.B. Weiner, L.R. Baden, N.H.V.T. Network, Safety and immunogenicity of an HIV-1 gag DNA vaccine with or without IL-12 and/or IL-15 plasmid cytokine adjuvant in healthy, HIV-1 uninfected adults, PLoS One 7(1) (2012) e29231.

[181] S.A. Kalams, S.D. Parker, M. Elizaga, B. Metch, S. Edupuganti, J. Hural, S. De Rosa, D.K. Carter, K. Rybczyk, I. Frank, J. Fuchs, B. Koblin, D.H. Kim, P. Joseph, M.C. Keefer, L.R. Baden, J. Eldridge, J. Boyer, A. Sherwat, M. Cardinali, M. Allen, M. Pensiero, C. Butler, A.S. Khan, J. Yan, N.Y. Sardesai, J.G. Kublin, D.B. Weiner, N.H.V.T. Network, Safety and comparative immunogenicity of an HIV-1 DNA vaccine in combination with plasmid interleukin 12 and impact of intramuscular electroporation for delivery, J Infect Dis 208(5) (2013) 818-29.

[182] D.J. Shedlock, C. Tingey, L. Mahadevan, N. Hutnick, E.L. Reuschel, S. Kudchodkar, S. Flingai, J. Yan, J.J. Kim, K.E. Ugen, D.B. Weiner, K. Muthumani, Co-Administration of Molecular Adjuvants Expressing NF-Kappa B Subunit p65/RelA or Type-1 Transactivator T-bet Enhance Antigen Specific DNA Vaccine-Induced Immunity, Vaccines (Basel) 2(2) (2014) 196-215.

[183] N. Bruffaerts, M. Romano, O. Denis, F. Jurion, K. Huygen, Increasing the Vaccine Potential of Live M. bovis BCG by Coadministration with Plasmid DNA Encoding a Tuberculosis Prototype Antigen, Vaccines (Basel) 2(1) (2014) 181-95.

[184] Y. Wan, X. Ren, Y. Ren, J. Wang, Z. Hu, X. Xie, J. Xu, As a genetic adjuvant, CTA improves the immunogenicity of DNA vaccines in an ADP-ribosyltransferase activity- and IL-6-dependent manner, Vaccine 32(19) (2014) 2173-80.

[185] S. Qiu, X. Ren, Y. Ben, Y. Ren, J. Wang, X. Zhang, Y. Wan, J. Xu, Fusion-expressed CTB improves both systemic and mucosal T-cell responses elicited by an intranasal DNA priming/intramuscular recombinant vaccinia boosting regimen, J Immunol Res 2014 (2014) 308732.

[186] H.K. Maity, S. Dey, C.M. Mohan, S.A. Khulape, D.C. Pathak, V.N. Vakharia, Protective efficacy of a DNA vaccine construct encoding the VP2 gene of infectious bursal disease and a truncated HSP70 of Mycobacterium tuberculosis in chickens, Vaccine 33(8) (2015) 1033-9.

[187] J. Ruan, Y. Duan, F. Li, Z. Wang, Enhanced synergistic anti-Lewis lung carcinoma effect of a DNA vaccine harboring a MUC1-VEGFR2 fusion gene used with GM-CSF as an adjuvant, Clin Exp Pharmacol Physiol 44(1) (2017) 71-78.

[188] J.C. Gilhodes, Y. Jule, S. Kreuz, B. Stierstorfer, D. Stiller, L. Wollin, Quantification of Pulmonary Fibrosis in a Bleomycin Mouse Model Using Automated Histological Image Analysis, PLoS One 12(1) (2017) e0170561.

[189] A. Ciabattini, E. Pettini, F. Fiorino, G. Pastore, P. Andersen, G. Pozzi, D. Medaglini, Modulation of Primary Immune Response by Different Vaccine Adjuvants, Front Immunol 7 (2016) 427.

[190] C. Schmidt, Clinical setbacks for toll-like receptor 9 agonists in cancer, Nat Biotechnol 25(8) (2007) 825-6.

[191] C.M. Sun, E. Deriaud, C. Leclerc, R. Lo-Man, Upon TLR9 signaling, CD5+ B cells control the IL-12-dependent Th1-priming capacity of neonatal DCs, Immunity 22(4) (2005) 467-77.

[192] S.C.T.P. Rts, S.T. Agnandji, B. Lell, S.S. Soulanoudjingar, J.F. Fernandes, B.P. Abossolo, C. Conzelmann, B.G. Methogo, Y. Doucka, A. Flamen, B. Mordmuller, S. Issifou, P.G. Kremsner, J. Sacarlal, P. Aide, M. Lanaspa, J.J. Aponte, A. Nhamuave, D. Quelhas, Q. Bassat, S. Mandjate, E. Macete, P. Alonso, S. Abdulla, N. Salim, O. Juma, M. Shomari, K. Shubis, F. Machera, A.S. Hamad, R. Minja, A. Mtoro, A. Sykes, S. Ahmed, A.M. Urassa, A.M. Ali, G. Mwangoka, M. Tanner, H. Tinto, U. D'Alessandro, H. Sorgho, I. Valea, M.C. Tahita, W. Kabore, S. Ouedraogo, Y. Sandrine, R.T. Guiguemde, J.B. Ouedraogo, M.J. Hamel, S. Kariuki, C. Odero, M. Oneko, K. Otieno, N. Awino, J. Omoto, J. Williamson, V. Muturi-Kioi, K.F. Laserson, L. Slutsker, W. Otieno, L. Otieno, O. Nekoye, S. Gondi, A. Otieno, B. Ogutu, R. Wasuna, V. Owira, D. Jones, A.A. Onyango, P. Njuguna, R. Chilengi, P.

Akoo, C. Kerubo, J. Gitaka, C. Maingi, T. Lang, A. Olotu, B. Tsofa, P. Bejon, N. Peshu, K. Marsh, S. Owusu-Agyei, K.P. Asante, K. Osei-Kwakye, O. Boahen, S. Ayamba, K. Kayan, R. Owusu-Ofori, D. Dosoo, I. Asante, G. Adjei, G. Adjei, D. Chandramohan, B. Greenwood, J. Lusingu, S. Gesase, A. Malabeja, O. Abdul, H. Kilavo, C. Mahende, E. Liheluka, M. Lemnge, T. Theander, C. Drakeley, D. Ansong, T. Agbenyega, S. Adjei, H.O. Boateng, T. Rettig, J. Bawa, J. Sylverken, D. Sambian, A. Agyekum, L. Owusu, F. Martinson, I. Hoffman, T. Mvalo, P. Kamthunzi, R. Nkomo, A. Msika, A. Jumbe, N. Chome, D. Nyakuipa, J. Chintedza, W.R. Ballou, M. Bruls, J. Cohen, Y. Guerra, E. Jongert, D. Lapierre, A. Leach, M. Lievens, O. Ofori-Anyinam, J. Vekemans, T. Carter, D. Leboulleux, C. Loucq, A. Radford, B. Savarese, D. Schellenberg, M. Sillman, P. Vansadia, First results of phase 3 trial of RTS,S/AS01 malaria vaccine in African children, N Engl J Med 365(20) (2011) 1863-75.

[193] F.M. Carbinatto, A.D. de Castro, R.C. Evangelista, B.S.F. Cury, Insights into the swelling process and drug release mechanisms from cross-linked pectin/high amylose starch matrices, Asian Journal of Pharmaceutical Sciences 9(1) (2014) 27-34.

[194] I. Tamayo, J.M. Irache, C. Mansilla, J. Ochoa-Reparaz, J.J. Lasarte, C. Gamazo, Poly(anhydride) nanoparticles act as active Th1 adjuvants through Toll-like receptor exploitation, Clin Vaccine Immunol 17(9) (2010) 1356-62.

[195] E.I. Wafa, S.M. Geary, J.T. Goodman, B. Narasimhan, A.K. Salem, The effect of polyanhydride chemistry in particle-based cancer vaccines on the magnitude of the anti-tumor immune response, Acta Biomater 50 (2017) 417-427.

[196] S. Dhakal, J. Goodman, K. Bondra, Y.S. Lakshmanappa, J. Hiremath, D.L. Shyu, K. Ouyang, K.I. Kang, S. Krakowka, M.J. Wannemuehler, C. Won Lee, B. Narasimhan, G.J. Renukaradhya, Polyanhydride nanovaccine against swine influenza virus in pigs, Vaccine 35(8) (2017) 1124-1131.

[197] K.A. Ross, H. Loyd, W. Wu, L. Huntimer, S. Ahmed, A. Sambol, S. Broderick, Z. Flickinger, K. Rajan, T. Bronich, S. Mallapragada, M.J. Wannemuehler, S. Carpenter, B. Narasimhan, Hemagglutinin-based polyanhydride nanovaccines against H5N1 influenza elicit protective virus neutralizing titers and cell-mediated immunity, Int J Nanomedicine 10 (2015) 229-43.

[198] A.K. Shakya, A. Kumar, R. Holmdahl, K.S. Nandakumar, Macrophage-derived reactive oxygen species protects against autoimmune priming with a defined polymeric adjuvant, Immunology 147(1) (2016) 125-32.

[199] A.L. Silva, P.C. Soema, B. Slutter, F. Ossendorp, W. Jiskoot, PLGA particulate delivery systems for subunit vaccines: Linking particle properties to immunogenicity, Hum Vaccin Immunother 12(4) (2016) 1056-69.

[200] G. Mittal, D.K. Sahana, V. Bhardwaj, M.N. Ravi Kumar, Estradiol loaded PLGA nanoparticles for oral administration: effect of polymer molecular weight and copolymer composition on release behavior in vitro and in vivo, J Control Release 119(1) (2007) 77-85.

196

[201] P. Li, C. Asokanathan, F. Liu, K.K. Khaing, D. Kmiec, X. Wei, B. Song, D. Xing, D. Kong, PLGA nano/micro particles encapsulated with pertussis toxoid (PTd) enhances Th1/Th17 immune response in a murine model, Int J Pharm 513(1-2) (2016) 183-190.

[202] L.J. Cruz, P.J. Tacken, C. Eich, F. Rueda, R. Torensma, C.G. Figdor, Controlled release of antigen and Toll-like receptor ligands from PLGA nanoparticles enhances immunogenicity, Nanomedicine (Lond) 12(5) (2017) 491-510.

[203] A. Ghanem, R. Healey, F.G. Adly, Current trends in separation of plasmid DNA vaccines: a review, Anal. Chim. Acta 760 (2013) 1-15.

[204] K. Zhu, H. Jin, Z. He, Q. Zhu, B. Wang, A continuous method for the large-scale extraction of plasmid DNA by modified boiling lysis, Nat. Protoc. 1(6) (2006) 3088-93.

[205] T. Vogl, M. Ahmad, F.W. Krainer, H. Schwab, A. Glieder, Restriction site free cloning (RSFC) plasmid family for seamless, sequence independent cloning in Pichia pastoris, Microb Cell Fact 14 (2015) 103.

[206] J.M. Cregg, K.J. Barringer, A.Y. Hessler, K.R. Madden, Pichia pastoris as a host system for transformations, Mol. Cell. Biol. 5(12) (1985) 3376-85.

[207] P.D. Williams, P.A. Kingston, Plasmid-mediated gene therapy for cardiovascular disease, Cardiovasc Res 91(4) (2011) 565-76.

[208] G.M. Borja, E. Meza Mora, B. Barron, G. Gosset, O.T. Ramirez, A.R. Lara, Engineering Escherichia coli to increase plasmid DNA production in high cell-density cultivations in batch mode, Microb Cell Fact 11 (2012) 132.

[209] K. Listner, L.K. Bentley, M. Chartrain, A simple method for the production of plasmid DNA in bioreactors, Methods Mol. Med. 127 (2006) 295-309.

[210] N. Miura, S.M. Shaheen, H. Akita, T. Nakamura, H. Harashima, A KALA-modified lipid nanoparticle containing CpG-free plasmid DNA as a potential DNA vaccine carrier for antigen presentation and as an immune-stimulative adjuvant, Nucleic Acids Res 43(3) (2015) 1317-31.

[211] M.M. Munye, A.D. Tagalakis, J.L. Barnes, R.E. Brown, R.J. McAnulty, S.J. Howe, S.L. Hart, Minicircle DNA Provides Enhanced and Prolonged Transgene Expression Following Airway Gene Transfer, Sci Rep 6 (2016) 23125.

[212] Q. Wang, W. Jiang, Y. Chen, P. Liu, C. Sheng, S. Chen, H. Zhang, C. Pan, S. Gao, W. Huang, In vivo electroporation of minicircle DNA as a novel method of vaccine delivery to enhance HIV-1-specific immune responses, J. Virol. 88(4) (2014) 1924-34.

[213] M.A. Kay, C.Y. He, Z.Y. Chen, A robust system for production of minicircle DNA vectors, Nat. Biotechnol. 28(12) (2010) 1287-9.

[214] Z.Y. Chen, C.Y. He, A. Ehrhardt, M.A. Kay, Minicircle DNA vectors devoid of bacterial DNA result in persistent and high-level transgene expression in vivo, Mol. Ther. 8(3) (2003) 495-500.

[215] N. Nafissi, R. Slavcev, Bacteriophage recombination systems and biotechnical applications, Appl. Microbiol. Biotechnol. 98(7) (2014) 2841-51.

[216] I. van der Heijden, J.H. Beijnen, B. Nuijen, Long term stability of lyophilized plasmid DNA pDERMATT, Int. J. Pharm. 453(2) (2013) 648-50.

[217] D. Pogocki, C. Schoneich, Chemical stability of nucleic acid-derived drugs, J. Pharm. Sci. 89(4) (2000) 443-56.

[218] A. Kronbichler, J. Kerschbaum, G. Mayer, The Influence and Role of Microbial Factors in Autoimmune Kidney Diseases: A Systematic Review, J Immunol Res 2015 (2015) 858027.

[219] R. Monjezi, C. Miskey, T. Gogishvili, M. Schleef, M. Schmeer, H. Einsele, Z. Ivics, M. Hudecek, Enhanced CAR T-cell engineering using non-viral Sleeping Beauty transposition from minicircle vectors, Leukemia 31(1) (2017) 186-194.

[220] V.T. Colluru, C.D. Zahm, D.G. McNeel, Mini-intronic plasmid vaccination elicits tolerant LAG3+ CD8+ T cells and inferior antitumor responses, Oncoimmunology 5(10) (2016) e1223002.

[221] S. Wong, P. Lam, N. Nafissi, S. Denniss, R. Slavcev, Production of Double-stranded DNA Ministrings, J. Vis. Exp. (108) (2016) 53177.

[222] C.H. Sum, N. Nafissi, R.A. Slavcev, S. Wettig, Physical Characterization of Gemini Surfactant-Based Synthetic Vectors for the Delivery of Linear Covalently Closed (LCC) DNA Ministrings, PLoS One 10(11) (2015) e0142875.

[223] L. Li, F. Saade, N. Petrovsky, The future of human DNA vaccines, J Biotechnol 162(2-3) (2012) 171-82.

[224] X. Jin, C. Morgan, X. Yu, S. DeRosa, G.D. Tomaras, D.C. Montefiori, J. Kublin, L. Corey, M.C. Keefer, N.H.V.T. Network, Multiple factors affect immunogenicity of DNA plasmid HIV vaccines in human clinical trials, Vaccine 33(20) (2015) 2347-53.

[225] G.S. Gilkeson, J.P. Grudier, D.G. Karounos, D.S. Pisetsky, Induction of anti-double stranded DNA antibodies in normal mice by immunization with bacterial DNA, J Immunol 142(5) (1989) 1482-6.

[226] D. Lilic, S.K. Ghosh, Liver dysfunction and DNA antibodies after hepatitis B vaccination, Lancet 344(8932) (1994) 1292-3.

[227] Y. Zafrir, N. Agmon-Levin, Z. Paz, T. Shilton, Y. Shoenfeld, Autoimmunity following hepatitis B vaccine as part of the spectrum of 'Autoimmune (Auto-inflammatory) Syndrome induced by Adjuvants' (ASIA): analysis of 93 cases, Lupus 21(2) (2012) 146-52.

[228] G. Mor, M. Singla, A.D. Steinberg, S.L. Hoffman, K. Okuda, D.M. Klinman, Do DNA vaccines induce autoimmune disease?, Hum. Gene Ther. 8(3) (1997) 293-300.

[229] H. Wurtele, K.C. Little, P. Chartrand, Illegitimate DNA integration in mammalian cells, Gene Ther 10(21) (2003) 1791-9.

[230] D.M. Klinman, S. Klaschik, D. Tross, H. Shirota, F. Steinhagen, FDA guidance on prophylactic DNA vaccines: analysis and recommendations, Vaccine 28(16) (2010) 2801-5.

[231] P. Crine, W.G. Verly, A study of DNA spontaneous degradation, Biochim Biophys Acta 442(1) (1976) 50-7.

[232] M. Karni, D. Zidon, P. Polak, Z. Zalevsky, O. Shefi, Thermal degradation of DNA, DNA Cell Biol 32(6) (2013) 298-301.

[233] T. Nguyen-Hieu, G. Aboudharam, M. Drancourt, Heat degradation of eukaryotic and bacterial DNA: an experimental model for paleomicrobiology, BMC Res Notes 5 (2012) 528.

[234] T. Lindahl, Instability and decay of the primary structure of DNA, Nature 362(6422) (1993) 709-15.

[235] C.J. Bishop, R.L. Majewski, T.M. Guiriba, D.R. Wilson, N.S. Bhise, A. Quinones-Hinojosa, J.J. Green, Quantification of Cellular and Nuclear Uptake Rates of Polymeric Gene Delivery Nanoparticles and DNA Plasmids via Flow Cytometry, Acta Biomater. doi:10.1016/j.actbio.2016.03.036 (2016).

[236] C.J. Bishop, K.L. Kozielski, J.J. Green, Exploring the role of polymer structure on intracellular nucleic acid delivery via polymeric nanoparticles, J Control Release 219 (2015) 488-99.

[237] R.K. Evans, Z. Xu, K.E. Bohannon, B. Wang, M.W. Bruner, D.B. Volkin, Evaluation of degradation pathways for plasmid DNA in pharmaceutical formulations via accelerated stability studies, J Pharm Sci 89(1) (2000) 76-87.

[238] H.V. Jain, S.L. Beaucage, An amphipathic trans-acting phosphorothioate DNA element delivers uncharged PNA and PMO nucleic acid sequences in mammalian cells, Curr Protoc Nucleic Acid Chem 64 (2016) 4 69 1-4 69 22.

[239] S. Siddiquee, K. Rovina, A. Azriah, A Review of Peptide Nucleic Acid, Advanced Techniques in Biology & Medicine (2015) 1-10.

[240] D. Takai, P.A. Jones, Comprehensive analysis of CpG islands in human chromosomes 21 and 22, Proc Natl Acad Sci U S A 99(6) (2002) 3740-5.

[241] P.A. Jones, Functions of DNA methylation: islands, start sites, gene bodies and beyond, Nat Rev Genet 13(7) (2012) 484-92.

[242] L.A. Mulcahy, R.C. Pink, D.R. Carter, Routes and mechanisms of extracellular vesicle uptake, J Extracell Vesicles 3 (2014).

[243] C.E. Adkins, R.K. Mittapalli, V.K. Manda, M.I. Nounou, A.S. Mohammad, T.B. Terrell, K.A. Bohn, C. Yasemin, T.R. Grothe, J.A. Lockman, P.R. Lockman, P-glycoprotein mediated efflux limits substrate and drug uptake in a preclinical brain metastases of breast cancer model, Front Pharmacol 4 (2013) 136.

[244] V.B. Lu, D.J. Williams, Y.J. Won, S.R. Ikeda, Intranuclear microinjection of DNA into dissociated adult mammalian neurons, J Vis Exp (34) (2009).

[245] H.N. Youn, D.H. Lee, Y.N. Lee, J.K. Park, S.S. Yuk, S.Y. Yang, H.J. Lee, S.H. Woo, H.M. Kim, J.B. Lee, S.Y. Park, I.S. Choi, C.S. Song, Intranasal administration of live Lactobacillus species facilitates protection against influenza virus infection in mice, Antiviral Res 93(1) (2012) 138-43.

[246] S. Sasaki, K. Sumino, K. Hamajima, J. Fukushima, N. Ishii, S. Kawamoto, H. Mohri, C.R. Kensil, K. Okuda, Induction of systemic and mucosal immune responses to human immunodeficiency virus type 1 by a DNA vaccine formulated with QS-21 saponin adjuvant via intramuscular and intranasal routes, J. Virol. 72(6) (1998) 4931-9.

[247] T.M. Pertmer, T.R. Roberts, J.R. Haynes, Influenza virus nucleoprotein-specific immunoglobulin G subclass and cytokine responses elicited by DNA vaccination are dependent on the route of vector DNA delivery, J Virol 70(9) (1996) 6119-25.

[248] J.W. Hooper, J.E. Moon, K.M. Paolino, R. Newcomer, D.E. McLain, M. Josleyn, D. Hannaman, C. Schmaljohn, A Phase 1 clinical trial of Hantaan virus and Puumala virus M-segment DNA vaccines for haemorrhagic fever with renal syndrome delivered by intramuscular electroporation, Clin Microbiol Infect 20 Suppl 5 (2014) 110-7.

[249] S.P. McBurney, J.E. Sunshine, S. Gabriel, J.P. Huynh, W.F. Sutton, D.H. Fuller, N.L. Haigwood, W.B. Messer, Evaluation of protection induced by a dengue virus serotype 2 envelope domain III protein scaffold/DNA vaccine in non-human primates, Vaccine 34(30) (2016) 3500-7.

[250] A.H. Choi, D.R. Knowlton, M.M. McNeal, R.L. Ward, Particle bombardment-mediated DNA vaccination with rotavirus VP6 induces high levels of serum rotavirus IgG but fails to protect mice against challenge, Virology 232(1) (1997) 129-38.

[251] H. Davtyan, A. Ghochikyan, N. Movsesyan, B. Ellefsen, I. Petrushina, D.H. Cribbs, D. Hannaman, C.F. Evans, M.G. Agadjanyan, Delivery of a DNA vaccine for Alzheimer's disease by electroporation versus gene gun generates potent and similar immune responses, Neurodegener Dis 10(1-4) (2012) 261-4.

[252] A. Sharei, J. Zoldan, A. Adamo, W.Y. Sim, N. Cho, E. Jackson, S. Mao, S. Schneider, M.J. Han, A. Lytton-Jean, P.A. Basto, S. Jhunjhunwala, J. Lee, D.A. Heller, J.W. Kang, G.C. Hartoularos, K.S. Kim, D.G. Anderson, R. Langer, K.F. Jensen, A vector-free microfluidic platform for intracellular delivery, Proc Natl Acad Sci U S A 110(6) (2013) 2082-7.

[253] R. Karshafian, P.D. Bevan, R. Williams, S. Samac, P.N. Burns, Sonoporation by ultrasound-activated microbubble contrast agents: effect of acoustic exposure parameters on cell membrane permeability and cell viability, Ultrasound Med Biol 35(5) (2009) 847-60.

[254] C.S. Kim, R. Mout, Y. Zhao, Y.C. Yeh, R. Tang, Y. Jeong, B. Duncan, J.A. Hardy, V.M. Rotello, Co-delivery of protein and small molecule therapeutics using nanoparticle-stabilized nanocapsules, Bioconjug Chem 26(5) (2015) 950-4.

[255] R. Tang, C.S. Kim, D.J. Solfiell, S. Rana, R. Mout, E.M. Velazquez-Delgado, A. Chompoosor, Y. Jeong, B. Yan, Z.J. Zhu, C. Kim, J.A. Hardy, V.M. Rotello, Direct delivery of functional proteins and enzymes to the cytosol using nanoparticle-stabilized nanocapsules, ACS Nano 7(8) (2013) 6667-6673.

[256] L.B. Sims, L.T. Curtis, H.B. Frieboes, J.M. Steinbach-Rankins, Enhanced uptake and transport of PLGA-modified nanoparticles in cervical cancer, J Nanobiotechnology 14 (2016) 33.

[257] C.J. Bishop, B. Abubaker-Sharif, T. Guiriba, S.Y. Tzeng, J.J. Green, Gene delivery polymer structure-function relationships elucidated via principal component analysis, Chem. Commun. 51(60) (2015) 12134-7.

[258] H. Guerrero-Cazares, S.Y. Tzeng, N.P. Young, A.O. Abutaleb, A. Quinones-Hinojosa, J.J. Green, Biodegradable Polymeric Nanoparticles Show High Efficacy and Specificity at DNA Delivery to Human Glioblastoma in Vitro and in Vivo, Acs Nano 8(5) (2014) 5141-5153.

[259] J.-P. Behr, The Proton Sponge: a Trick to Enter Cells the Viruses Did Not Exploit, CHIMIA International Journal for Chemistry 51(1-2) (1997) 34-36.

[260] R.V. Benjaminsen, M.A. Mattebjerg, J.R. Henriksen, S.M. Moghimi, T.L. Andresen, The possible "proton sponge " effect of polyethylenimine (PEI) does not include change in lysosomal pH, Mol Ther 21(1) (2013) 149-57.

[261] I. Nakase, S. Futaki, Combined treatment with a pH-sensitive fusogenic peptide and cationic lipids achieves enhanced cytosolic delivery of exosomes, Sci Rep 5 (2015) 10112.

[262] Y. Hu, B. Xu, J. Xu, D. Shou, E. Liu, J. Gao, W. Liang, Y. Huang, Microneedle-assisted dendritic cell-targeted nanoparticles for transcutaneous DNA immunization, Polymer Chemistry 6(3) (2015) 373-379.

[263] T.F. Martens, K. Remaut, J. Demeester, S.C. De Smedt, K. Braeckmans, Intracellular delivery of nanomaterials: How to catch endosomal escape in the act, Nano Today 9(3) (2014) 344-364.

[264] J. Hu, L. Qiu, X. Wang, X. Zou, M. Lu, J. Yin, Carbohydrate-based vaccine adjuvants - discovery and development, Expert Opin Drug Discov 10(10) (2015) 1133-44.

[265] Q. Hu, J. Wang, J. Shen, M. Liu, X. Jin, G. Tang, P.K. Chu, Intracellular pathways and nuclear localization signal peptide-mediated gene transfection by cationic polymeric nanovectors, Biomaterials 33(4) (2012) 1135-45.

[266] M.A. Badding, E.E. Vaughan, D.A. Dean, Transcription factor plasmid binding modulates microtubule interactions and intracellular trafficking during gene transfer, Gene Ther. 19(3) (2012) 338-46.

[267] C.J. Bishop, K.L. Kozielski, J.J. Green, Exploring the role of polymer structure on intracellular nucleic acid delivery via polymeric nanoparticles, J. Control. Release 219 (2015) 488-499.

[268] J.C. Sunshine, C.J. Bishop, J.J. Green, Advances in polymeric and inorganic vectors for nonviral nucleic acid delivery, Ther Deliv 2(4) (2011) 493-521.

[269] P.P. Hung, C.M. Ling, L.R. Overby, Self-assembly of Q-beta and MS2 phage particles: possible function of initiation complexes, Science 166(3913) (1969) 1638-40.

[270] B. Akache, R.D. Weeratna, A. Deora, J.M. Thorn, B. Champion, J.R. Merson, H.L. Davis, M.J. McCluskie, Anti-IgE Qb-VLP Conjugate Vaccine Self-Adjuvants through Activation of TLR7, Vaccines (Basel) 4(1) (2016).

[271] P.A. Goepfert, M.L. Elizaga, K. Seaton, G.D. Tomaras, D.C. Montefiori, A. Sato, J. Hural, S.C. DeRosa, S.A. Kalams, M.J. McElrath, M.C. Keefer, L.R. Baden, J.R. Lama, J. Sanchez, M.J. Mulligan, S.P. Buchbinder, S.M. Hammer, B.A. Koblin, M. Pensiero, C. Butler, B. Moss, H.L. Robinson, H.S. Group, A. National Institutes of, H.I.V.V.T.N. Infectious Diseases, Specificity and 6-month durability of immune responses induced by DNA and recombinant modified vaccinia Ankara vaccines expressing HIV-1 virus-like particles, J Infect Dis 210(1) (2014) 99-110.

[272] N. Noranate, N. Takeda, P. Chetanachan, P. Sittisaman, A.N. A, S. Anantapreecha, Characterization of chikungunya virus-like particles, PLoS One 9(9) (2014) e108169.

[273] L.J. Chang, K.A. Dowd, F.H. Mendoza, J.G. Saunders, S. Sitar, S.H. Plummer, G. Yamshchikov, U.N. Sarwar, Z. Hu, M.E. Enama, R.T. Bailer, R.A. Koup, R.M. Schwartz, W. Akahata, G.J. Nabel, J.R. Mascola, T.C. Pierson, B.S. Graham, J.E. Ledgerwood, V.R.C.S. Team, Safety and tolerability of chikungunya virus-like particle vaccine in healthy adults: a phase 1 dose-escalation trial, Lancet 384(9959) (2014) 2046-52.

[274] J.G. Low, L.S. Lee, E.E. Ooi, K. Ethirajulu, P. Yeo, A. Matter, J.E. Connolly, D.A. Skibinski, P. Saudan, M. Bachmann, B.J. Hanson, Q. Lu, S. Maurer-Stroh, S. Lim, V. Novotny-Diermayr, Safety and immunogenicity of a virus-like particle pandemic influenza A (H1N1) 2009 vaccine: results from a double-blinded, randomized Phase I clinical trial in healthy Asian volunteers, Vaccine 32(39) (2014) 5041-8.

[275] M. Safaeian, C. Porras, Y. Pan, A. Kreimer, J.T. Schiller, P. Gonzalez, D.R. Lowy, S. Wacholder, M. Schiffman, A.C. Rodriguez, R. Herrero, T. Kemp, G. Shelton, W. Quint, L.J. van Doorn, A. Hildesheim, L.A. Pinto, C.V.T. Group, Durable antibody responses following one dose of the bivalent human papillomavirus L1 virus-like particle vaccine in the Costa Rica Vaccine Trial, Cancer Prev Res (Phila) 6(11) (2013) 1242-50.

[276] M.A. Kotterman, D.V. Schaffer, Engineering adeno-associated viruses for clinical gene therapy, Nat Rev Genet 15(7) (2014) 445-51.

[277] C.E. Thomas, A. Ehrhardt, M.A. Kay, Progress and problems with the use of viral vectors for gene therapy, Nat Rev Genet 4(5) (2003) 346-58.

[278] S.C. Harrison, Viral membrane fusion, Virology 479-480 (2015) 498-507.

[279] T. Gargett, B. Grubor-Bauk, D. Miller, T. Garrod, S. Yu, S. Wesselingh, A. Suhrbier, E.J. Gowans, Increase in DNA vaccine efficacy by virosome delivery and co-expression of a cytolytic protein, Clin Transl Immunology 3(6) (2014) e18.

[280] G. Leroux-Roels, C. Maes, F. Clement, F. van Engelenburg, M. van den Dobbelsteen, M. Adler, M. Amacker, L. Lopalco, M. Bomsel, A. Chalifour, S. Fleury, Randomized Phase I: Safety, Immunogenicity and Mucosal Antiviral Activity in Young Healthy Women Vaccinated with HIV-1 Gp41 P1 Peptide on Virosomes, PLoS One 8(2) (2013) e55438.

[281] J.F. Aldrich, M.H. Shearer, D.B. Lowe, R.E. Winn, C.A. Jumper, R.C. Kennedy, R.K. Bright, The role of gamma interferon in DNA vaccine-induced tumor immunity targeting simian virus 40 large tumor antigen, Cancer Immunol. Immunother. 62(2) (2013) 371-82.

[282] L. Redding, D.B. Weiner, DNA vaccines in veterinary use, Expert Rev Vaccines 8(9) (2009) 1251-76.

[283] Y. Wang, S. Wu, Z.C. Wang, X.M. Zhu, X.T. Yin, K. Gao, Z.Y. Du, G.Z. Chen, J.Y. Yu, Enhanced immunity and antiviral effects of an HBV DNA vaccine delivered by a DC-targeting protein, J Viral Hepat 23(10) (2016) 798-804.

[284] S.K. Khattar, A.L. DeVico, C.C. LaBranche, A. Panda, D.C. Montefiori, S.K. Samal, Enhanced Immune Responses to HIV-1 Envelope Elicited by a Vaccine Regimen Consisting of Priming with Newcastle Disease Virus Expressing HIV gp160 and Boosting with gp120 and SOSIP gp140 Proteins, J Virol 90(3) (2015) 1682-6.

[285] S. Gupta, E.S. Clark, J.M. Termini, J. Boucher, S. Kanagavelu, C.C. LeBranche, S. Abraham, D.C. Montefiori, W.N. Khan, G.W. Stone, DNA vaccine molecular adjuvants SP-D-BAFF and SP-D-APRIL enhance anti-gp120 immune response and increase HIV-1 neutralizing antibody titers, J Virol 89(8) (2015) 4158-69.

[286] H.C. Birnboim, J. Doly, A rapid alkaline extraction procedure for screening recombinant plasmid DNA, Nucleic Acids Res 7(6) (1979) 1513-23.

[287] G.A. Goncalves, K.L. Prather, G.A. Monteiro, D.M. Prazeres, Engineering of Escherichia coli strains for plasmid biopharmaceutical production: scale-up challenges, Vaccine 32(24) (2014) 2847-50.

[288] A.M. Darquet, B. Cameron, P. Wils, D. Scherman, J. Crouzet, A new DNA vehicle for nonviral gene delivery: supercoiled minicircle, Gene Ther 4(12) (1997) 1341-9.

[289] M. Huang, Z. Chen, S. Hu, F. Jia, Z. Li, G. Hoyt, R.C. Robbins, M.A. Kay, J.C. Wu, Novel minicircle vector for gene therapy in murine myocardial infarction, Circulation 120(11 Suppl) (2009) S230-7.

[290] T.L. Deans, A. Singh, M. Gibson, J.H. Elisseeff, Regulating synthetic gene networks in 3D materials, Proc. Natl. Acad. Sci. U. S. A. 109(38) (2012) 15217-22.

[291] A.M. Krieg, Therapeutic potential of Toll-like receptor 9 activation, Nat Rev Drug Discov 5(6) (2006) 471-84.

[292] J. Scheiermann, D.M. Klinman, Clinical evaluation of CpG oligonucleotides as adjuvants for vaccines targeting infectious diseases and cancer, Vaccine 32(48) (2014) 6377-89.

[293] Y. Qiu, L. Guo, S. Zhang, B. Xu, Y. Gao, Y. Hu, J. Hou, B. Bai, H. Shen, P. Mao, DNA-based vaccination against hepatitis B virus using dissolving microneedle arrays adjuvanted by cationic liposomes and CpG ODN, Drug Deliv 23(7) (2016) 2391-2398.

[294] Y.Z. Yu, Y. Ma, W.H. Xu, S. Wang, Z.W. Sun, Combinations of various CpG motifs cloned into plasmid backbone modulate and enhance protective immunity of viral replicon DNA anthrax vaccines, Med Microbiol Immunol 204(4) (2015) 481-91.

[295] Z. He, J. Xu, W. Tao, T. Fu, F. He, R. Hu, L. Jia, Y. Hong, A recombinant plasmid containing CpG motifs as a novel vaccine adjuvant for immune protection against herpes simplex virus 2, Mol Med Rep 14(2) (2016) 1823-8.

[296] X. Shen, A.K. Pitol, V. Bachmann, D.L. Hacker, L. Baldi, F.M. Wurm, A simple plasmid-based transient gene expression method using High Five cells, J Biotechnol 216 (2015) 67-75.

[297] L. Cervera, S. Gutierrez-Granados, M. Martinez, J. Blanco, F. Godia, M.M. Segura, Generation of HIV-1 Gag VLPs by transient transfection of HEK 293

suspension cell cultures using an optimized animal-derived component free medium, J Biotechnol 166(4) (2013) 152-65.

[298] J. Sun, D. Li, Y. Hao, Y. Zhang, W. Fan, J. Fu, Y. Hu, Y. Liu, Y. Shao, Posttranscriptional regulatory elements enhance antigen expression and DNA vaccine efficacy, DNA Cell Biol 28(5) (2009) 233-40.

[299] K. Li, L. Gao, H. Gao, X. Qi, Y. Gao, L. Qin, Y. Wang, X. Wang, Codon optimization and woodchuck hepatitis virus posttranscriptional regulatory element enhance the immune responses of DNA vaccines against infectious bursal disease virus in chickens, Virus Res 175(2) (2013) 120-7.

[300] R. Grantham, C. Gautier, M. Gouy, R. Mercier, A. Pave, Codon catalog usage and the genome hypothesis, Nucleic Acids Res 8(1) (1980) r49-r62.

[301] T. Nagata, M. Uchijima, A. Yoshida, M. Kawashima, Y. Koide, Codon optimization effect on translational efficiency of DNA vaccine in mammalian cells: analysis of plasmid DNA encoding a CTL epitope derived from microorganisms, Biochem Biophys Res Commun 261(2) (1999) 445-51.

[302] T.M. Jacobs, H. Yumerefendi, B. Kuhlman, A. Leaver-Fay, SwiftLib: rapid degenerate-codon-library optimization through dynamic programming, Nucleic Acids Res 43(5) (2015) e34.

[303] D. Hannaman, L.C. Dupuy, B. Ellefsen, C.S. Schmaljohn, A Phase 1 clinical trial of a DNA vaccine for Venezuelan equine encephalitis delivered by intramuscular or intradermal electroporation, Vaccine 34(31) (2016) 3607-12.

[304] D. Datta, G.P. Bansal, D.L. Gerloff, B. Ellefsen, D. Hannaman, N. Kumar, Immunogenicity and malaria transmission reducing potency of Pfs48/45 and Pfs25 encoded by DNA vaccines administered by intramuscular electroporation, Vaccine 35(2) (2017) 264-272.

[305] A. Stachyra, P. Redkiewicz, P. Kosson, A. Protasiuk, A. Gora-Sochacka, G. Kudla, A. Sirko, Codon optimization of antigen coding sequences improves the immune potential of DNA vaccines against avian influenza virus H5N1 in mice and chickens, Virol J 13(1) (2016) 143.

[306] B. Sendy, D.J. Lee, S.J. Busby, J.A. Bryant, RNA polymerase supply and flux through the lac operon in Escherichia coli, Philos. Trans. R. Soc. Lond. B. Biol. Sci. 371(1707) (2016).

[307] J.A.N. Brophy, C.A. Voigt, Principles of genetic circuit design, Nat Meth 11(5) (2014) 508-520.

[308] J.A. Brophy, C.A. Voigt, Antisense transcription as a tool to tune gene expression, Mol. Syst. Biol. 12(1) (2016) 854.

[309] B.S. Der, E. Glassey, B.A. Bartley, C. Enghuus, D.B. Goodman, D.B. Gordon, C.A. Voigt, T.E. Gorochowski, DNAplotlib: programmable visualization of genetic designs and associated data, ACS Synth Biol (2016).

[310] K. Temme, R. Hill, T.H. Segall-Shapiro, F. Moser, C.A. Voigt, Modular control of multiple pathways using engineered orthogonal T7 polymerases, Nucleic Acids Res. 40(17) (2012) 8773-81.

[311] T.S. Moon, C. Lou, A. Tamsir, B.C. Stanton, C.A. Voigt, Genetic programs constructed from layered logic gates in single cells, Nature 491(7423) (2012) 249-53.

[312] R. Racz, X. Li, M. Patel, Z. Xiang, Y. He, DNAVaxDB: the first web-based DNA vaccine database and its data analysis, BMC Bioinformatics 15(4) (2014) S2.

[313] V.B. Pereira, M. Zurita-Turk, T.D.L. Saraiva, C.P. De Castro, B.M. Souza, P.M. Agresti, F.A. Lima, V.N. Pfeiffer, M.S.P. Azevedo, C.S. Rocha, DNA vaccines approach: from concepts to applications, World Journal of Vaccines 2014 (2014).

[314] L. Redding, D.B. Weiner, DNA vaccines in veterinary use, Expert Rev. Vaccines 8(9) (2009) 1251-1276.

[315] M.A. Kutzler, D.B. Weiner, DNA vaccines: ready for prime time?, Nature Reviews Genetics 9(10) (2008) 776-788.

[316] Y. Nakayama, A. Aruga, Comparison of current regulatory status for gene-based vaccines in the US, europe and japan, Vaccines 3(1) (2015) 186-202.

[317] M.A. Liu, J.B. Ulmer, Human clinical trials of plasmid DNA vaccines, Adv. Genet. 55 (2005) 25-40.

[318] M. Thompson, S.L. Heath, B. Sweeton, K. Williams, P. Cunningham, B.F. Keele, S. Sen, B.E. Palmer, N. Chomont, Y. Xu, DNA/MVA Vaccination of HIV-1 Infected Participants with Viral Suppression on Antiretroviral Therapy, followed by Treatment Interruption: Elicitation of Immune Responses without Control of Re-Emergent Virus, PLoS ONE 11(10) (2016) e0163164.

[319] C. Nilsson, B. Hejdeman, K. Godoy-Ramirez, T. Tecleab, G. Scarlatti, A. Bråve, P.L. Earl, R.R. Stout, M.L. Robb, R.J. Shattock, HIV-DNA given with or without

intradermal electroporation is safe and highly immunogenic in healthy swedish HIV-1 DNA/MVA vaccinees: a phase I randomized trial, PLoS ONE 10(6) (2015) e0131748.

[320] Q. Wang, W. Jiang, Y. Chen, P. Liu, C. Sheng, S. Chen, H. Zhang, C. Pan, S. Gao, W. Huang, In vivo electroporation of minicircle DNA as a novel method of vaccine delivery to enhance HIV-1-specific immune responses, J. Virol. 88(4) (2014) 1924-1934.

[321] D. Bose, J. Chandra, R. Dutta, M. Jais, S. Ray, R.A. Gupta, A. Seth, P. Kumar, Immune Response to Double Dose Hepatitis-B Vaccine using Four Dose Schedule in HIV Infected Children, Indian J Pediatr 83(8) (2016) 772-6.

[322] R.L. McCall, R.W. Sirianni, PLGA nanoparticles formed by single- or double-emulsion with vitamin E-TPGS, J Vis Exp (82) (2013) 51015.

[323] V.R. Sinha, A. Trehan, Biodegradable microspheres for protein delivery, J Control Release 90(3) (2003) 261-80.

[324] S. Luthra, J.P. Obert, D.S. Kalonia, M.J. Pikal, Investigation of drying stresses on proteins during lyophilization: differentiation between primary and secondary-drying stresses on lactate dehydrogenase using a humidity controlled mini freeze-dryer, J. Pharm. Sci. 96(1) (2007) 61-70.

[325] S. Luthra, J.P. Obert, D.S. Kalonia, M.J. Pikal, Impact of critical process and formulation parameters affecting in-process stability of lactate dehydrogenase during the secondary drying stage of lyophilization: a mini freeze dryer study, J. Pharm. Sci. 96(9) (2007) 2242-50.

[326] O.H. El-Nesr, S.A. Yahiya, O.N. El-Gazayerly, Effect of formulation design and freeze-drying on properties of fluconazole multilamellar liposomes, Saudi Pharm J 18(4) (2010) 217-24.

[327] P.V. Date, A. Samad, P.V. Devarajan, Freeze thaw: a simple approach for prediction of optimal cryoprotectant for freeze drying, AAPS PharmSciTech 11(1) (2010) 304-13.

[328] S. Bosch, L. de Beaurepaire, M. Allard, M. Mosser, C. Heichette, D. Chretien, D. Jegou, J.M. Bach, Trehalose prevents aggregation of exosomes and cryodamage, Sci Rep 6 (2016) 36162.

[329] P. Fonte, S. Reis, B. Sarmento, Facts and evidences on the lyophilization of polymeric nanoparticles for drug delivery, J Control Release 225 (2016) 75-86.

[330] M. Zheng, J. Luo, Z. Chen, Development of universal influenza vaccines based on influenza virus M and NP genes, Infection 42(2) (2014) 251-62.